NASA TECHNICAL NOTE

NASA TN D-8210

NASA TN D-8210

AN EXPERIMENTAL AND ANALYTICAL INVESTIGATION OF THE EFFECT ON ISOLATED BOATTAIL DRAG OF VARYING REYNOLDS NUMBER UP TO 130 × 10^6

David E. Reubush and Lawrence E. Putnam

Langley Research Center
Hampton, Va. 23665

NATIONAL AERONAUTICS AND SPACE ADMINISTRATION • WASHINGTON, D. C. • MAY 1976

1. Report No.	2. Government Accession No.	3. Recipient's Catalog No.
NASA TN D-8210		

4. Title and Subtitle	5. Report Date
AN EXPERIMENTAL AND ANALYTICAL INVESTIGATION OF THE EFFECT ON ISOLATED BOATTAIL DRAG OF VARYING REYNOLDS NUMBER UP TO 130×10^6	May 1976
	6. Performing Organization Code
7. Author(s)	8. Performing Organization Report No.
David E. Reubush and Lawrence E. Putnam	L-10521
	10. Work Unit No.
9. Performing Organization Name and Address	505-04-11-01
NASA Langley Research Center Hampton, Va. 23665	11. Contract or Grant No.
	13. Type of Report and Period Covered
12. Sponsoring Agency Name and Address	Technical Note
National Aeronautics and Space Administration Washington, D.C. 20546	14. Sponsoring Agency Code

15. Supplementary Notes

16. Abstract

An investigation was conducted to determine whether large Reynolds number effects occur on isolated boattails. The investigation included an analytical study and tests in the Langley 1/3-meter transonic cryogenic tunnel. This investigation was conducted at an angle of attack of 0^o at Mach numbers from 0.6 to 0.9 for Reynolds numbers up to 130×10^6. Results from this investigation indicate that as the Reynolds number was increased, the boattail static pressure coefficients in the expansion region of the boattail became more negative whereas those in the recompression region became more positive. These two trends were compensating and, as a result, there was only a small effect (if any) of Reynolds number on boattail pressure drag.

17. Key Words (Suggested by Author(s))	18. Distribution Statement
Boattail drag Reynolds number	Unclassified – Unlimited Subject Category 02

19. Security Classif. (of this report)	20. Security Classif. (of this page)	21. No. of Pages	22. Price*
Unclassified	Unclassified	83	$4.75

*For sale by the National Technical Information Service, Springfield, Virginia 22161

AN EXPERIMENTAL AND ANALYTICAL INVESTIGATION OF THE EFFECT ON ISOLATED BOATTAIL DRAG OF VARYING REYNOLDS NUMBER UP TO 130×10^6

David E. Reubush and Lawrence E. Putnam
Langley Research Center

SUMMARY

An investigation was conducted to determine whether large Reynolds number effects occur on isolated boattails. The investigation included an analytical study and tests in the Langley 1/3-meter transonic cryogenic tunnel. This investigation was conducted at an angle of attack of 0^o at Mach numbers from 0.6 to 0.9. Reynolds number based on the distance from the nose to the start of the boattail was varied from about 2.5×10^6 to 106×10^6 at a Mach number of 0.6 and from about 3.4×10^6 to 130×10^6 at a Mach number of 0.9. Reynolds number was varied by operating the tunnel at stagnation pressures which ranged from about 1.2 to 5.0 atmospheres at stagnation temperatures which ranged from about 103 K to 308 K.

Results from this investigation indicate that as the Reynolds number was increased, the boattail static pressure coefficients in the expansion region of the boattail became more negative whereas those in the recompression region became more positive. These two trends were compensating and, as a result, there was only a small effect (if any) of Reynolds number on boattail pressure drag.

INTRODUCTION

Current methods of prediction for propulsion-system installation drag in full-scale aircraft rely heavily on wind-tunnel simulation of actual conditions. Wind-tunnel tests are required because the drag-producing components of the propulsion system are usually installed in areas where the flow field is extremely complex; at present, there are no adequate theoretical techniques with which to predict these complex flows. High slopes and large boundary-layer runs, especially in the afterbody nozzle region, result in large and unpredictable viscous effects on boattail pressure drag. Attention has recently been focused on scaling effects, with particular notice given to the effects of Reynolds number variation on boattail pressure drag. Investigations by the Lewis Research Center of the National Aeronautics and Space Administration (refs. 1 to 5) have identified possible large effects of Reynolds number variation on installed boattail drag. At the Lewis Research

Center, flight tests were conducted by using an F-106B airplane which had two research nacelles mounted under the wings. The boattails to be tested were mounted on these nacelles and the F-106B airplane was flown over a range of altitudes to obtain boattail pressure drag data over a significant range of Reynolds numbers. In addition to the flight tests, tests of two scale models (5 and 22 percent) of the F-106B airplane were performed in the Lewis 8- by 6-foot supersonic tunnel in order to obtain data at Reynolds numbers lower than those achievable in flight. These tests also made possible a comparison between flight and wind-tunnel data. Results from these investigations have shown large apparent effects of Reynolds number variation on boattail pressure drag and have indicated that the wind-tunnel boattail pressure drags could not be extrapolated to flight. These data have accentuated the need for further research in this area.

The current investigation was initiated to determine whether large Reynolds number effects occur on isolated boattails. This investigation used a series of six isolated, sting-mounted, cone-cylinder nacelle models (2.54 cm in diameter) with four different boattail geometries. These models were tested in the Langley 1/3-meter transonic cryogenic tunnel because of the large range of Reynolds numbers available there. The tests and the analytical study were made primarily at the subsonic Mach numbers of 0.6 and 0.9 at an angle of attack of 0°. Reynolds number based on the distance from the nose to the start of the boattail varied from about 2.5×10^6 to 106×10^6 at a Mach number of 0.6 and from about 3.4×10^6 to 130×10^6 at a Mach number of 0.9. Limited data on this subject have been previously published in reference 6.

SYMBOLS

A cross-sectional area

A_m maximum cross-sectional area of model

A_β incremental cross-sectional area assigned to boattail static-pressure orifice for drag integration

$C_{D,\beta}$ boattail pressure drag coefficient, $\frac{1}{A_m} \sum_{i=1}^{30} C_{p,i} A_{\beta,i}$

C_p static pressure coefficient, $\frac{p - p_\infty}{q}$

d_b base diameter of boattail

d_m maximum diameter of model

d_s sting diameter

L	length of model from nose to start of boattail (characteristic length)
l	length of boattail
M	free-stream Mach number
p	local static pressure on model
p_t	free-stream total pressure
p_∞	free-stream static pressure
q	free-stream dynamic pressure
R	Reynolds number (based on distance from nose to start of boattail)
T_t	free-stream total temperature
V_x	ratio of component of local velocity on boattail in axial direction to free-stream velocity
V_y	ratio of local velocity on boattail in radial direction to free-stream velocity
x	axial distance from start of boattail, positive aft
y	radial distance from center line of model
δ^*	boundary-layer displacement thickness
θ_s	divergence angle of discriminating streamline, deg
ϕ	meridian angle about model axis, clockwise positive facing upstream, 0^o at top of model, deg

Subscripts:

a	analogous configuration
c	configuration corrected for boundary-layer displacement thickness

min	conditions at point of minimum static pressure on boattail
s	conditions at point of separation on boattail

APPARATUS AND PROCEDURE

Wind Tunnel

This investigation was conducted in the Langley 1/3-meter transonic cryogenic tunnel, a single-return, continuous-flow pressure tunnel. The test section is a regular octagon in cross section (34.29 cm across the flats) with slots at the corners of the octagon; it is essentially a model of the Langley 16-foot transonic tunnel test section. (See ref. 7.) This facility is capable of operating at stagnation pressures from about 1 to 5 atmospheres and at stagnation temperatures from about 78 K to 350 K over the tunnel operating Mach number range of about 0.1 to 1.2. Further description of the Langley 1/3-meter transonic cryogenic tunnel can be found in references 8 to 14.

Models and Support System

A generalized sketch of the boattailed cone-cylinder nacelle models used in this investigation is shown in figure 1. Figure 2 is a photograph of all six models. There were four short models of differing boattail geometry with a length of 20.32 cm from the nose to the start of the boattail (characteristic length); there were two long models with a length from the nose to the start of the boattail of 40.64 cm. The boattail geometry of the two long models duplicated the boattail geometry of two of the short models. Details of the geometry of the four boattails are shown in figure 3. The four boattail geometries were: circular arc with a length to maximum diameter ratio (fineness ratio, l/d_m) of 0.8 (both short and long models), circular arc with a fineness ratio of 1.77, circular-arc–conic with a fineness ratio of 0.96 (both short and long models), and contoured with a fineness ratio of 0.95. The two circular-arc boattails are scale models of two boattails which have been tested in the Langley 16-foot transonic tunnel (refs. 15 and 16 and unpublished data); the circular-arc–conic and the contoured boattails are isolated scale models of two boattails which have been wind tunnel tested in the Lewis 8- by 6-foot supersonic wind tunnel on models of the F-106B and flight tested on the F-106B airplane. (See refs. 1 to 5.)

The models were all sting mounted with the sting simulating the geometry of a jet exhaust plume for a nozzle operating at its design point. (See ref. 16.) The two circular-arc boattails and the circular-arc–conic boattail had ratios of sting diameter to maximum diameter of 0.50 whereas the contoured nozzle had a ratio of sting diameter to maximum diameter of 0.544. The length of the constant-diameter portion of the stings was such that, based on reference 17, there should be no effect of the tunnel support-sting flare on

the boattail pressure coefficients. In addition, the sum of the boattail and sting lengths (before the flare) was constant so that the noses of all four of the short models were at the same tunnel station. The noses of the two long models were at the same tunnel station, but this station was not the same as that for the short models. (Start of the boattail was at the same tunnel station for all six models.)

The models were constructed of cast aluminum with stainless-steel pressure tubes cast as an integral part of each model. The tubes were placed in the sand mold in the proper position, the aluminum was poured, and the model was machined to the proper contours.

Figure 4 is a photograph of one of the short models mounted in the Langley 1/3-meter transonic cryogenic tunnel. The models had a maximum diameter of 2.54 cm and a resulting tunnel blockage of about 0.52 percent. The test medium for the Langley 1/3-meter transonic cryogenic tunnel is nitrogen.

Instrumentation and Tests

The six boattails were instrumented with 30 static-pressure orifices in three rows of 10 orifices each (ϕ = 0°, 120°, and 240°) at the locations given in table I. These orifices were connected to a remotely located pressure scanning valve.

All tests were conducted in the Langley 1/3-meter transonic cryogenic tunnel at Mach numbers from about 0.6 to 0.9 (primarily at about M = 0.6 and 0.9) at an angle of attack of 0°. The Reynolds number based on the distance from the nose to the beginning of the boattail varied from about 2.5×10^6 to 106×10^6 at a Mach number of 0.6 and from about 3.4×10^6 to 130×10^6 at a Mach number of 0.9. The Reynolds number was varied by operating the tunnel at stagnation pressures which ranged from about 1.2 to 5.0 atmospheres at stagnation temperatures from about 103 K to 308 K. (Tests were conducted at two temperatures primarily: 117 K and 308 K.) Table II gives the approximate test conditions for both model lengths. Boundary-layer transition was natural for all tests.

Data Reduction

Model and wind-tunnel data were recorded on magnetic tape and a digital computer was used to compute standard force and pressure coefficients. Pressure drag coefficients were computed from the measured pressures on each boattail. These coefficients were based on the maximum cross-sectional area of the model and were obtained from the pressure data by assigning an area to each orifice and computing the coefficients from the equation

$$C_{D,\beta} = \frac{1}{qA_m} \sum_{i=1}^{30} \left(p_i - p_\infty\right) A_{\beta,i} \tag{1}$$

Accuracy of this step integration scheme was spot-checked by plotting the pressure coefficients as a function of A/A_m and integrating with a planimeter.

ANALYTICAL METHOD

The analytical method used in this study has been developed to calculate the flow over axisymmetric boattailed bodies at subsonic speeds. It is assumed that a viscous layer near the body and an inviscid external flow compose the flow. The effect of the viscous layer is taken into account by modifying the body shape with an appropriate displacement thickness. In the framework of this representation, any boundary-layer separation on the boattail surface is taken into account by properly modifying the afterbody geometry. In the present investigation, the models were sting supported with the diameter of the stings essentially equal to the base diameter of the body. Therefore, it was not necessary to develop an analytical model of a wake or jet exhaust plume, and the sting was treated as a body connected to and downstream of the boattail.

Inviscid Flow Solution

The Neumann solution of reference 18 for incompressible flow over bodies of revolution was used to calculate the external inviscid flow. Since this is a solution for incompressible flow, the compressibility correction of reference 19 was used to correct for Mach number effects. The incompressible flow field considered is that for an "analogous" configuration obtained by means of the affine coordinate transformation given by the following equations:

$$x_a = \frac{x}{\beta} \tag{2}$$

$$y_a = y \tag{3}$$

where

$$\beta = \sqrt{1 - M^2} \tag{4}$$

The calculated flow velocities of the "analogous" configuration are then corrected using the following equations:

$$V_x = \frac{V_{x,a}}{B^2} \tag{5}$$

$$V_y = \frac{\beta V_{y,a}}{B^2} \tag{6}$$

where

$$B = \sqrt{1 - M^2\left(1 + V_{x,a}\right)} \tag{7}$$

The pressure coefficients are obtained from the corrected velocities by using the isentropic flow relation. Experience to date has shown that this compressibility correction provides better agreement with experimental results for flow over boattails than the classical Goethert compressibility correction.

Viscous Flow Solution

The displacement-thickness distribution along the body is calculated by the method of reference 20 for turbulent boundary layers. This method is a modified version of the Reshotko-Tucker integral boundary-layer solution (ref. 21).

If boundary-layer separation occurs on the boattail, the boundary-layer equations become singular at the separation point. Although the boundary-layer solution of reference 20 is calculated through the separation point, the predicted values of displacement thickness in the region of separated flow are incorrect. To overcome this difficulty, the separation model of Presz (ref. 22) is used for the present calculations. In Presz's model of the separated region, a discriminating streamline is used to separate the reverse flow from the outer boundary-layer flow. (See fig. 5.) Presz modeled this discriminating streamline as a conical surface diverging from the model surface at an angle which is dependent on the local Mach number at the separation point. A straight-line curve fit through the experimental data of Presz (fig. 6) is used in the calculations of this paper to determine the divergence angle of the discriminating streamline. This curve fit is given by the following equation:

$$\theta_s = 14.4 - 4.89M_s \tag{8}$$

Experience has shown that although this divergence angle is not critical, the location of the separation point is extremely critical to good results. To approximate the boundary-layer displacement-thickness effect of the outer flow in the separation region, the displacement thickness calculated by the method of reference 20 is added to the discriminating streamline.

The use of Presz's model of the separated flow region requires that some method be available for predicting the location of the separation point. For the calculations of this paper, the location of separation is predicted by using the method of Page (ref. 23) as modified in reference 24. This relatively simple technique is based on the pressure rise from the minimum pressure on the afterbody to the pressure at separation; that is,

$$C_{p,s}\frac{p_\infty M^2}{p_s M_s^2} = C_{p,m}\frac{p_\infty M^2}{p_{min}M_{min}^2} + 0.38 \tag{9}$$

Presz found that this method did not give good results when the experimental pressure distribution on the afterbody was used with equation (9) to predict the separation location (ref. 22). However, if the inviscid pressure distribution predicted by the method of this study is used instead, a reasonable prediction of the separation location results. (The point x_s is the point on the boattail where $C_{p,s}$ found from eq. (9) occurs.) (See fig. 7.) This procedure is the separation prediction technique used in this investigation. With this method (that is, using the inviscid pressure distribution), the predicted location of separation is not a function of Reynolds number.

Viscous-Inviscous Interaction

Since the boundary-layer displacement thickness is a function of the pressure distribution along the body, the final converged solution must be obtained by iteration between the inviscid outer flow solution and the inner boundary-layer solution. The iteration algorithm used by the present method follows:

(1) Calculate the inviscid pressure distribution on the body of revolution.

(2) Determine whether the boattail boundary-layer flow is attached or whether the boundary-layer flow separates. The present method for predicting the location of separation predicts a separation point for any boattail. In order to determine whether the boattail flow is separated or attached, it is first necessary to calculate a solution assuming attached flow. If the solution diverges, it can be assumed that the flow is not attached, and calculation of the solution by assuming separated flow is necessary.

(3) If a separated boattail flow solution is required, the following calculations are necessary:

(a) Calculate the location of the separation point.

(b) Correct body geometry for separated flow discriminating streamline.

(c) Calculate inviscid pressure distribution for effective body.

(4) Calculate boundary-layer displacement thickness δ^*.

(5) Correct body geometry for boundary-layer displacement effects by using the following equation (subscript I indicates iteration number):

$$y_c = y + \frac{\delta_I^* + \delta_{I-1}^*}{2} \tag{10}$$

where $\delta_0^* = 0$.

(6) Calculate inviscid pressure distribution for corrected body.

(7) Repeat steps (4) to (6) for desired number of iterations. In the present algorithm, no convergence criteria are specified. Convergence is taken to occur when two successive iterations give essentially the same results when plotted to a reasonable scale. To obtain this result, most configurations required from 7 to 9 iterations only.

DISCUSSION

Boattail Pressure Coefficient Distributions

Boattail pressure coefficient distributions for the six models at various Reynolds numbers for Mach numbers of 0.6 and 0.9 are shown in figures 8 to 13. These basic data are not discussed as such but are summarized and discussed in the following sections. The slight scatter shown when the three rows of pressures are compared for the same data point, however, is discussed briefly before the major results are presented.

The scatter shown in the data presented in the basic data figures is caused by two factors. First, at the time these data were obtained, the Langley 1/3-meter transonic cryogenic tunnel still had the status of a pilot proof-of-concept facility and its control systems were not refined. (Tunnel controls have been considerably improved since that time.) As a result, the tunnel conditions (free-stream Mach number, stagnation pressure, and stagnation temperature) could not be held constant during the approximately 1-minute recording time for each data point. In addition, a given set of tunnel conditions could not be repeated to close tolerances. With a slight variation in tunnel conditions came a slight variation in model pressures. The second possible reason for the slight scatter was the small amount of misalinement of the various models with the flow (varied from model to model) so that the models were not exactly at an angle of attack or sideslip of 0°. The small amounts of scatter shown in these data are not believed to have altered in any way the conclusions which were drawn from these data.

Theoretical Predictions of Boattail Pressure Coefficients

Included on each of the basic data figures are the boattail pressure coefficient distributions predicted by the analytical method described previously. (Theory is not applicable to configurations where flow has reached sonic velocity, that is, all configurations at $M = 0.9$ except $\frac{l}{d_m} = 1.77$ circular arc.) In general, the method yields reasonable predictions for the boattail pressure coefficients. Agreement was especially good for the $\frac{l}{d_m} = 1.77$ circular arc which had attached flow at both $M = 0.6$ and 0.9 (fig. 10). For the other configurations, all of which had flow separation, the method gave good results except in the separated region. For the $\frac{l}{d_m} = 0.80$ circular-arc boattails (figs. 8 and 9)

and the contoured boattail (fig. 13), the pressure level in the separated region was overpredicted, while for the circular-arc–conic boattails, the pressure level in the separated region was underpredicted (figs. 11 and 12). This problem with the separated region is believed to be a result of an inaccurate separation location prediction technique. In order to achieve better results in the separated region, a better separation location prediction technique needs to be developed.

Effect of Reynolds Number on Boattail Pressure Coefficient Distributions

Boattail pressure coefficient distributions (all three rows) for the $\frac{l}{d_m} = 0.8$ circular arc boattail $\left(\frac{L}{d_m} = 8.0 \text{ model}\right)$ obtained at four Reynolds numbers (spanning the range of those tested for the Mach numbers of 0.6 and 0.9) are shown in figure 14. On the cylindrical portion of the model just upstream of the beginning of the boattail $\left(\frac{x}{d_m} = 0.0\right)$, the pressure coefficients at all four Reynolds numbers generally agree. However, as the flow expands around the shoulder of the boattail, the pressure coefficients at the different Reynolds numbers begin to spread apart so that the higher the Reynolds number, the more negative the pressure coefficients in this expansion region. As the flow begins to recompress over the aft portion of the boattail, the trend is reversed; that is, the higher the Reynolds number, the more positive the pressure coefficients. It is also believed that for this configuration on which the flow separated, the separation point may have moved aft slightly as the Reynolds number was increased.

The result shown in figure 14 is typical of that found for all four boattail geometries tested. The pressure coefficient distributions for all of the other boattails (figs. 15 to 19) show trends identical to those previously discussed. As Reynolds number is increased, the expansion pressure coefficients become more negative while the recompression pressure coefficients become more positive. Similar trends have been reported in references 25 and 26.

Results from the theoretical predictions of the previously described method show the same trends in boattail pressure coefficient variation with Reynolds number as the experimental data. Figure 20 shows the theoretically predicted boattail pressure coefficient distributions at $M = 0.6$ for the circular-arc–conic boattail $\left(\frac{L}{d_m} = 8.0\right)$ at three Reynolds numbers from 2.6×10^6 to 42.9×10^6. These results are typical of those found for all the configurations. As with the experimental data, the pressure coefficients in the expansion region become more negative with increasing Reynolds number whereas those in the recompression region become more positive.

It is believed that the effects of Reynolds number shown in the pressure coefficient distributions are caused by the relative thickness of the boundary layer at the various

Reynolds numbers. At the lower Reynolds numbers, the boundary layer is relatively thicker than at the higher Reynolds numbers. As a result, the thick boundary layer "softens" the shoulder that the flow must negotiate; thus, the peak expansion pressures are lower than at the higher Reynolds numbers where the boundary layer is thinner and the shoulder "sharper." However, this thicker boundary layer for the lower Reynolds numbers reduces the effective area ratio for the diffuser effect in the recompression region of the boattail; thus there are lower pressures in the recompression region for the lower Reynolds numbers than for the higher Reynolds numbers. In addition, the thicker boundary layer at the lower Reynolds numbers is less energetic than the boundary layer at the higher Reynolds numbers; thus, the flow cannot penetrate the adverse pressure gradient in the recompression region as far as at the higher Reynolds numbers. This condition results in an earlier separation for the lower Reynolds numbers; the early separation also yields lower pressures in the recompression region.

Effect of Reynolds Number on Boattail Pressure Drag Coefficients

Boattail pressure drag coefficients as a function of Reynolds number for the Mach numbers of 0.6 and 0.9 and as a function of Mach number are shown in figures 21 to 26. These figures show that the trends shown for the boattail pressure coefficients are compensating. As a result, there is generally only a small effect (if any) of Reynolds number on boattail pressure drag. The curves of boattail pressure drag as a function of Mach number show that some of the small amount of scatter in the $M = 0.9$ Reynolds number curves can be attributed to differences in Mach number among data obtained in the drag rise region.

Theoretical predictions of the effect of Reynolds number on boattail pressure drag coefficients are shown in figure 27. Although the absolute levels of drag coefficient do not agree very well with the experimental drag coefficients, the trend of essentially no change in boattail pressure drag with changes in Reynolds number agrees with experiment. There seems to be a contradiction between the relatively good agreement of theory with experiment in pressure coefficient distributions and the poor agreement when these pressure coefficients are integrated to yield drag. Boattail pressure drag coefficients are extremely sensitive to changes in boattail pressure coefficients. As a result, a theoretical pressure coefficient distribution which is judged to be in good agreement with an experimental distribution can yield integrated drag coefficients which are in poor agreement.

These experimental and analytical results are different from those found in the work with installed configurations at the Lewis Research Center. Therefore, it must be

concluded that the large effects shown in that work are caused by installation effects and not by a fundamental effect of Reynolds number on boattail flow.

It must be noted at this point that had the portion of the model considered to be the boattail not included all the aft-facing, axially projected area, the results from this investigation could be interpreted in a vastly different manner. For instance, had the boattail been broken down into two regions (e.g., afterbody and nozzle) divided at a point between the expansion and recompression regions, the results would show the two regions to have exactly opposite trends of drag coefficient with Reynolds number. The forward afterbody region which includes the expansion region would show an increase in drag with Reynolds number because the expansion pressures become more negative. The nozzle region would show a decrease in drag with Reynolds number because the recompression pressures become more positive. Only when both regions are considered together does the true picture of no effect of Reynolds number emerge. Similarly, had the boattail been considered as a single region which started at some point downstream of the maximum diameter point, a portion of the aft-facing, axially projected area (containing a portion of the expansion region) would not be considered in the drag measurement. The existence of this unmeasured portion would result in integrated pressure drag coefficients which decrease with Reynolds number. This conclusion is again false. These comments are illustrated by figure 28 which shows the drag buildup as a function of axial distance from the start of the boattail at two extremes of Reynolds number for the circular-arc–conic boattail at $M = 0.6$ which is typical of all those tested. Although the drag buildups follow different paths at the two different Reynolds numbers, the final drag values are about the same. If there is an area of the boattail with inadequate pressure instrumentation, there is the possibility of a problem similar to that created by the exclusion of the total amount of aft-facing, axially projected area in the drag calculations. This occurrence would bias the results toward those regions with more extensive instrumentation. Such a bias would yield higher or lower drag with Reynolds number depending on where the instrumentation was located.

Comparison of Data Obtained in Two Different Facilities

As mentioned previously, the two circular-arc boattails are models of two models which had been previously tested in the Langley 16-foot transonic tunnel (blockage is approximately 0.1 percent). A comparison of some previously unpublished data from the sting-mounted Langley 16-foot transonic tunnel models with the corresponding data for the models of this investigation is shown in figures 29 and 30. Figure 29 shows the comparisons at $M = 0.6$ and 0.9 (Reynolds numbers as close as possible) for the $\frac{l}{d_m} = 0.8$ circular-arc boattail $\left(\frac{L}{d_m} = 8.0\right)$. At $M = 0.6$, the pressure coefficients agree quite well. At $M = 0.9$, the pressure coefficients agree except for the slightly different pressure

coefficients in the separated region. However, the pressure drag coefficients agree only fairly well at both Mach numbers. This difference in the pressure drag levels is believed to be caused by differences between the two tests with regard to blockage and other wall interference effects. Figure 30 shows the comparisons at $M = 0.6$ and 0.9 for the $\frac{l}{d_m} = 1.77$ circular-arc boattail $\left(\frac{L}{d_m} = 8.0\right)$. At both $M = 0.6$ and 0.9 the pressure coefficients and pressure drag coefficients agree quite well for this unseparated boattail.

SUMMARY OF RESULTS

An investigation at an angle of attack of 0^o has been conducted in the Langley 1/3-meter transonic cryogenic tunnel at Mach numbers from 0.6 to 0.9 with Reynolds numbers to 130×10^6 to determine the effects of variations in Reynolds number on the boattail pressure drag of several isolated boattails. An analytical study was also part of this investigation. The results of this investigation indicate the following:

1. As the Reynolds number was increased, the boattail static pressure coefficients in the expansion region of the boattails became more negative, although those pressure coefficients in the recompression region of the boattails became more positive. These trends were compensating and, as a result, there was only a small effect (if any) of Reynolds number on isolated boattail pressure drag.

2. Use of the theoretical method reported in this paper yielded reasonable predictions of the boattail static pressure coefficient distributions for the various boattails but poor prediction of the drag levels (because of the extreme sensitivity of drag to changes in pressure coefficients). However, the trends of both boattail static pressure coefficient and boattail pressure drag coefficient with Reynolds number were predicted.

Langley Research Center
National Aeronautics and Space Administration
Hampton, Va. 23665
April 9, 1976

REFERENCES

1. Chamberlin, Roger: Flight Investigation of 24° Boattail Nozzle Drag at Varying Subsonic Flight Conditions. NASA TM X-2626, 1972.

2. Chamberlin, Roger; and Blaha, Bernard J.: Flight and Wind Tunnel Investigation of the Effects of Reynolds Number on Installed Boattail Drag at Subsonic Speeds. NASA TM X-68162, [1973].

3. Wilcox, Fred A.: Comparison of Ground and Flight Test Results Using a Modified F106B Aircraft. AIAA Paper No. 73-1305, Nov. 1973.

4. Chamberlin, Roger: Flight Reynolds Number Effects on a Contoured Boattail Nozzle at Subsonic Speeds. NASA TM X-3053, 1974.

5. Wilcox, F. A.; and Chamberlin, R.: Reynolds Number Effects on Boattail Drag of Exhaust Nozzles From Wind Tunnel and Flight Tests. Airframe/Propulsion Interference, AGARD-CP-150, Sept. 1974.

6. Reubush, David E.: The Effect of Reynolds Number on Boattail Drag. AIAA Paper No. 75-63, Jan. 1975.

7. Corson, Blake W., Jr.; Runckel, Jack F.; and Igoe, William B.: Calibration of the Langley 16-Foot Transonic Tunnel With Test Section Air Removal. NASA TR R-423, 1974.

8. Goodyer, Michael J.; and Kilgore, Robert A.: The High Reynolds Number Cryogenic Wind Tunnel. AIAA Paper No. 72-995, Sept. 1972.

9. Kilgore, Robert A.; Adcock, Jerry B.; and Ray, Edward J.: Flight Simulation Characteristics of the Langley High Reynolds Number Cryogenic Transonic Tunnel. AIAA Paper No. 74-80, Jan.-Feb. 1974.

10. Ray, Edward J.; Kilgore, Robert A.; Adcock, Jerry B.; and Davenport, Edwin E.: Test Results From the Langley High Reynolds Number Cryogenic Transonic Tunnel. AIAA Paper No. 74-631, July 1974.

11. Polhamus, E. C.; Kilgore, R. A.; Adcock, J. B.; and Ray, E. J.: The Langley Cryogenic High Reynolds Number Wind-Tunnel Program. Astronaut. & Aeronaut., vol. 12, no. 10, Oct. 1974, pp. 30-40.

12. Kilgore, Robert A.; Goodyer, Michael J.; Adcock, Jerry B.; and Davenport, Edwin E.: The Cryogenic Wind-Tunnel Concept for High Reynolds Number Testing. NASA TN D-7762, 1974.

13. Kilgore, Robert A.; Adcock, Jerry B.; and Ray, Edward J.: Simulation of Flight Test Conditions in the Langley Pilot Transonic Cryogenic Tunnel. NASA TN D-7811, 1974.

14. Ray, Edward J.; Kilgore, Robert A.; Adcock, Jerry B.; and Davenport, Edwin E.: Analysis of Validation Tests of the Langley Pilot Transonic Cryogenic Tunnel. NASA TN D-7828, 1975.

15. Reubush, David E.; and Runckel, Jack F.: Effect of Fineness Ratio on the Boattail Drag of Circular-Arc Afterbodies Having Closure Ratios of 0.50 With Jet Exhaust at Mach Numbers Up to 1.30. NASA TN D-7192, 1973.

16. Reubush, David E.: Experimental Study of the Effectiveness of Cylindrical Plume Simulators for Predicting Jet-On Boattail Drag at Mach Numbers up to 1.30. NASA TN D-7795, 1974.

17. Cahn, Maurice S.: An Experimental Investigation of Sting-Support Effects on Drag and a Comparison With Jet Effects at Transonic Speeds. NACA Rep. 1353, 1958. (Supersedes NACA RM L56F18a.)

18. Hess, J. L.; and Smith, A. M. O.: Calculation of Potential Flow About Arbitrary Bodies. Progress in Aeronautical Sciences, Vol. 8, D. Küchemann, P. Carrière, B. Etkin, W. Fiszdon, N. Rott, J. Smolderen, I. Tani, and W. Wuest, eds., Pergamon Press, Inc., c.1967, pp. 1-138.

19. Labrujere, Th. E.; Loeve, W.; and Slooff, J. W.: An Approximate Method for the Calculation of the Pressure Distribution on Wing-Body Combinations at Subcritical Speeds. Aerodynamic Interference, AGARD-CP-71-71, Sept. 1970.

20. Users Manual for the External Drag and Internal Nozzle Performance Deck (Deck XI) – Supersonic Flow Analysis (Applicable to Deck VI). PWA-3465, Suppl. F, Pt. I (Contract No. AF 33(615)-3128), Pratt & Whitney Aircraft, Sept. 1, 1968.

21. Reshotko, Eli; and Tucker, Maurice: Approximate Calculation of the Compressible Turbulent Boundary Layer With Heat Transfer and Arbitrary Pressure Gradient. NACA TN 4154, 1957.

22. Presz, Walter Michael, Jr.: Turbulent Boundary Layer Separation of Axisymmetric Afterbodies. Ph. D. Thesis, Univ. of Connecticut, 1974.

23. Page, R. H.: A Theory for Incipient Separation. Developments in Mechanics, Vol. 1, J. E. Lay and L. E. Malvern, eds., Plenum Press, 1961, pp. 563-577.

24. Presz, Walter M., Jr.; and Pitkin, Edward T.: Flow Separation Over Axisymmetric Afterbody Models. AIAA Paper No. 74-17, Jan.-Feb. 1974.

25. Zonars, D.; Laughrey, James A.; and Bowers, Douglas L.: Effects of Varying Reynolds Number and Boundary Layer Displacement Thickness on the External Flow Over Nozzle Boattails. Improved Nozzle Testing Techniques in Transonic Flow, A. Ferri, ed., AGARD-AG-208, Sept. 1974, pp. I-F1 – I-F28.

26. Lee, John D.: An Experimental Study of Boattail Pressures at High Subsonic Mach Numbers and High Reynolds Numbers. ARL TR 75-0014, U.S. Air Force, Mar. 1975.

TABLE I.- BOATTAIL SURFACE ORIFICE LOCATIONS

Boattail configuration	$\frac{x}{d_m}$ for $\frac{L}{d_m}$ = 8 at ϕ, deg, of –			$\frac{x}{d_m}$ for $\frac{L}{d_m}$ = 16 at ϕ, deg, of –		
	0	120	240	0	120	240
Circular arc; $\frac{l}{d_m}$ = 0.8	-0.2771	-0.2761	-0.2850	-0.4491	-0.4660	-0.4561
	-.0256	-.0731	-.0700	-.1637	-.2201	-.1552
	.0770	.0256	.0345	-.0600	-.1281	-.0590
	.1765	.1287	.1270	.0337	-.0260	.0390
	.2750	.2257	.2260	.1268	.0744	.1342
	.3679	.3240	.3279	.2279	.1729	.2713
	.4675	.4180	.4200	.3210	.2696	.3718
	.5749	.5166	.5220	.4199	.3679	.4680
	.6698	.6165	.6376	.5231	.4640	.5749
	.7746	.7280	.7400	.6279	.6758	.7304
Circular arc; $\frac{l}{d_m}$ = 1.77	-0.3006	-0.3028	-0.3090			
	-.0086	.2554	-.1088			
	.3515	.5057	-.0113			
	.6314	.7364	.3543			
	.8271	.9091	.5072			
	.9975	1.0652	.8204			
	1.1500	1.2075	.9910			
	1.2776	1.3581	1.3528			
	1.4144	1.4817	1.4846			
	1.5447	1.6202	1.6936			
Circular-arc–conic; $\frac{l}{d_m}$ = 0.96	-0.2842	-0.2843	-0.2847	-0.2612	-0.2773	-0.2613
	.0001	.0352	.0059	.0228	-.0292	.0307
	.1090	.0640	.1044	.1227	.0707	.1246
	.1917	.1577	.2069	.2158	.1705	.2308
	.3000	.2542	.3031	.3107	.2638	.3237
	.4027	.3528	.4453	.4148	.3638	.4648
	.5022	.4499	.5483	.5097	.4607	.5737
	.5991	.5518	.6516	.5967	.5557	.6628
	.6948	.6522	.7494	.7068	.6558	.7706
	.8036	.8488	.9069	.8188	.8678	.9156
Contoured; $\frac{l}{d_m}$ = 0.95	-0.2951	-0.2950	-0.3011			
	-.0084	-.0500	-.0021			
	.0925	.0500	.0934			
	.1930	.1485	.1976			
	.2861	.2433	.2913			
	.3759	.3449	.4350			
	.4786	.4417	.5355			
	.5797	.5404	.6335			
	.6840	.6415	.7366			
	.7909	.8425	.8951			

TABLE II.- APPROXIMATE TEST CONDITIONS

T_t, K	p_t, atm*	M	R for $\frac{L}{d_m} = 8.0$	R for $\frac{L}{d_m} = 16.0$
103	5.00	0.6		106×10^6
103	5.00	.9		130
117	5.00	.6	43×10^6	86
117	5.00	.9	55	110
117	4.15	.8	43	86
117	4.02	.85	43	86
117	4.00	.6	34	68
117	4.00	.9	44	88
117	3.00	.6	26	52
117	3.00	.9	33	66
117	2.50	.6	21.5	43
117	2.50	.9	27.5	55
117	2.00	.6	17	34
117	2.00	.9	22	44
117	1.50	.6	13	26
117	1.50	.9	16.5	33
117	1.30	.6	11.5	23
117	1.30	.9	13.5	27
308	5.00	.6	11.5	23
308	5.00	.9	14	28
308	3.80	.6	8.5	17
308	3.80	.9	11	22
308	3.14	.6	7	14
308	2.63	.8	7	14
308	2.56	.85	7	14
308	2.50	.6	5.5	11
308	2.50	.9	7	14
308	1.25	.6	3	6
308	1.25	.9	3.5	7

*1 atm = 0.101325 MPa.

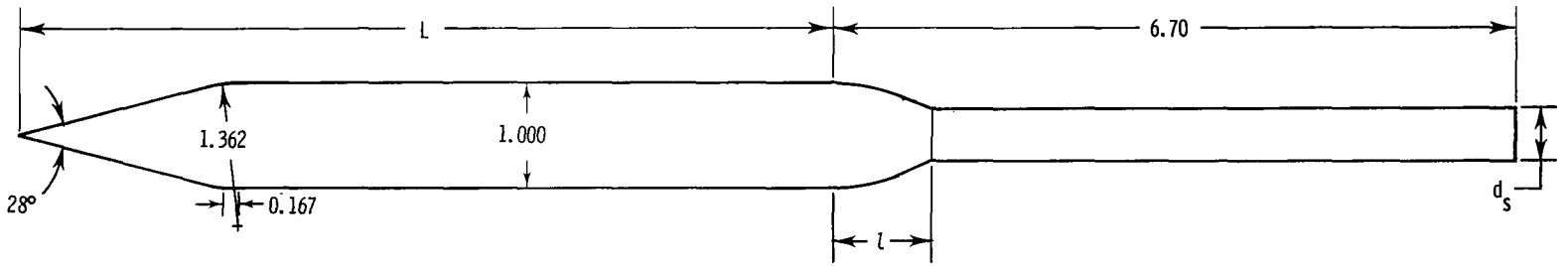

Boattail	L/d_m	d_s/d_m
Circular arc; l/d_m = 0.80	8.00 and 16.00	0.500
Circular arc; l/d_m = 1.77	8.00	.500
Circular-arc—conic	8.00 and 16.00	.500
Contoured	8.00	.544

Figure 1.- Sketch of cone-cylinder nacelle model. All dimensions are nondimensionalized by model maximum diameter (2.54 cm).

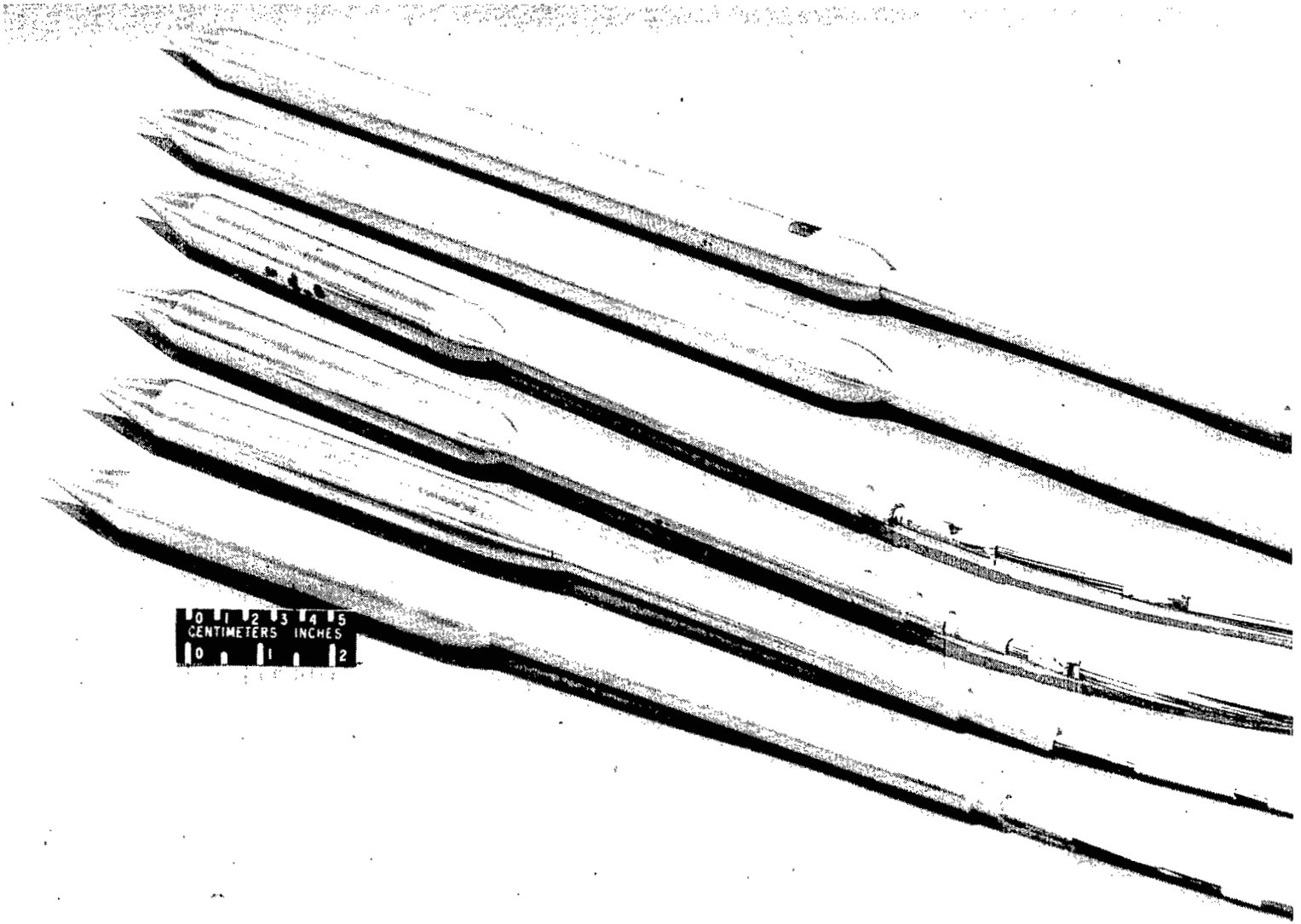

L-74-2518

Figure 2.- Six models used in this investigation.

Circular arc

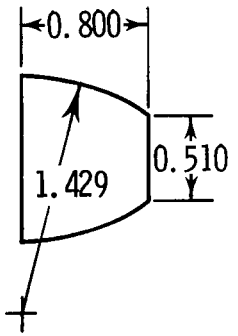

Circular-arc—conic

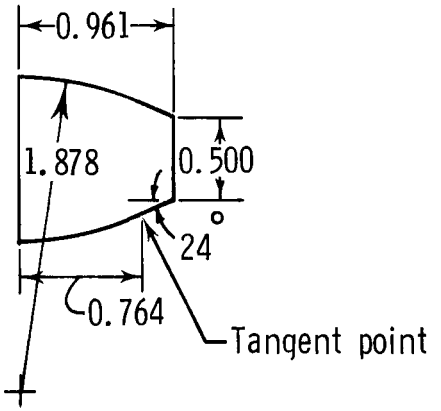

Circular arc

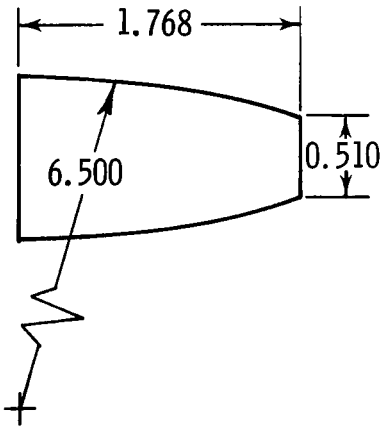

Contoured

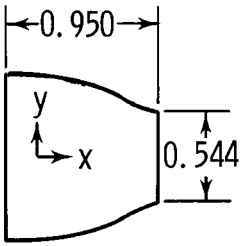

Coordinates for contoured boattail

x/d_m	y/d_m	x/d_m	y/d_m
0.0	0.500	0.640	0.409
.080	.499	.720	.372
.160	.497	.800	.328
.240	.494	.840	.304
.320	.487	.880	.288
.400	.475	.920	.276
.480	.461	.950	.272
.560	.439		

Figure 3.- Sketch showing details of boattail geometries. All dimensions are nondimensionalized by model maximum diameter (2.54 cm).

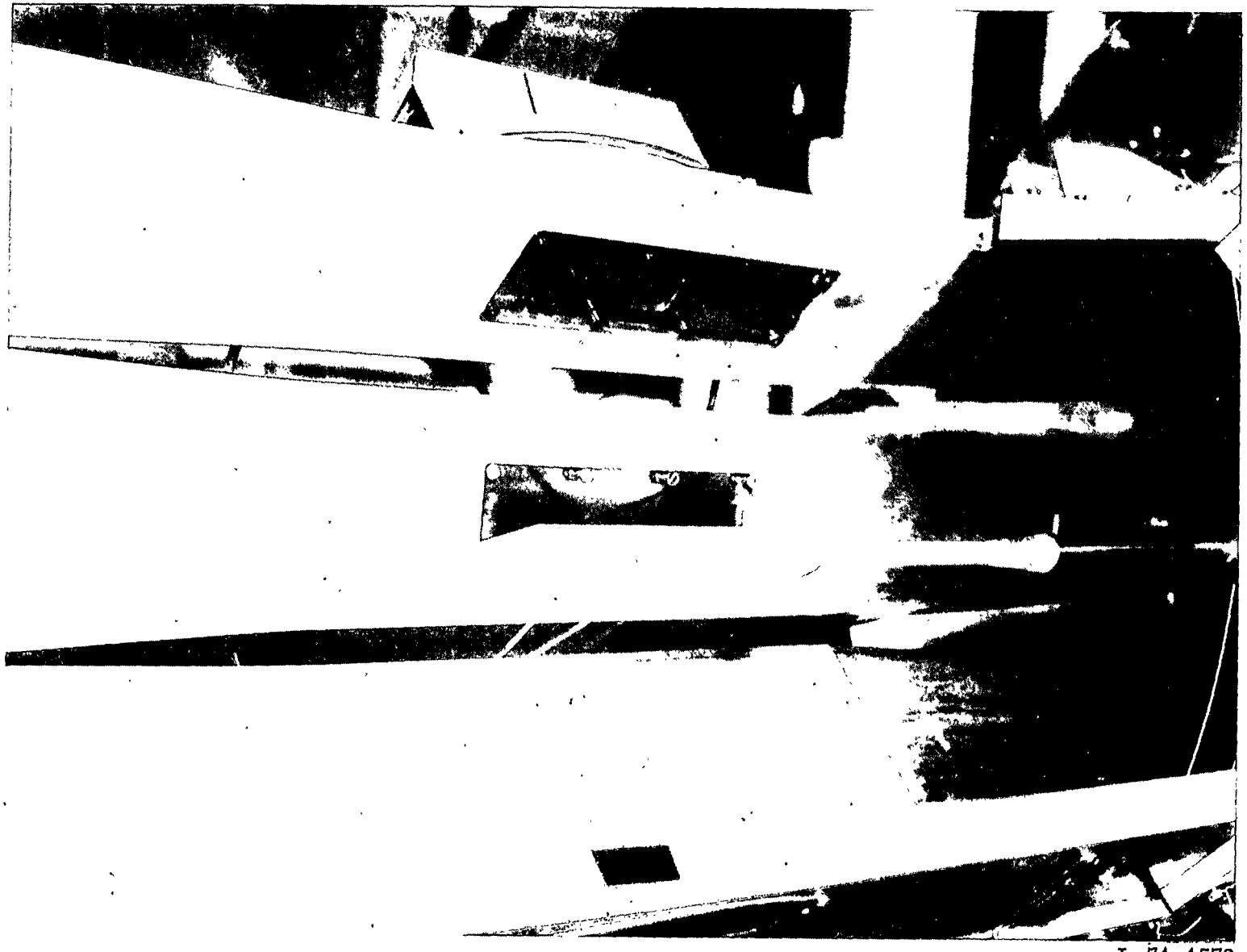

L-74-4572

Figure 4.- Typical installation of $\frac{L}{d_m} = 8.0$ nacelle model in cryogenic tunnel.

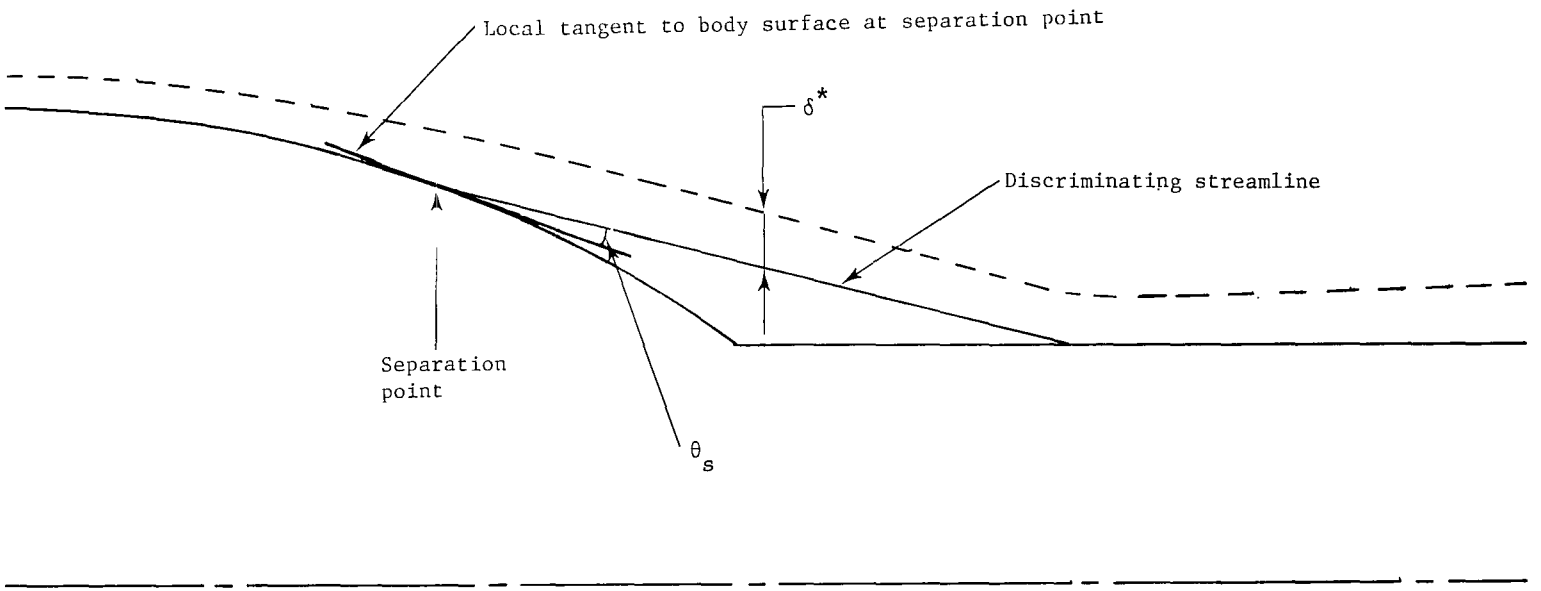

Figure 5.- Analytical model of separated flow region on afterbody.

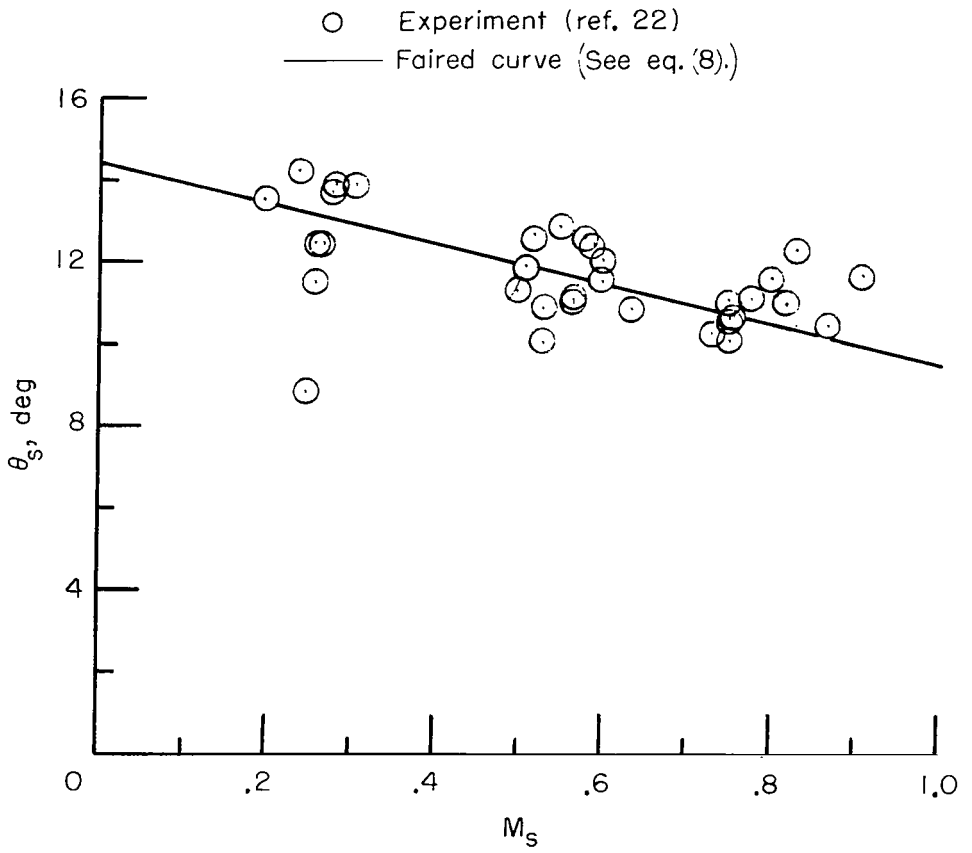

Figure 6.- Variation of separation discriminating streamline divergence angle with Mach number at separation.

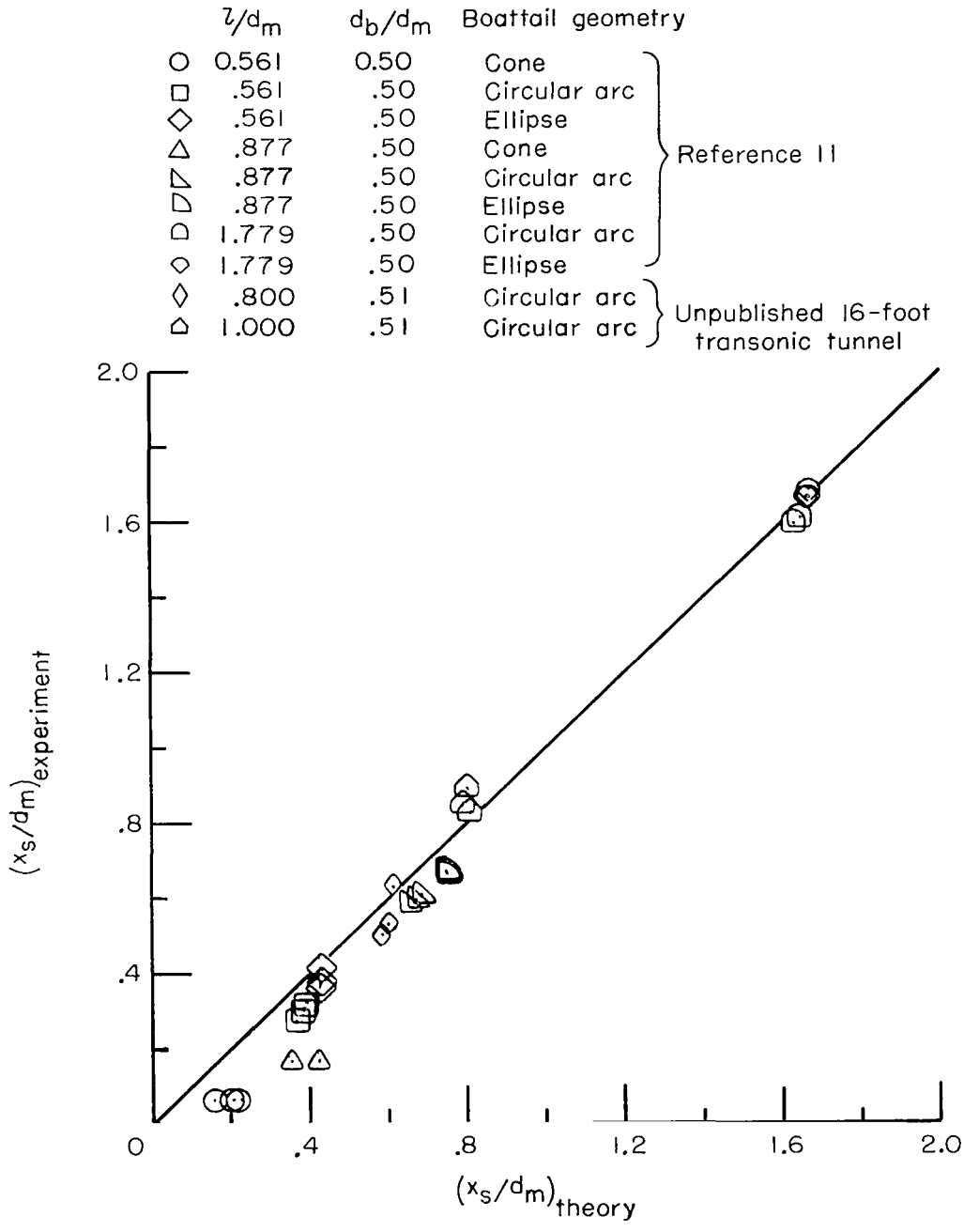

Figure 7.- Comparison of separation location predicted by modified Page method with experiment. M = 0.25 to 0.70.

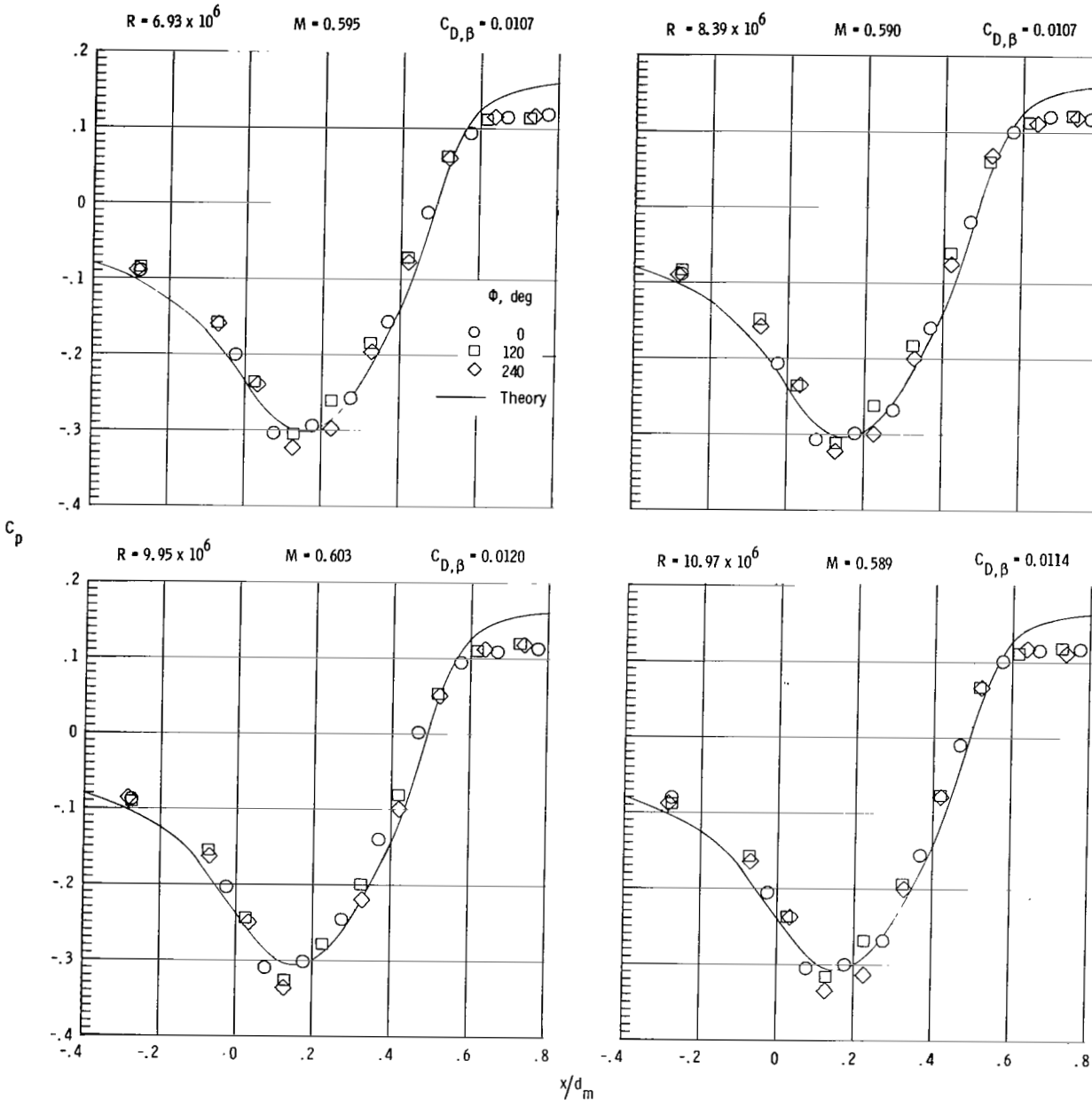

(a) M = 0.6.

Figure 8.- Boattail static pressure coefficients for $\frac{l}{d_m} = 0.80$ circular-arc boattail $\left(\frac{L}{d_m} = 8.0\right)$ at various Reynolds numbers for M = 0.6 and 0.9.

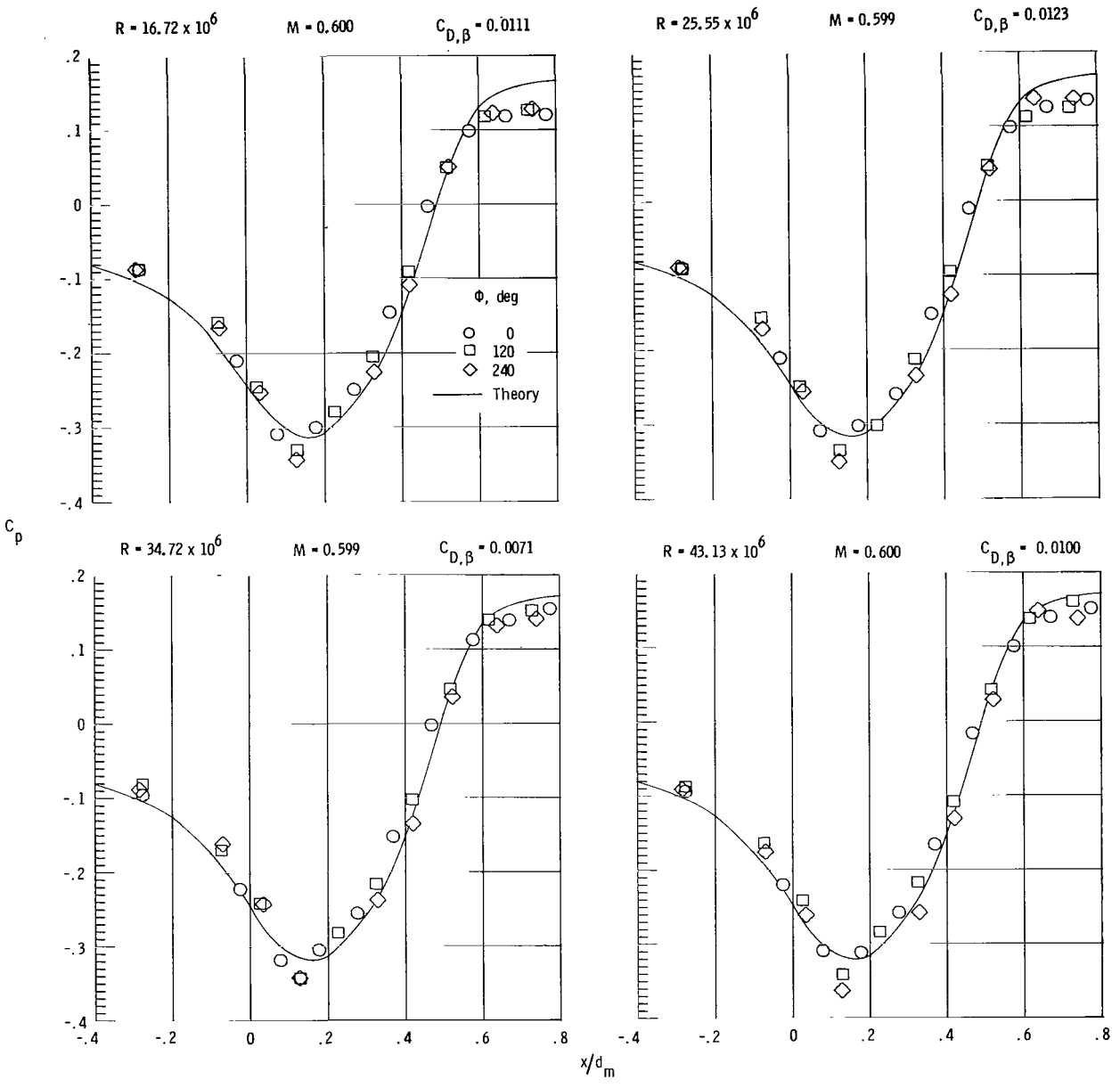

(a) Concluded.

Figure 8.- Continued.

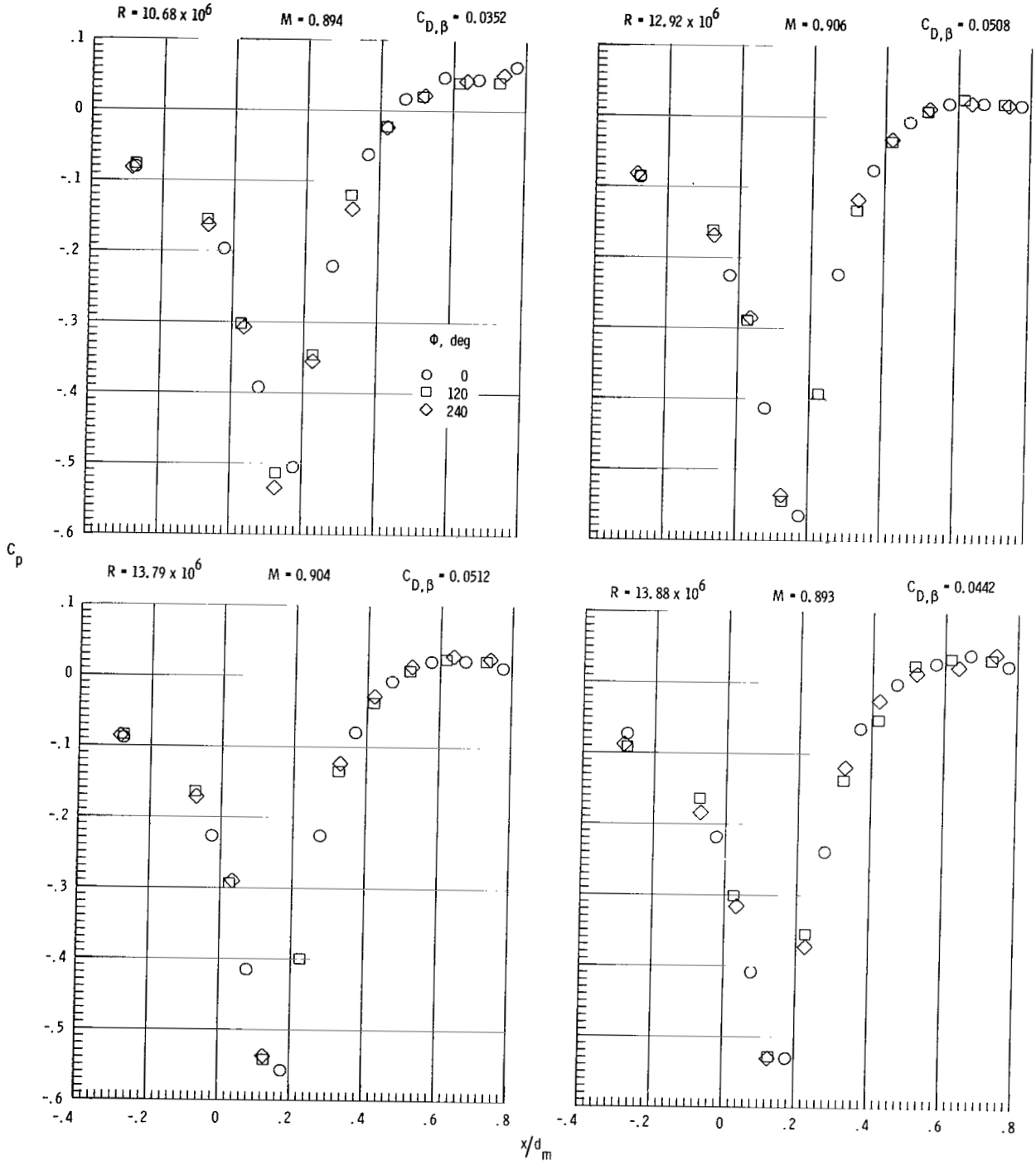

(b) M = 0.9.

Figure 8.- Continued.

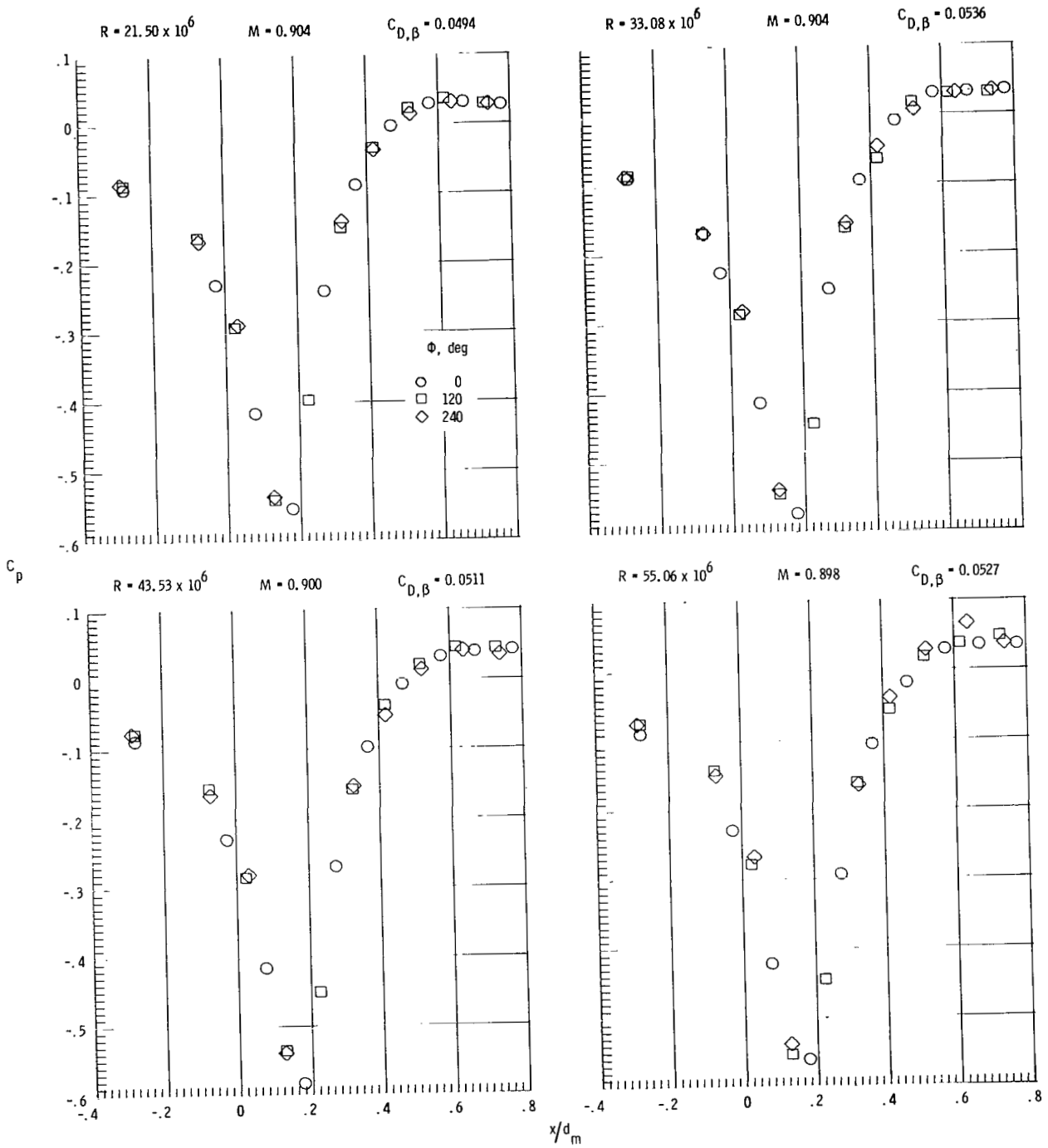

(b) Concluded.

Figure 8.- Concluded.

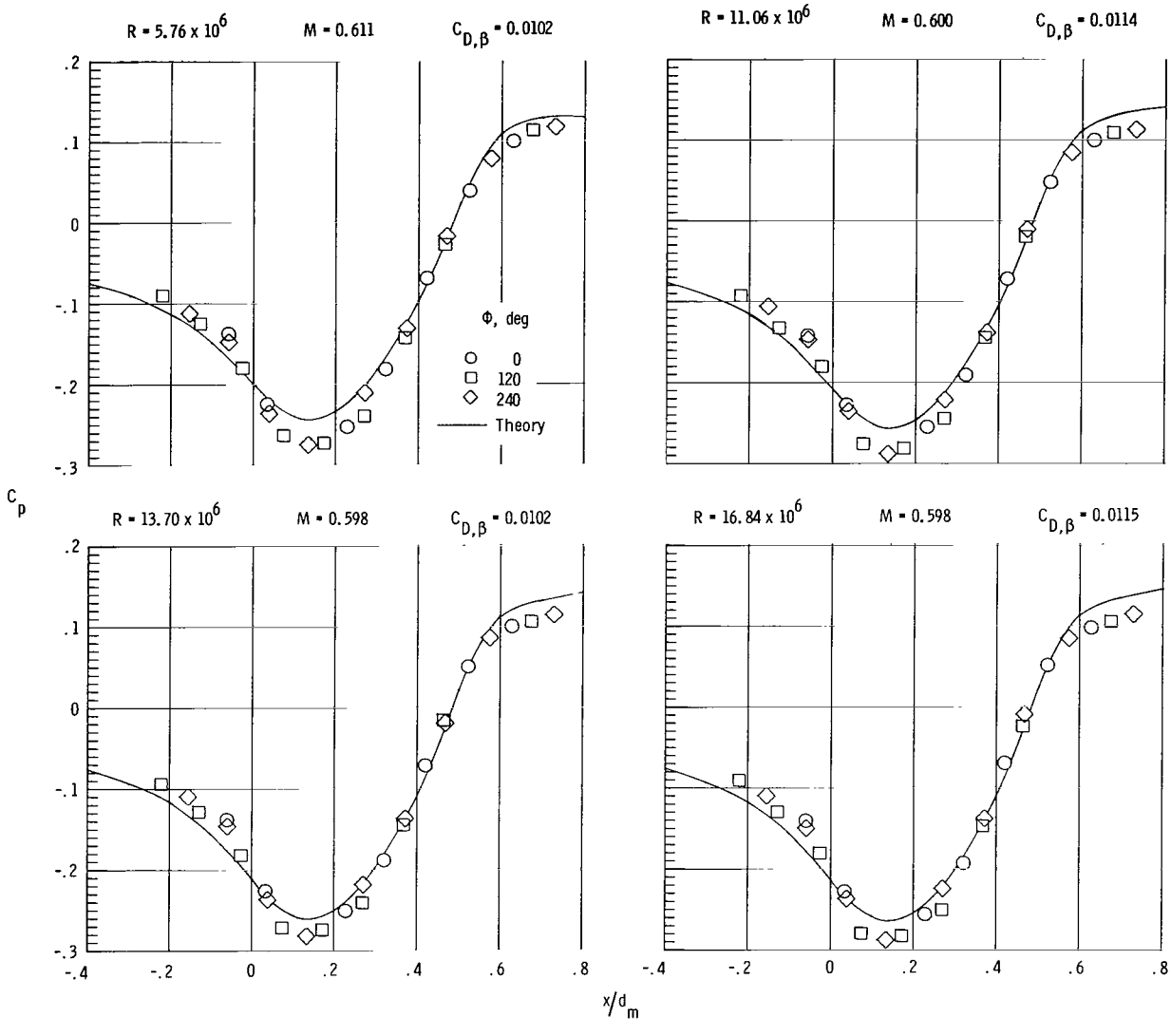

(a) M = 0.6.

Figure 9.- Boattail static pressure coefficients for $\frac{l}{d_m} = 0.80$ circular-arc boattail $\left(\frac{L}{d_m} = 16.0\right)$ at various Reynolds numbers for M = 0.6 and 0.9.

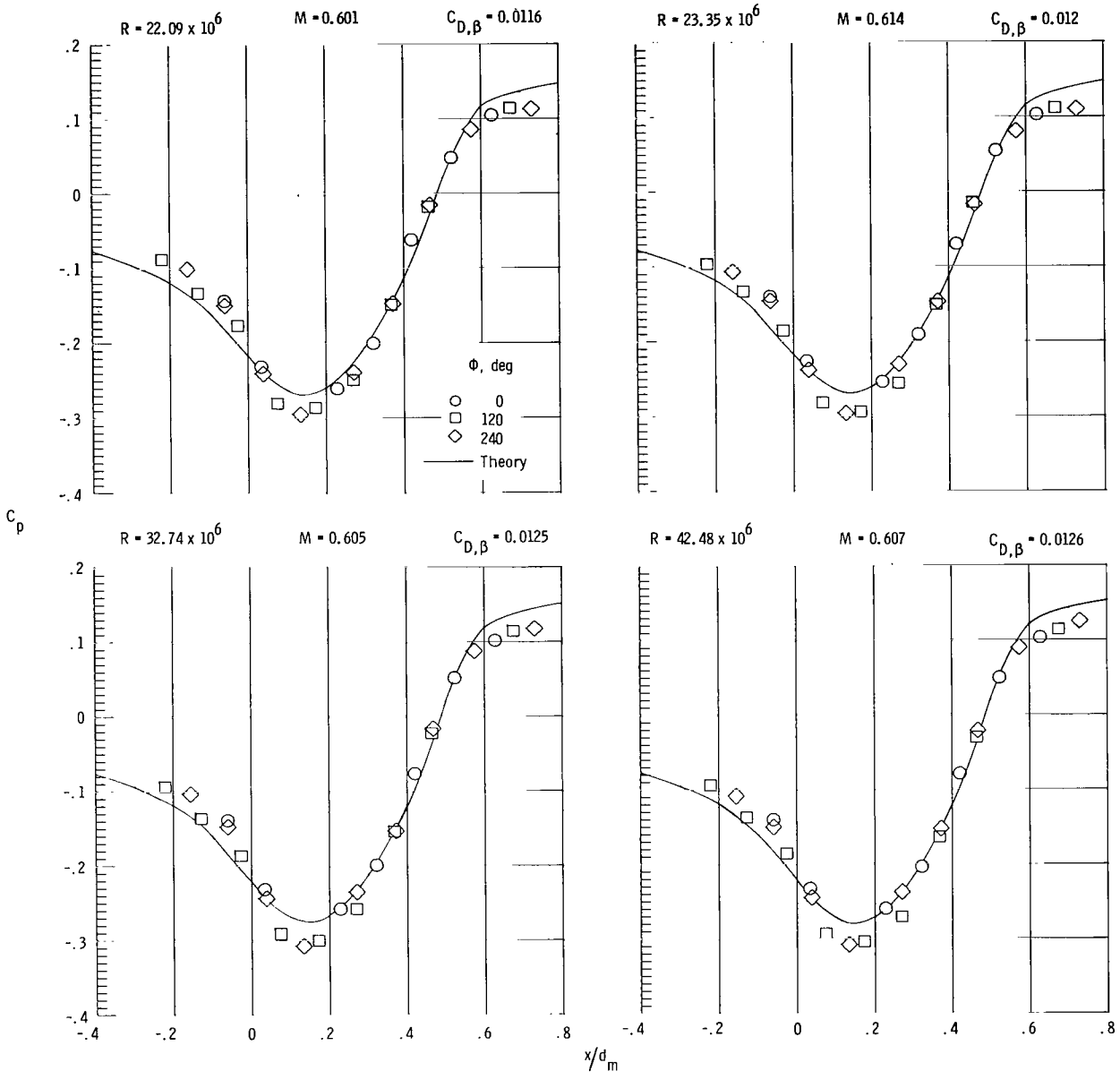

(a) Continued.

Figure 9.- Continued.

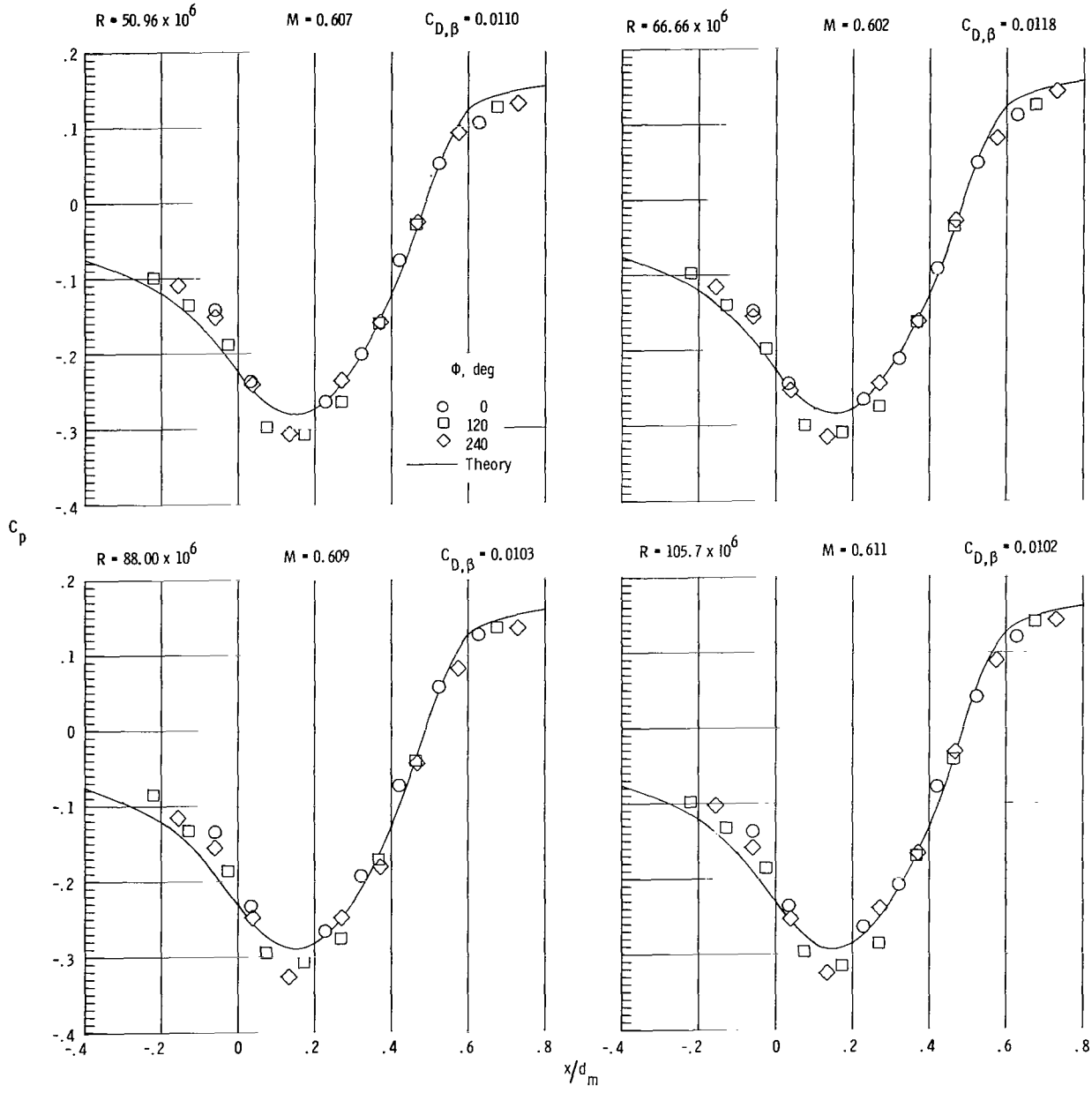

(a) Concluded.

Figure 9.- Continued.

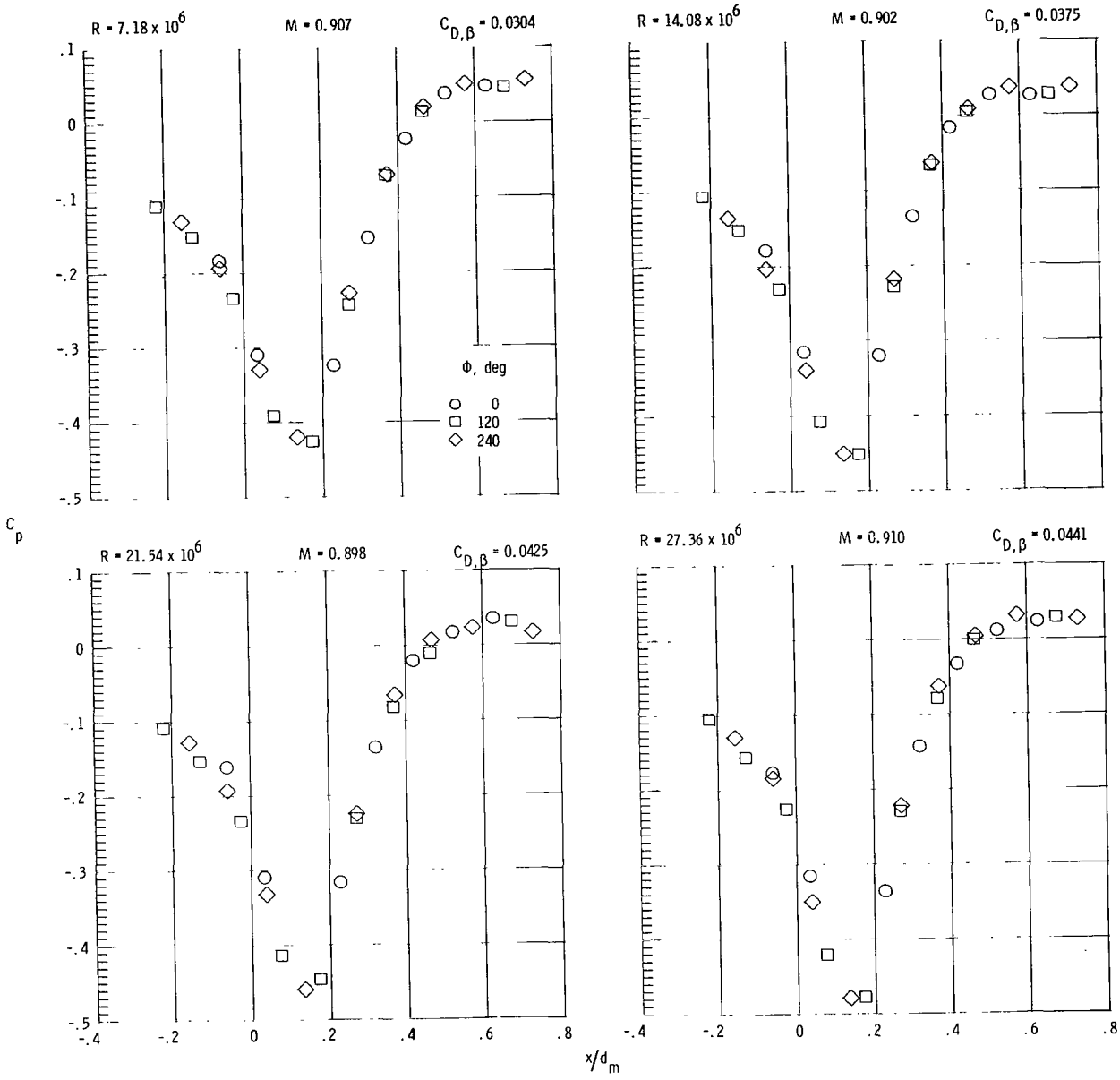

(b) M = 0.9.

Figure 9.- Continued.

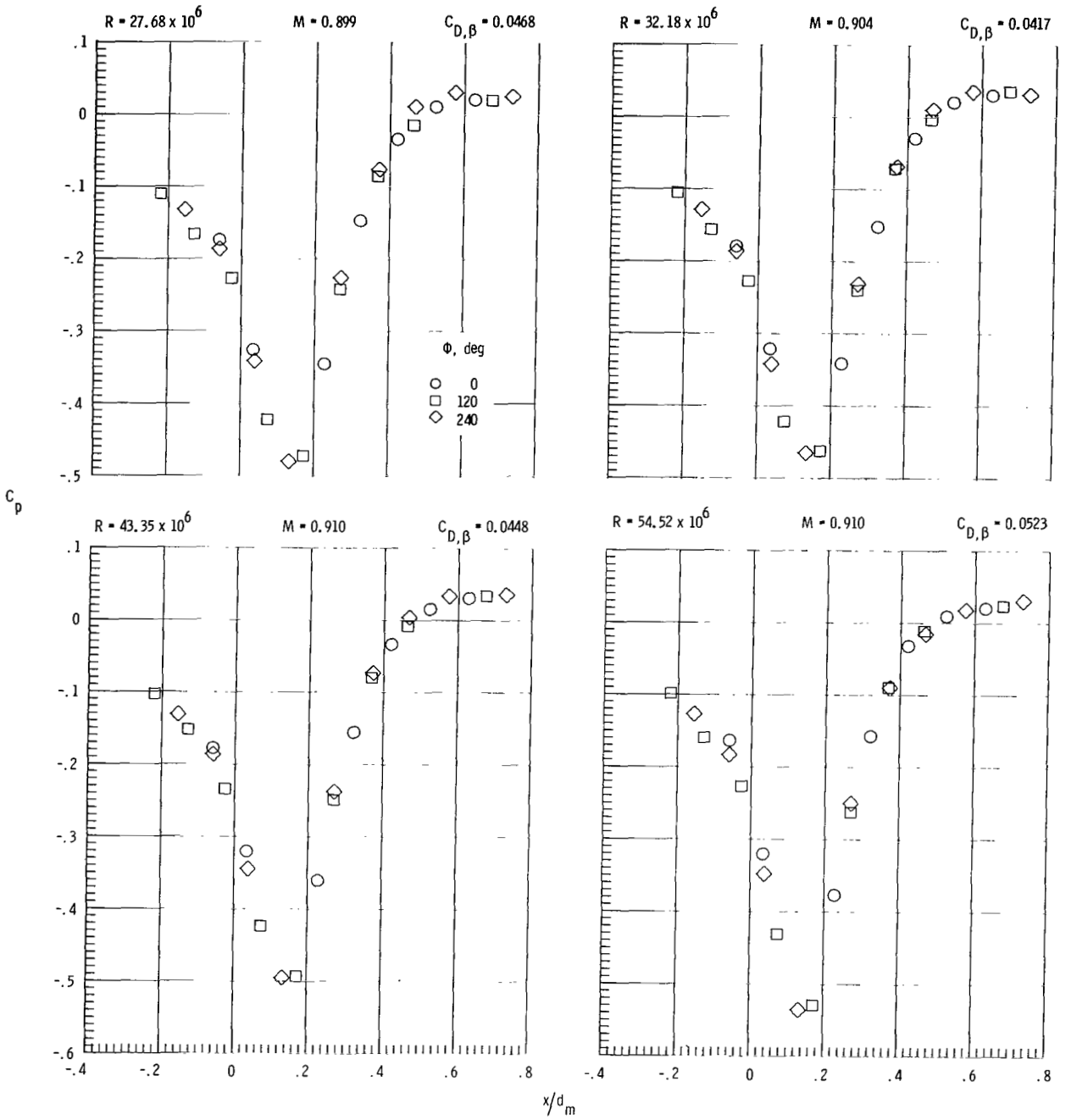

(b) Continued.

Figure 9.- Continued.

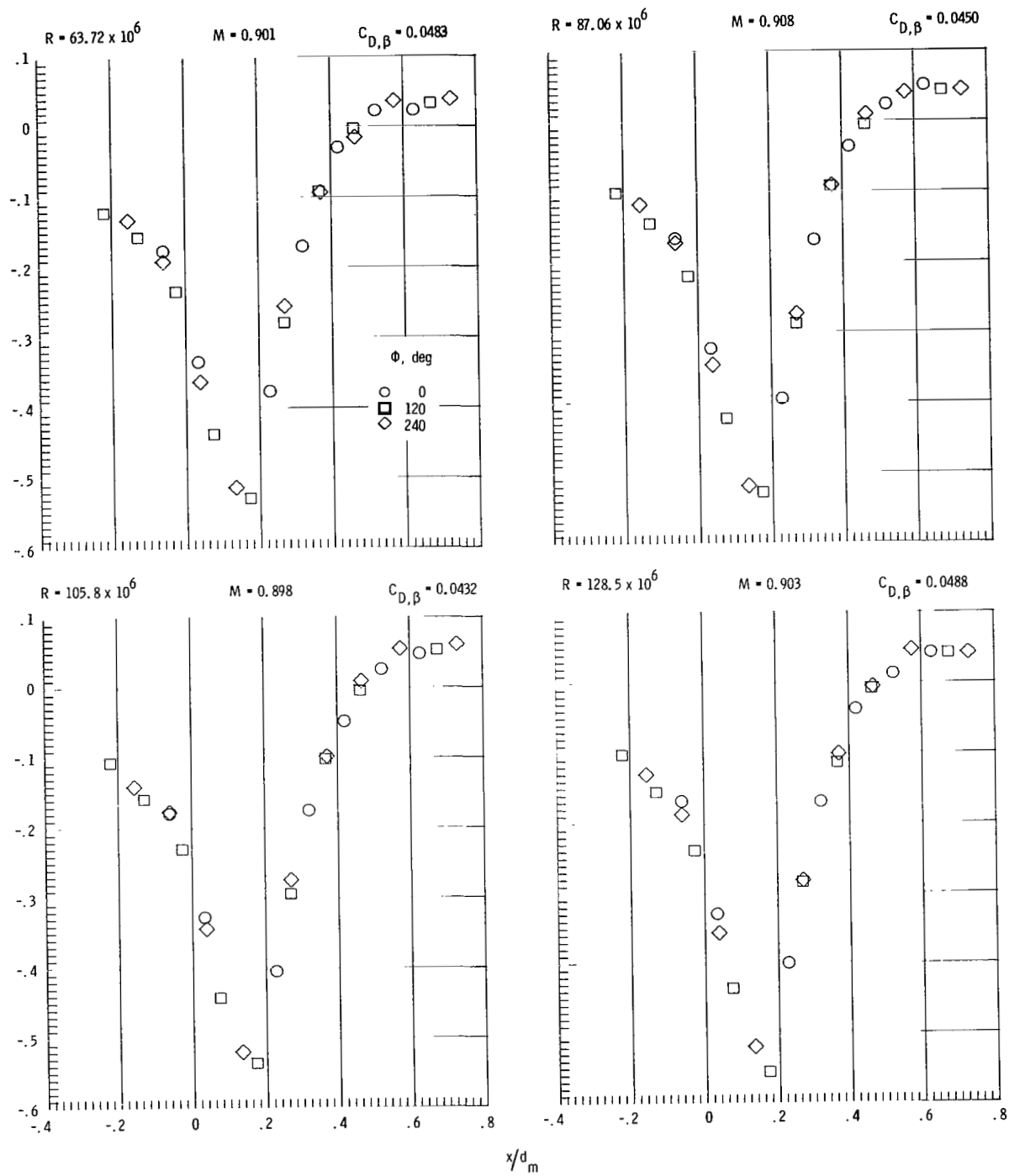

(b) Concluded.

Figure 9.- Concluded.

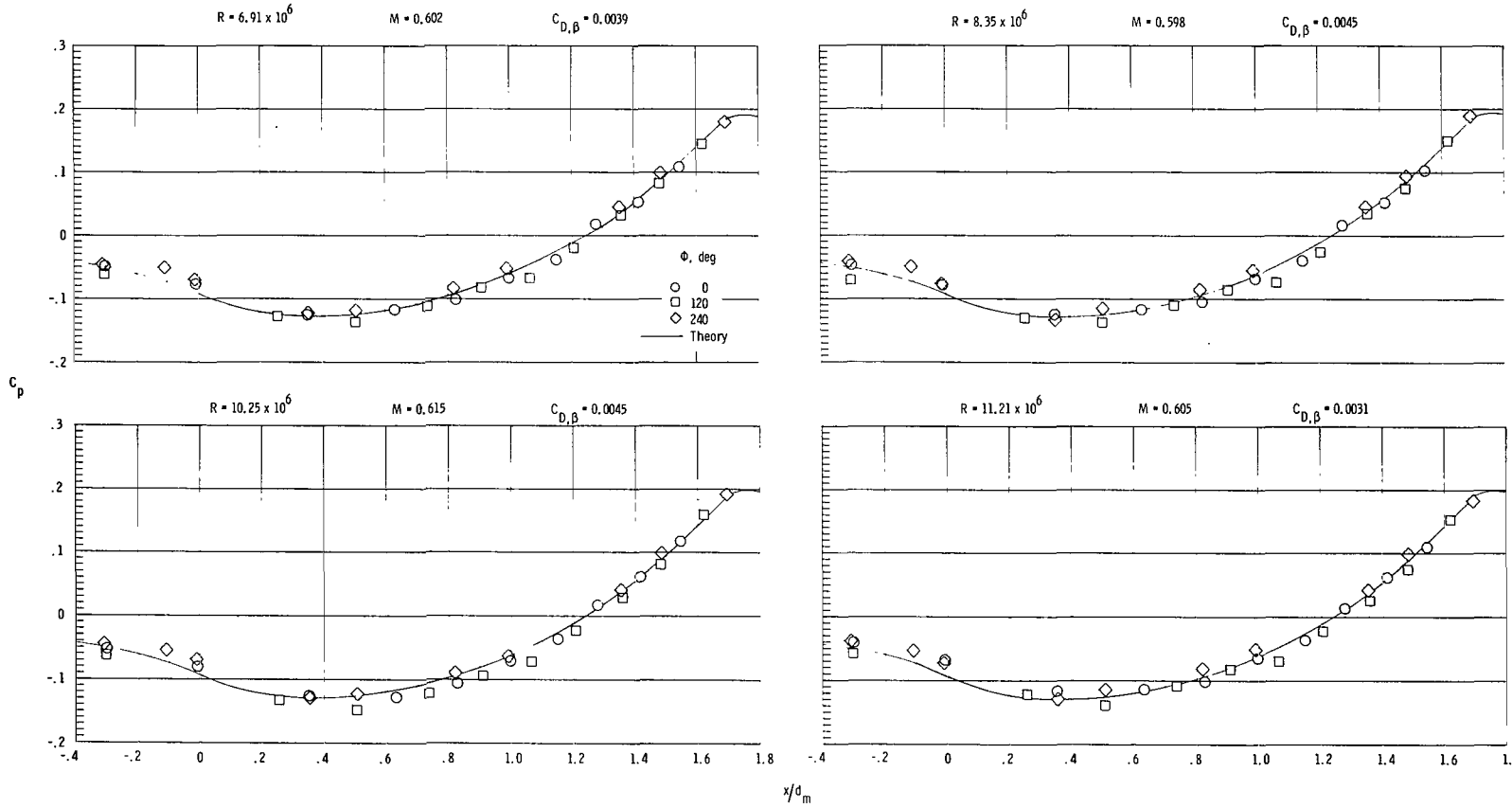

(a) M = 0.6.

Figure 10.- Boattail static pressure coefficients for $\frac{l}{d_m} = 1.77$ circular-arc boattail $\left(\frac{L}{d_m} = 8.0\right)$ at various Reynolds numbers for M = 0.6 and 0.9.

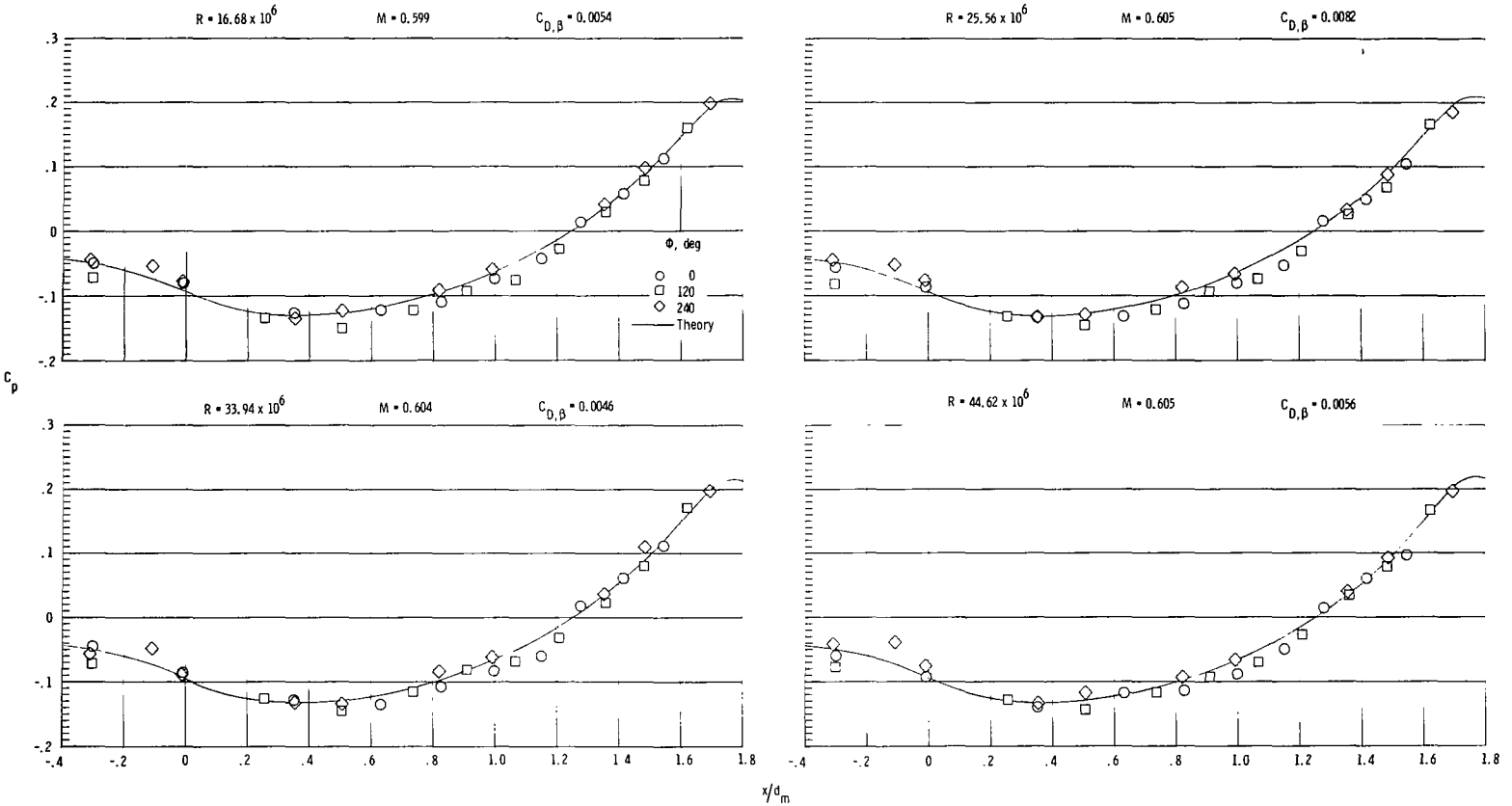

(a) Concluded.

Figure 10.- Continued.

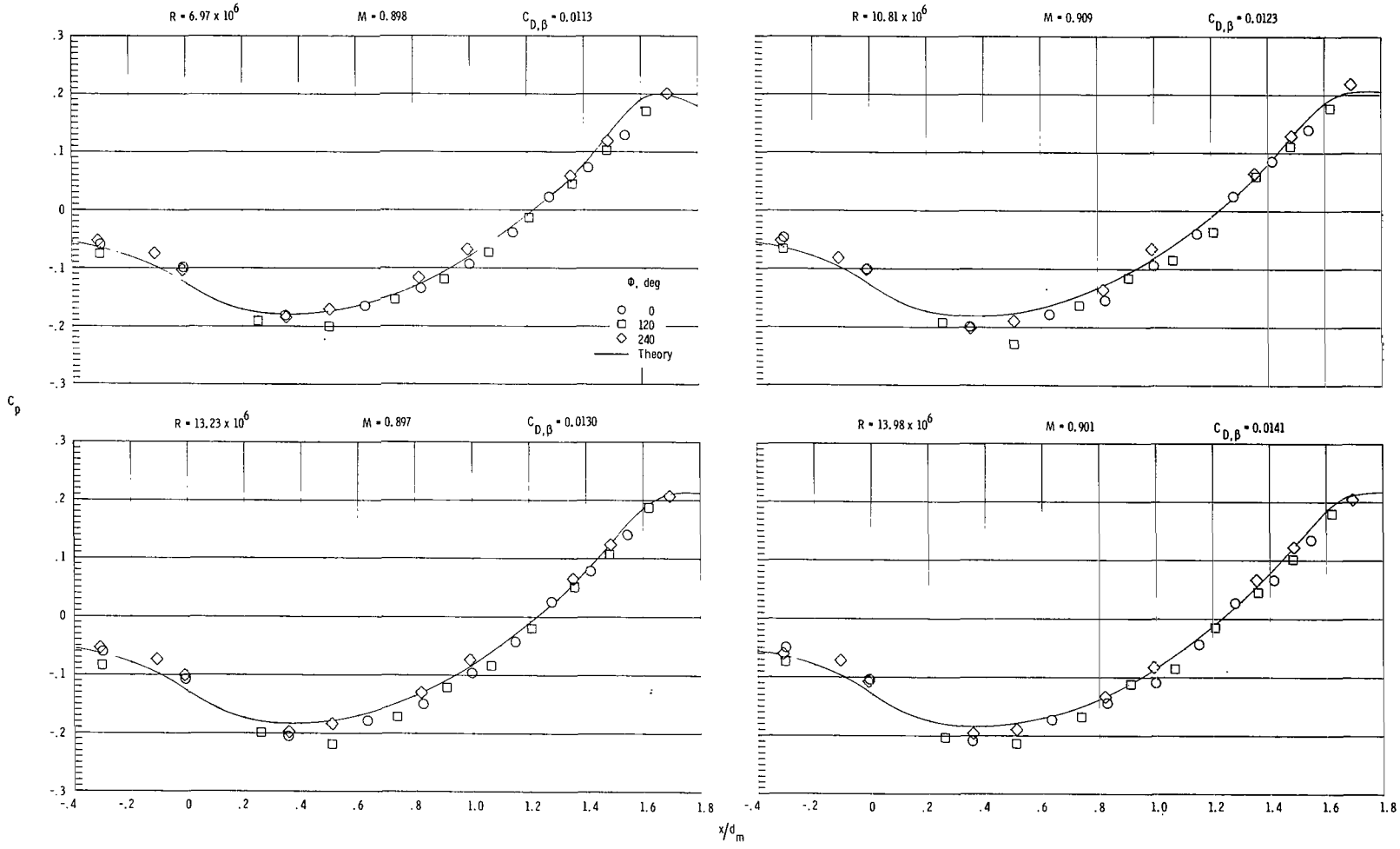

(b) M = 0.9.

Figure 10.- Continued.

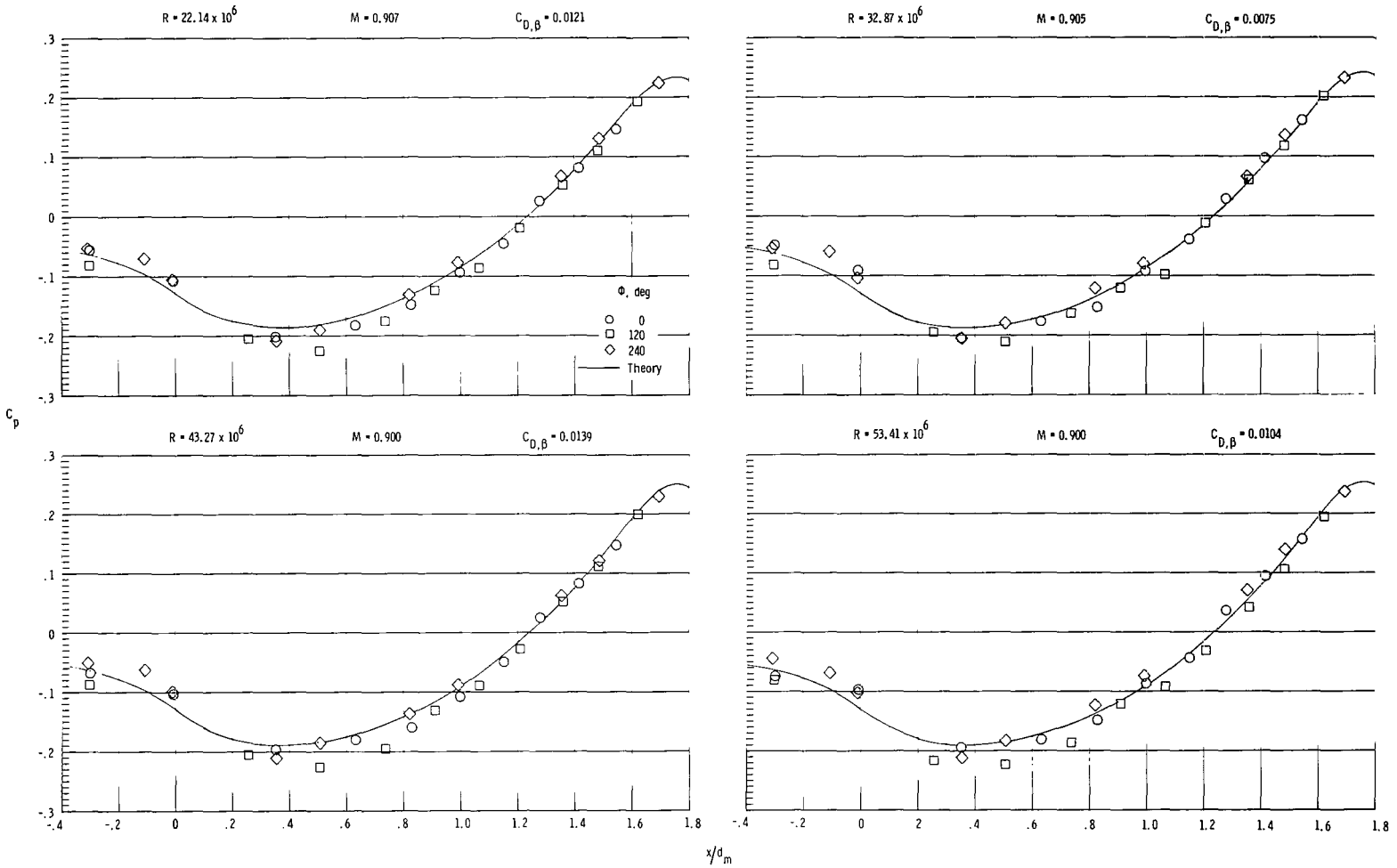

(b) Concluded.

Figure 10.- Concluded.

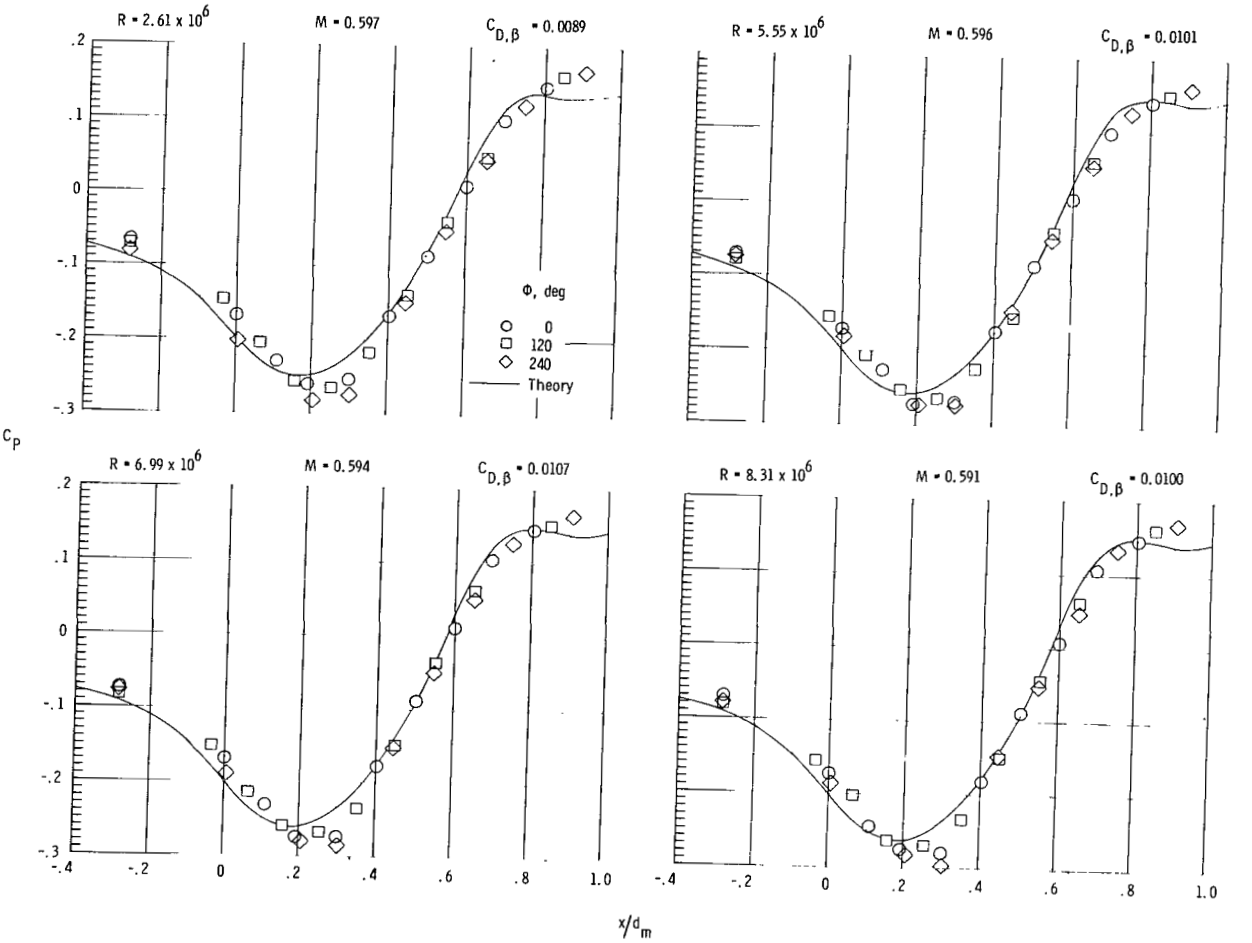

(a) M = 0.6.

Figure 11.- Boattail static pressure coefficients for circular-arc–conic boattail $\left(\frac{L}{d_m} = 8.0\right)$ at various Reynolds numbers for M = 0.6 and 0.9.

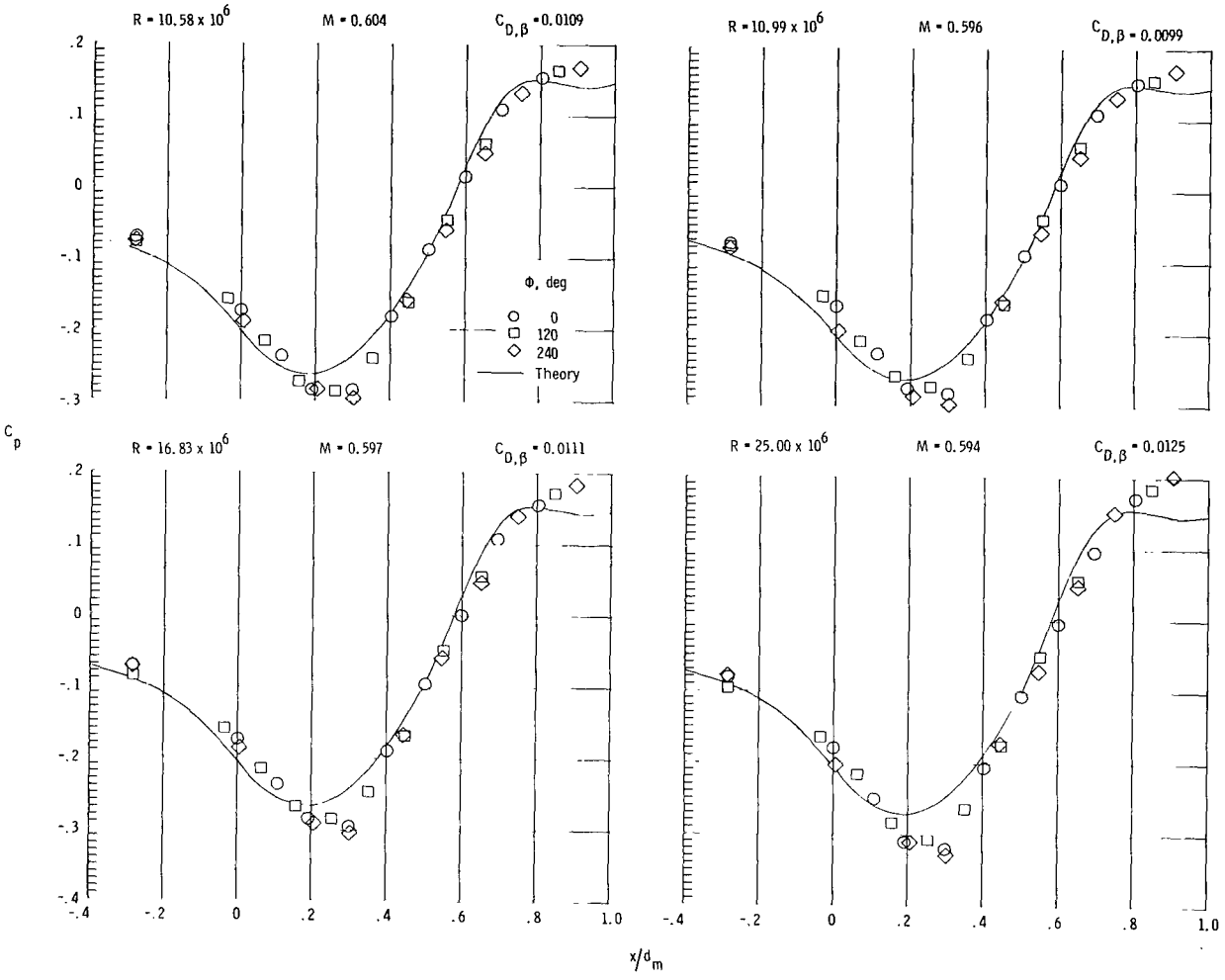

(a) Continued.

Figure 11.- Continued.

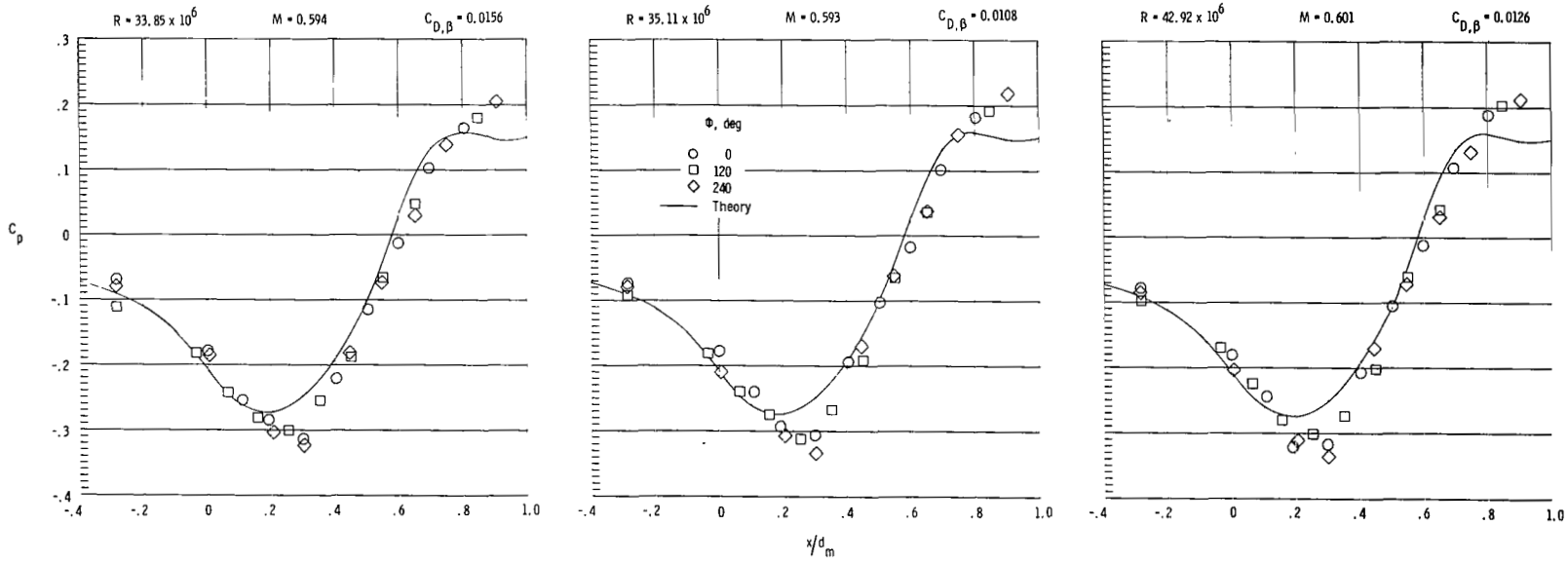

(a) Concluded.

Figure 11.- Continued.

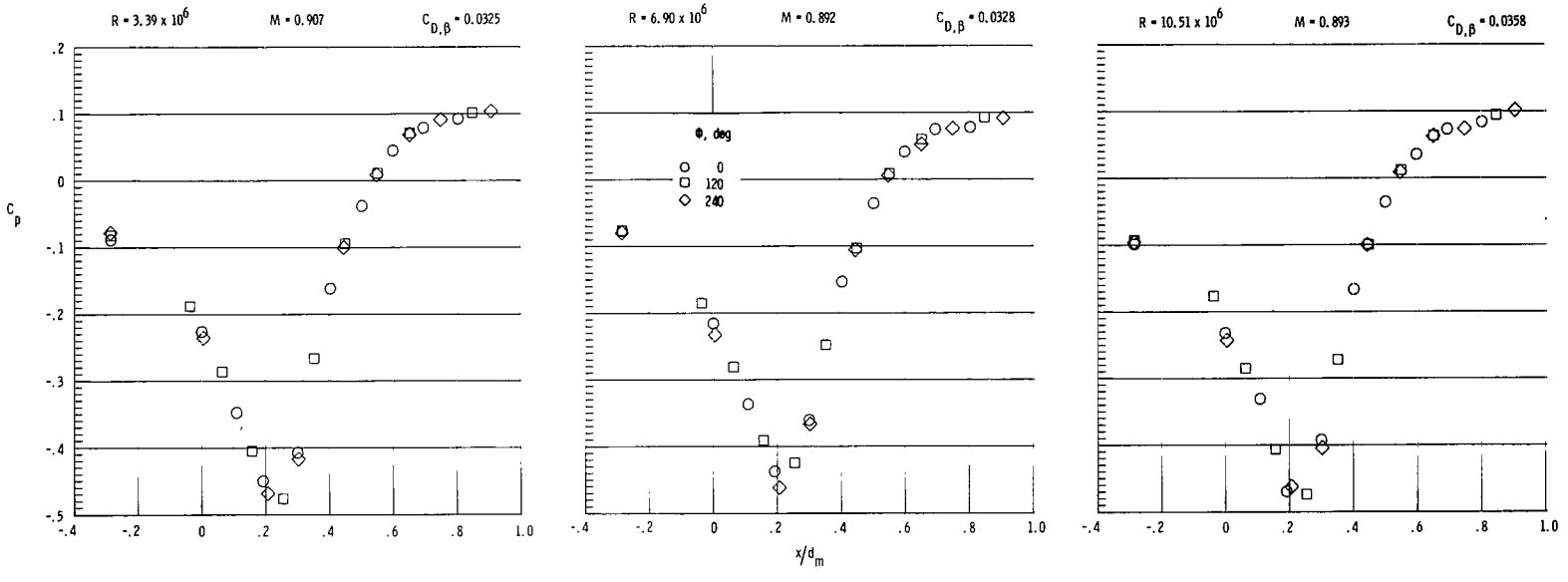

(b) M = 0.9.

Figure 11.- Continued.

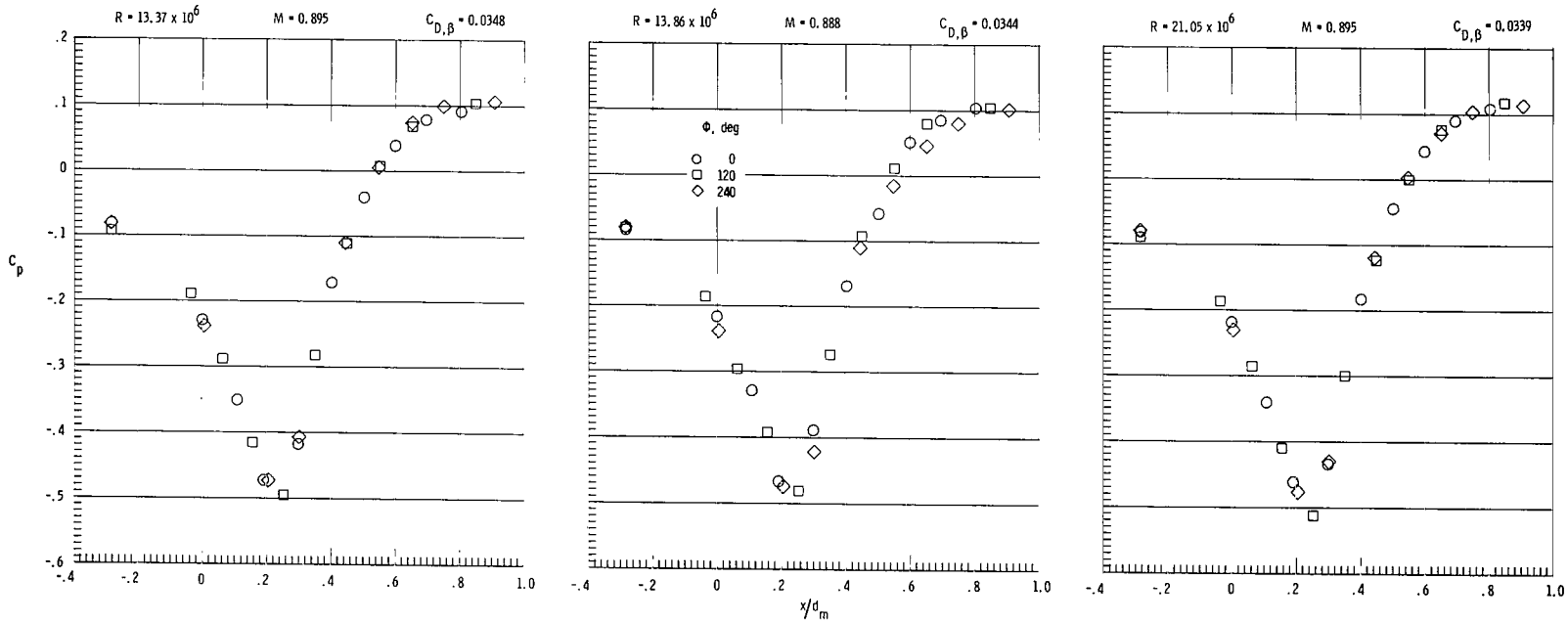

(b) Continued.

Figure 11.- Continued.

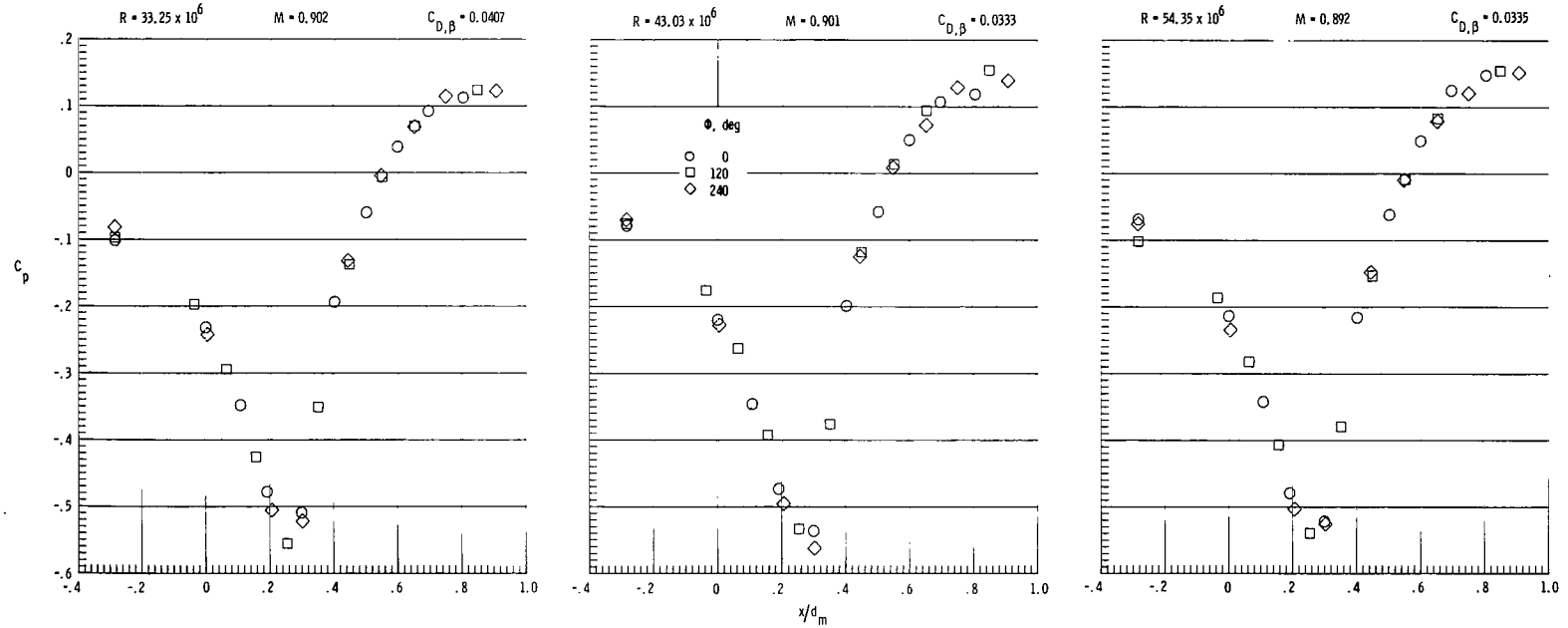

(b) Concluded.

Figure 11.- Concluded.

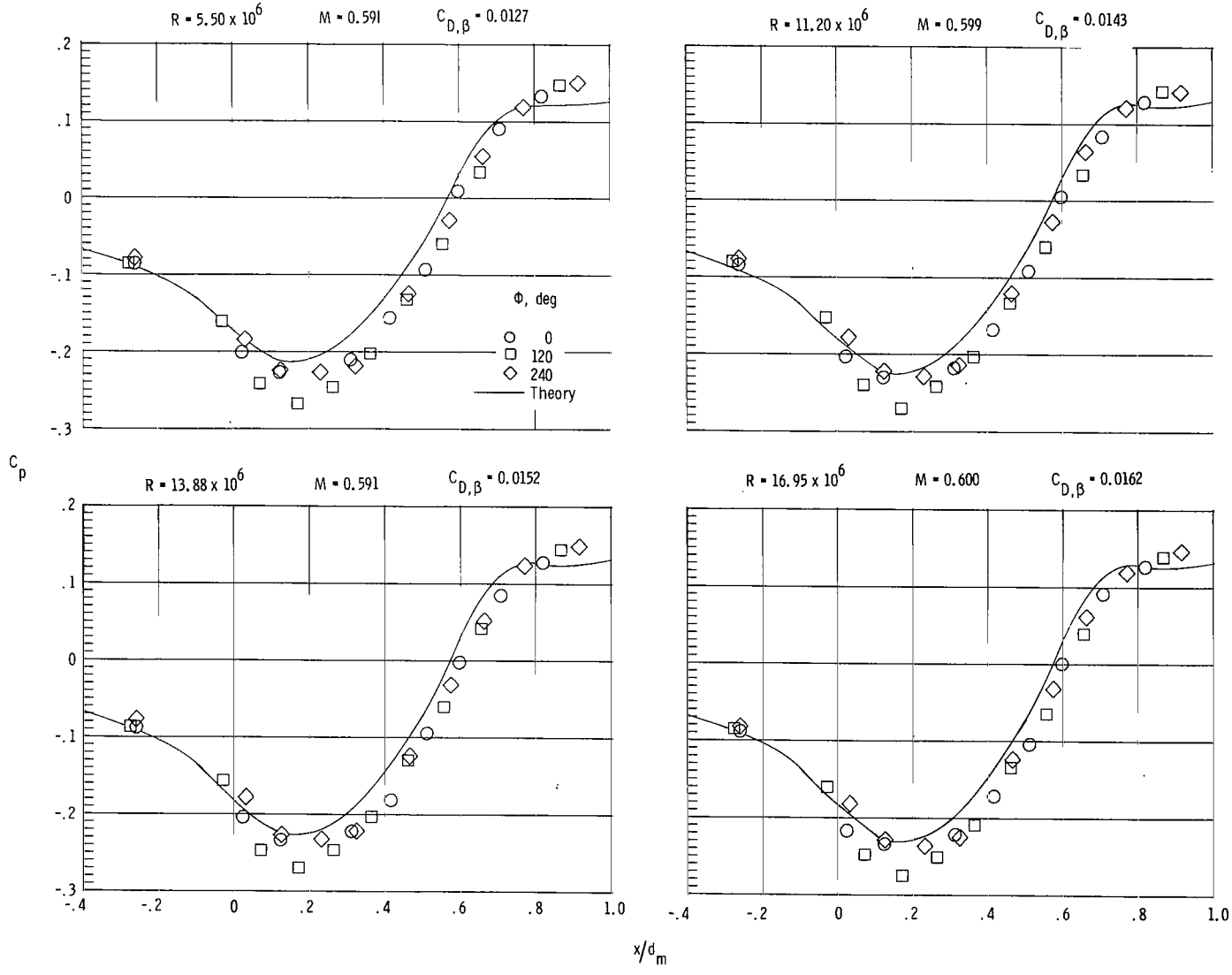

(a) M = 0.6.

Figure 12.- Boattail static pressure coefficients for circular-arc–conic boattail $\left(\frac{L}{d_m} = 16.0\right)$ at various Reynolds numbers for M = 0.6 and 0.9.

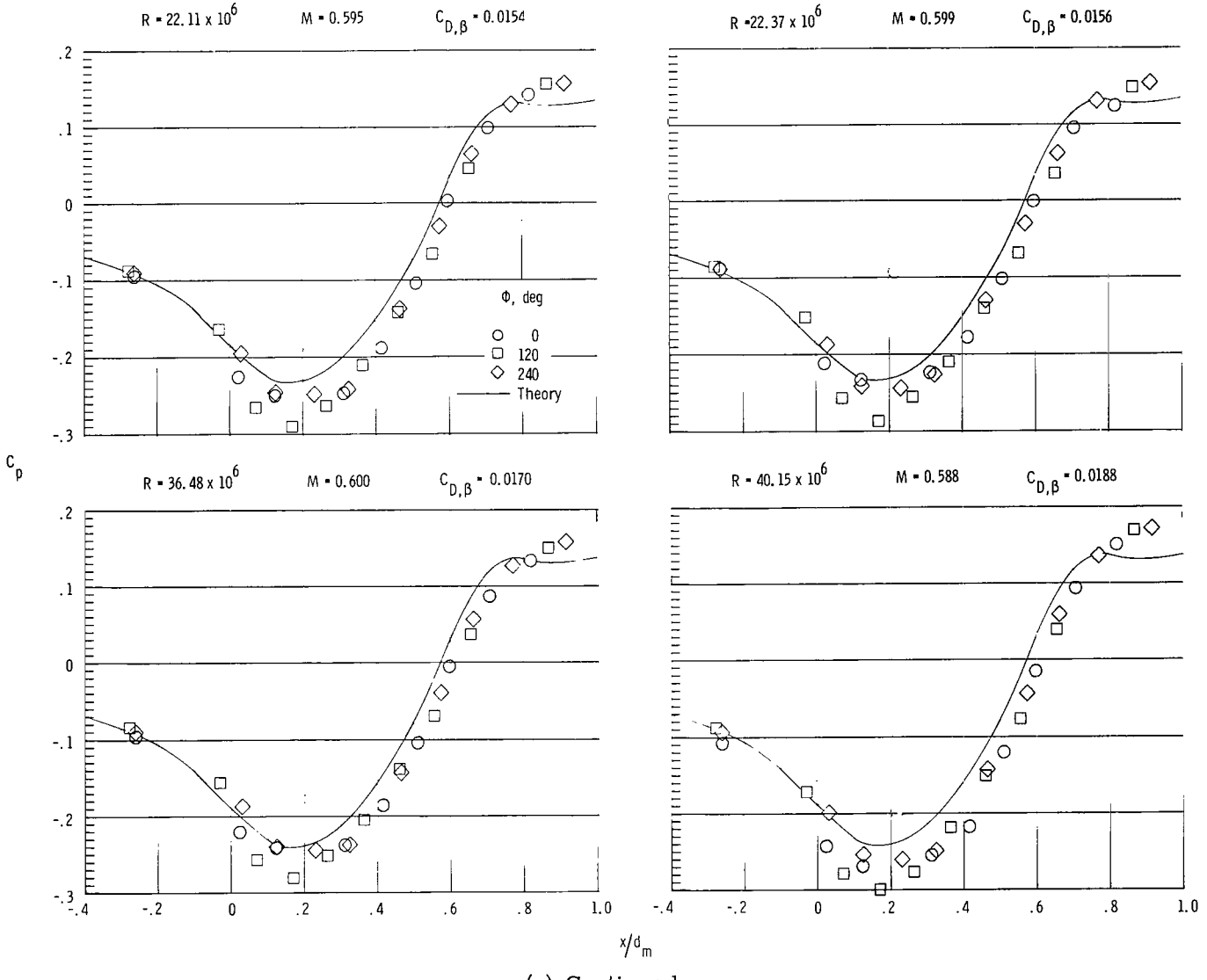

(a) Continued.

Figure 12.- Continued.

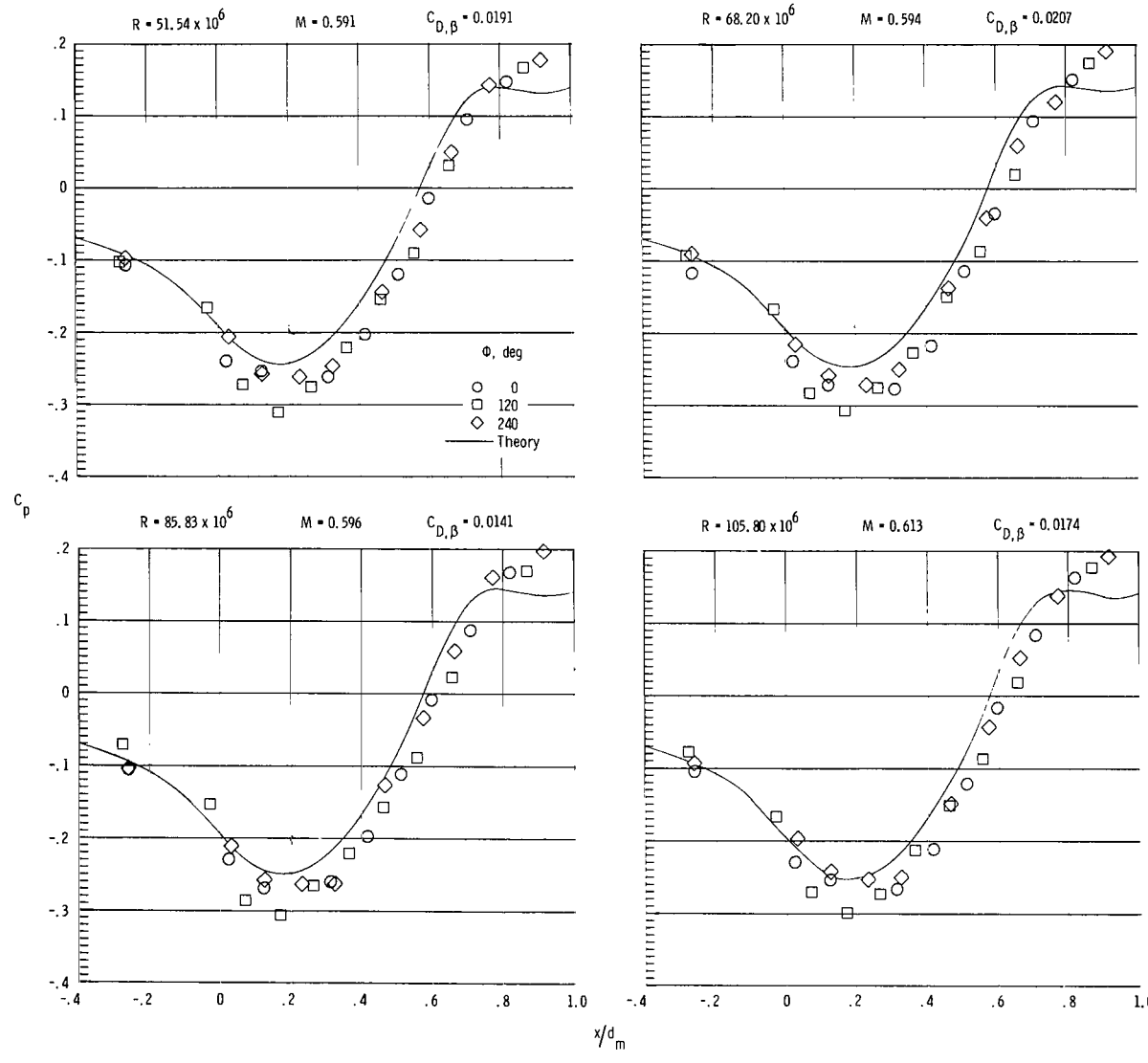

(a) Concluded.

Figure 12.- Continued.

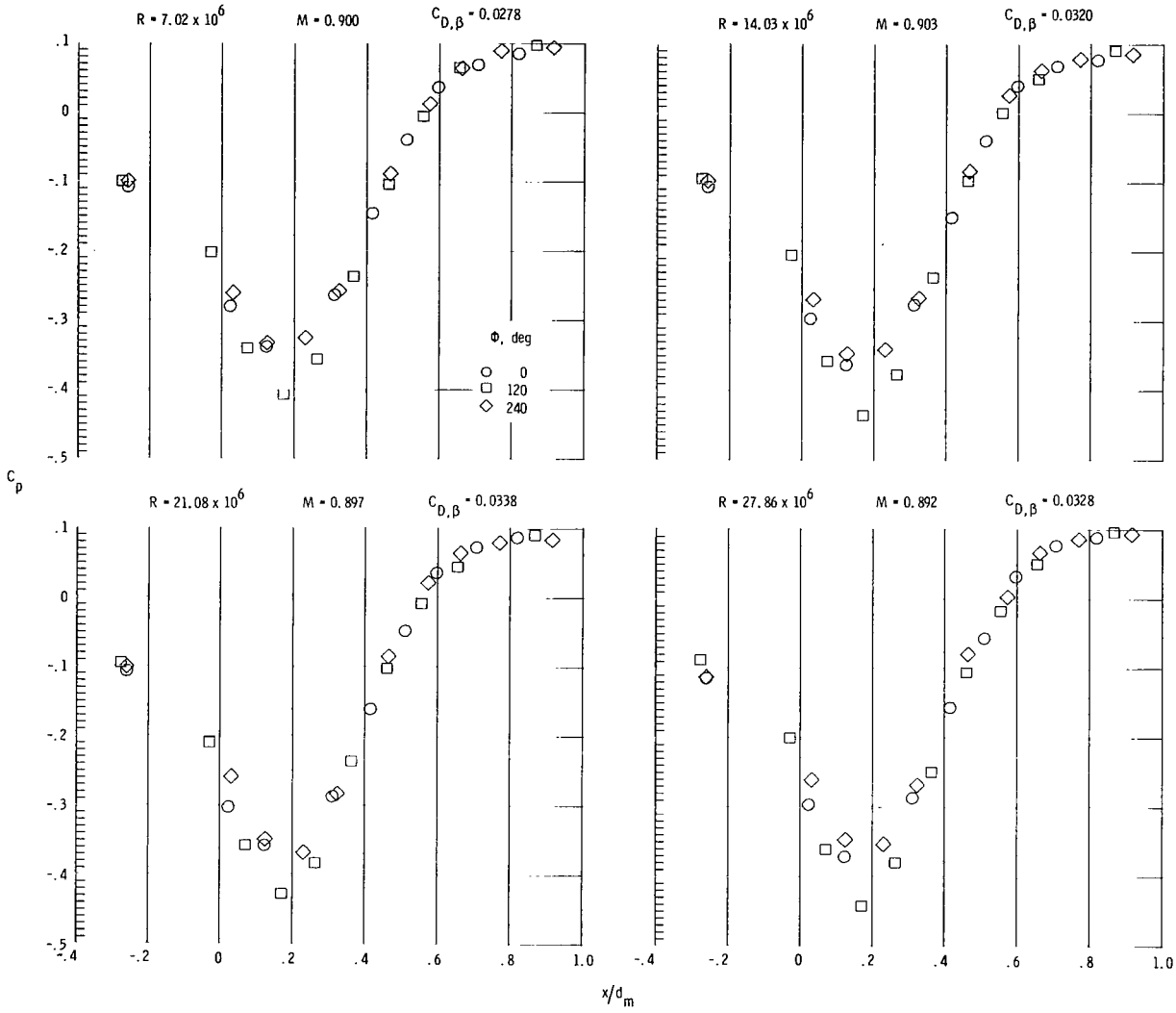

(b) M = 0.9.

Figure 12.- Continued.

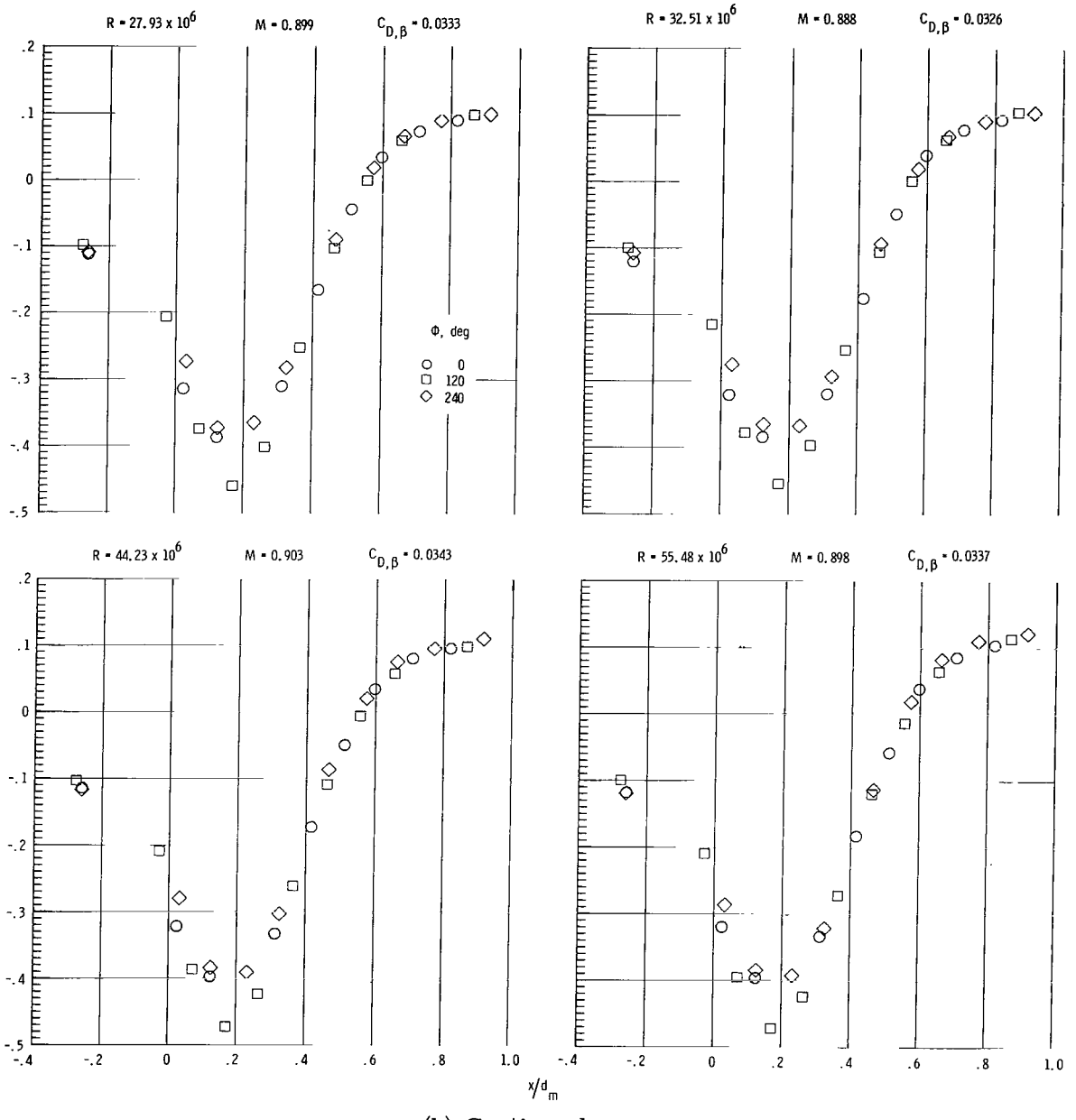

(b) Continued.

Figure 12.- Continued.

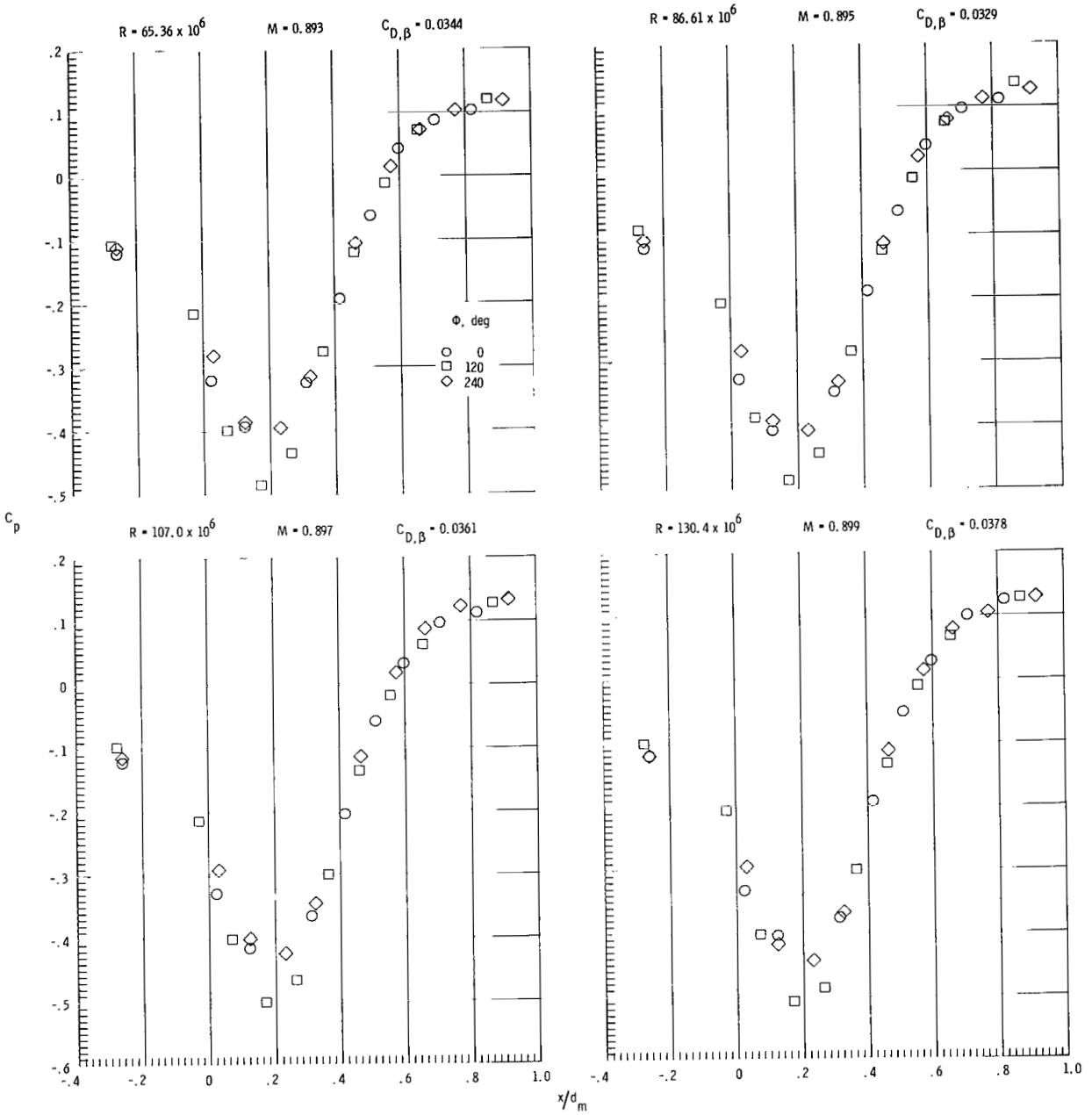

(b) Concluded.

Figure 12.- Concluded.

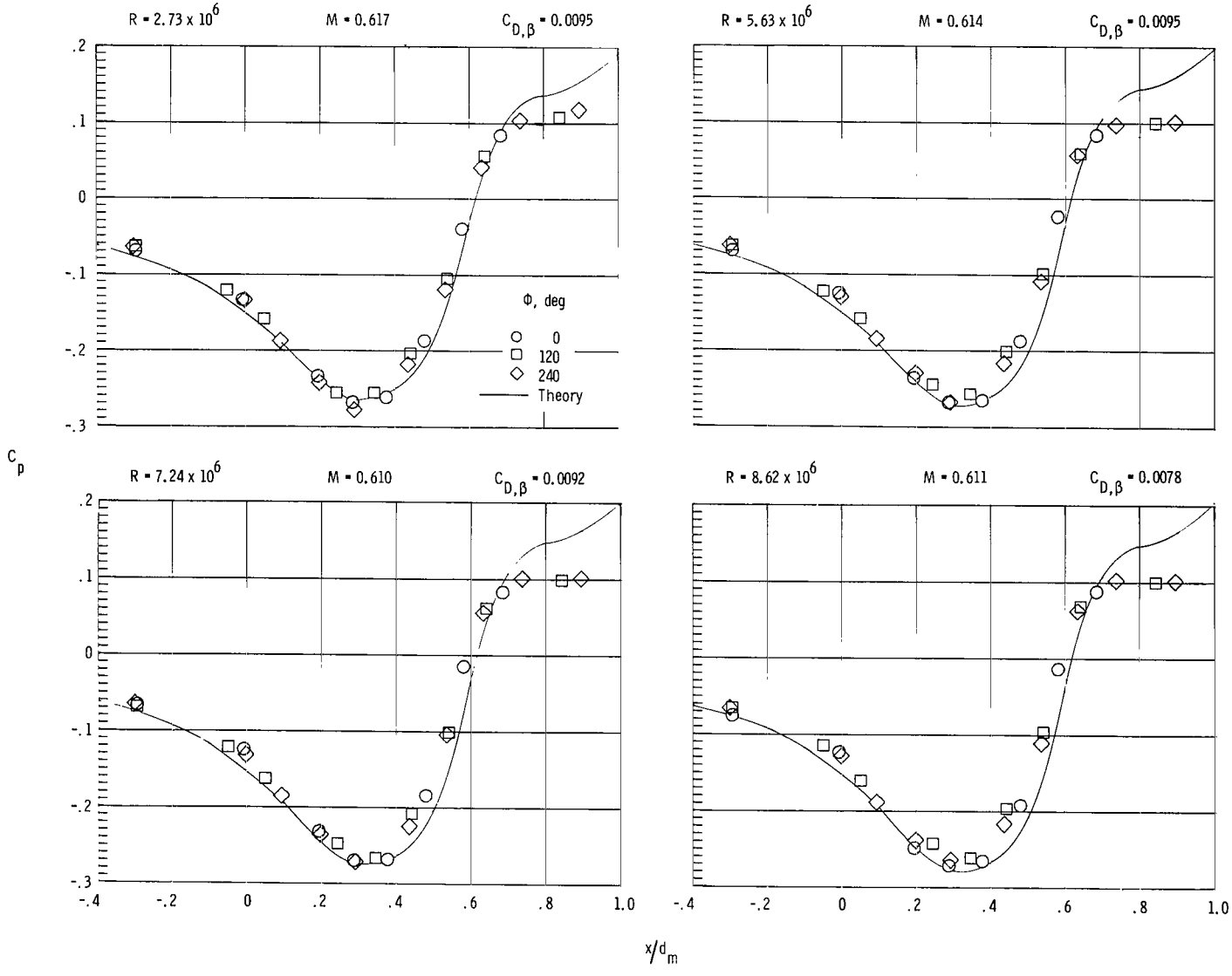

(a) M = 0.6.

Figure 13.- Boattail static pressure coefficients for contoured boattail $\left(\frac{L}{d_m} = 8.0\right)$ at various Reynolds numbers for M = 0.6 and 0.9.

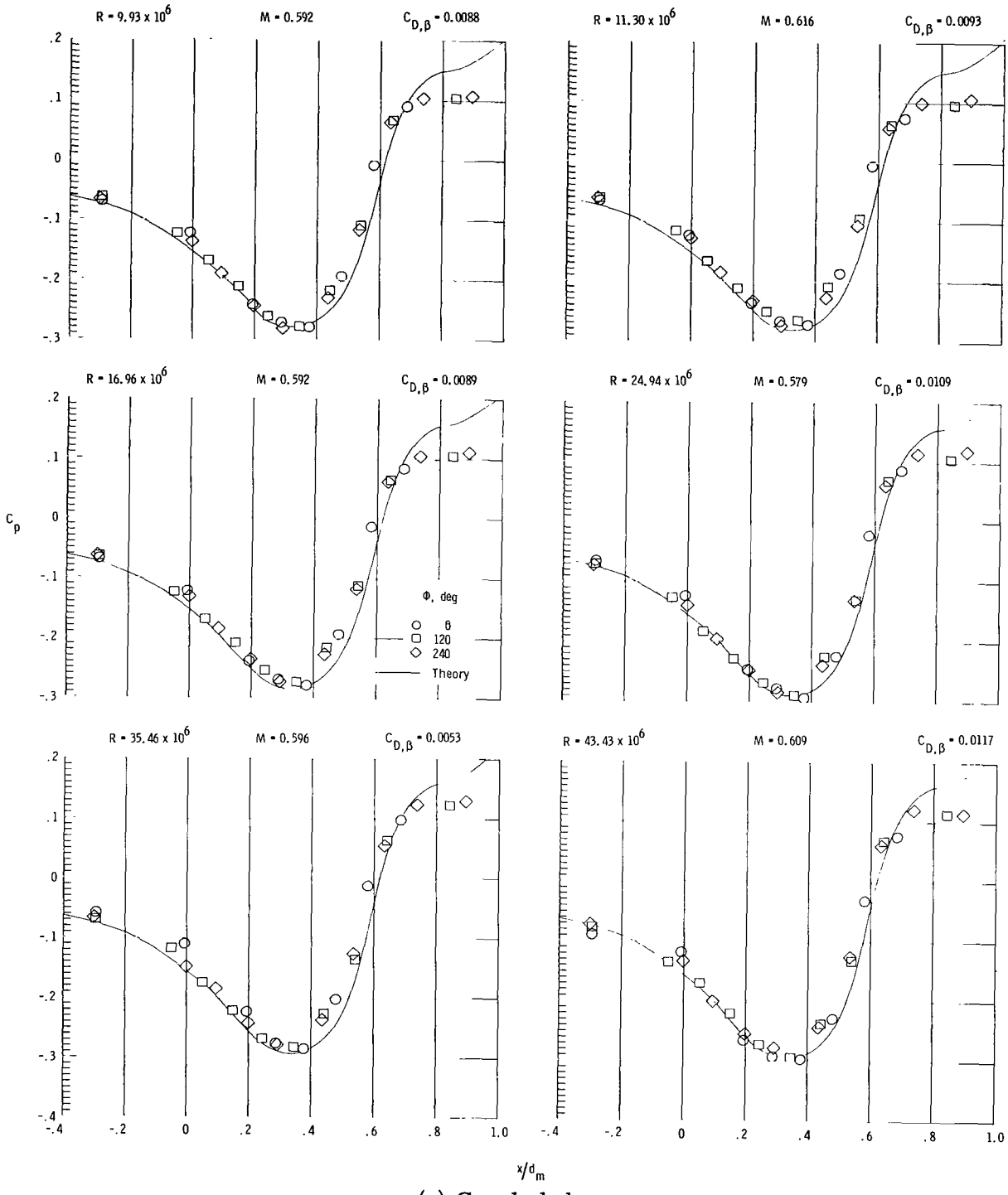

(a) Concluded.

Figure 13.- Continued.

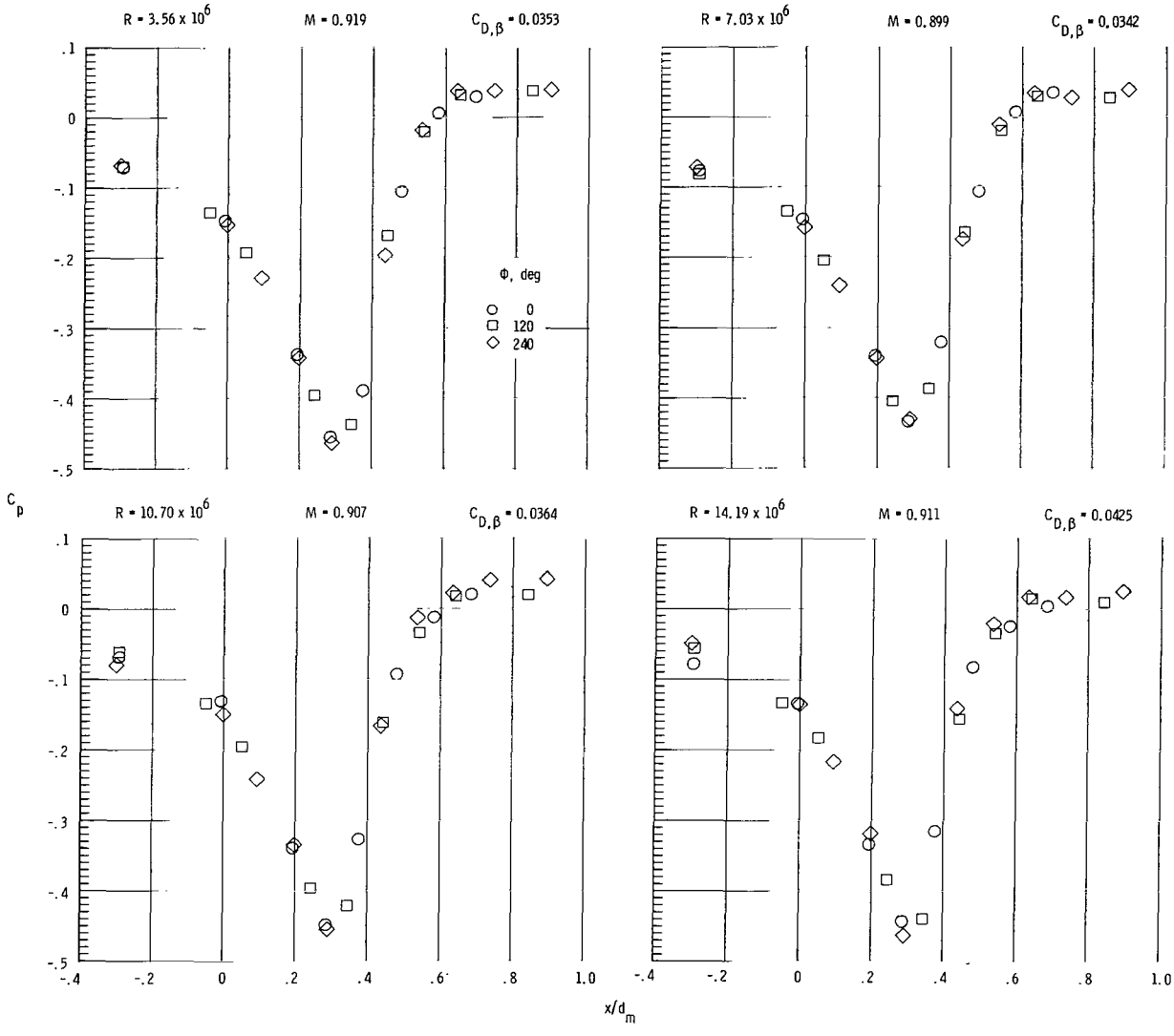

(b) M = 0.9.

Figure 13.- Continued.

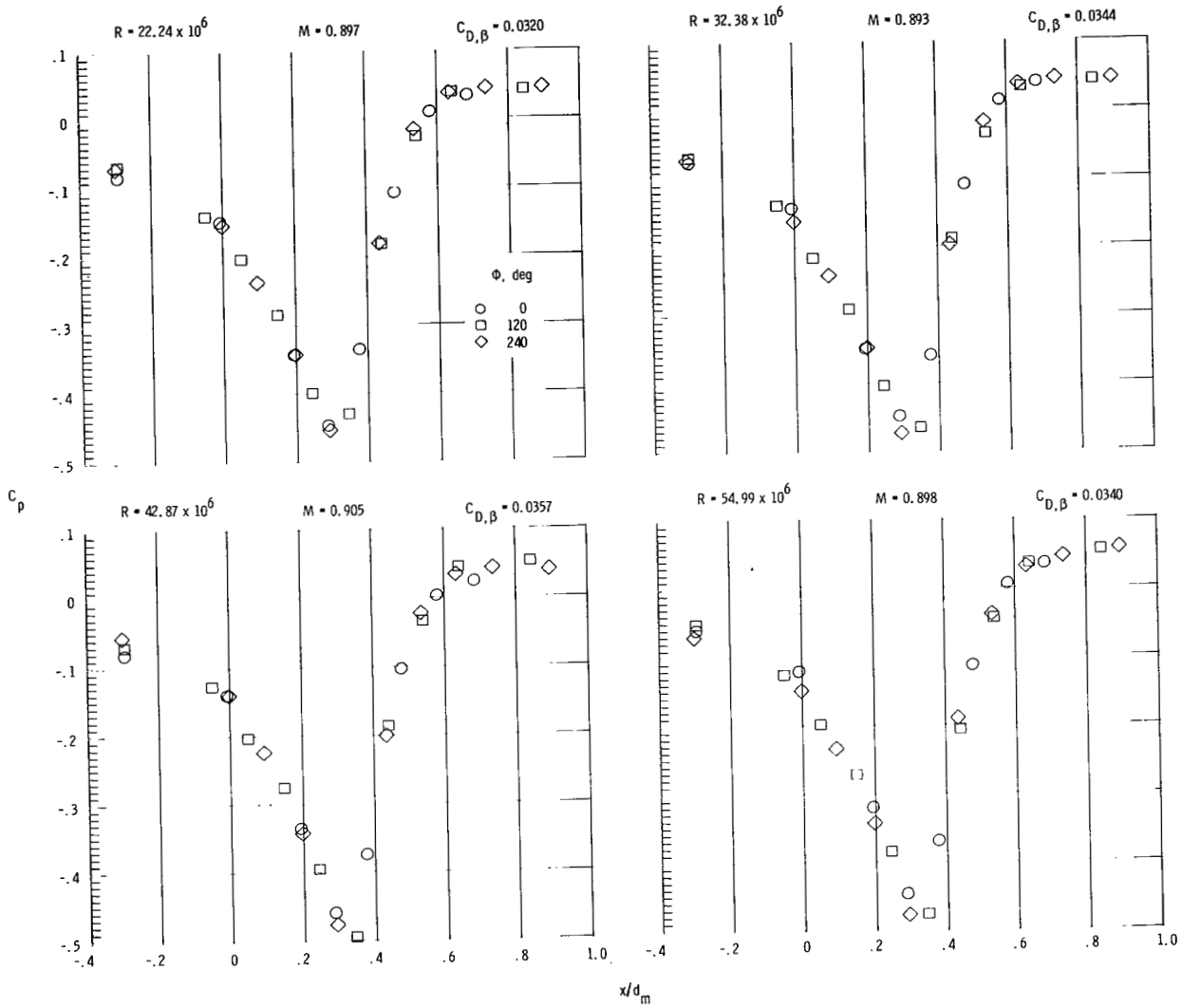

(b) Concluded.

Figure 13.- Concluded.

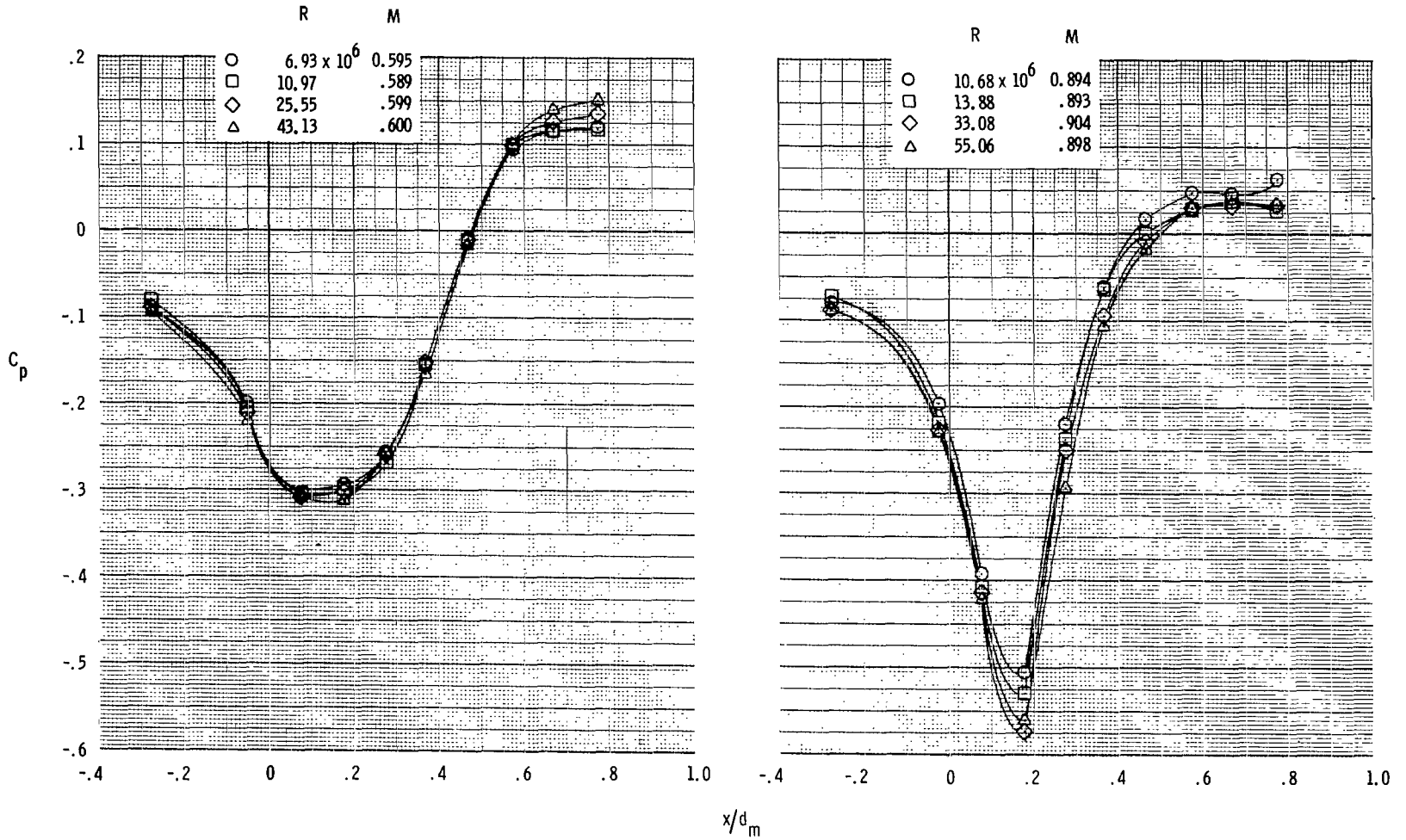

(a) $\phi = 0^{o}$.

Figure 14.- Comparison of boattail static pressure coefficients at four values of Reynolds number for $\frac{l}{d_m} = 0.80$ circular-arc boattail $\left(\frac{L}{d_m} = 8.0\right)$ for $M = 0.6$ and 0.9.

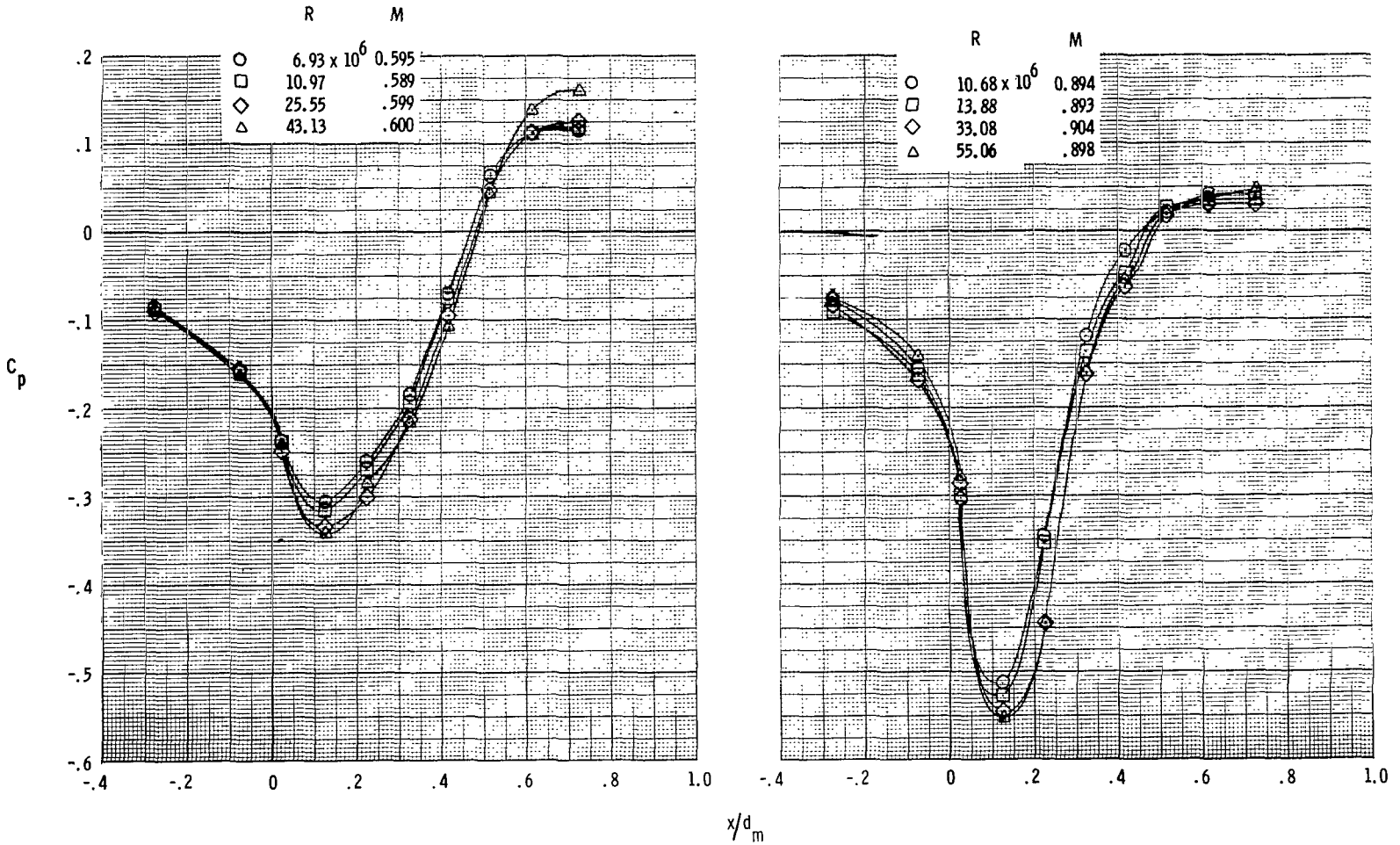

(b) $\phi = 120^{\circ}$.

Figure 14.- Continued.

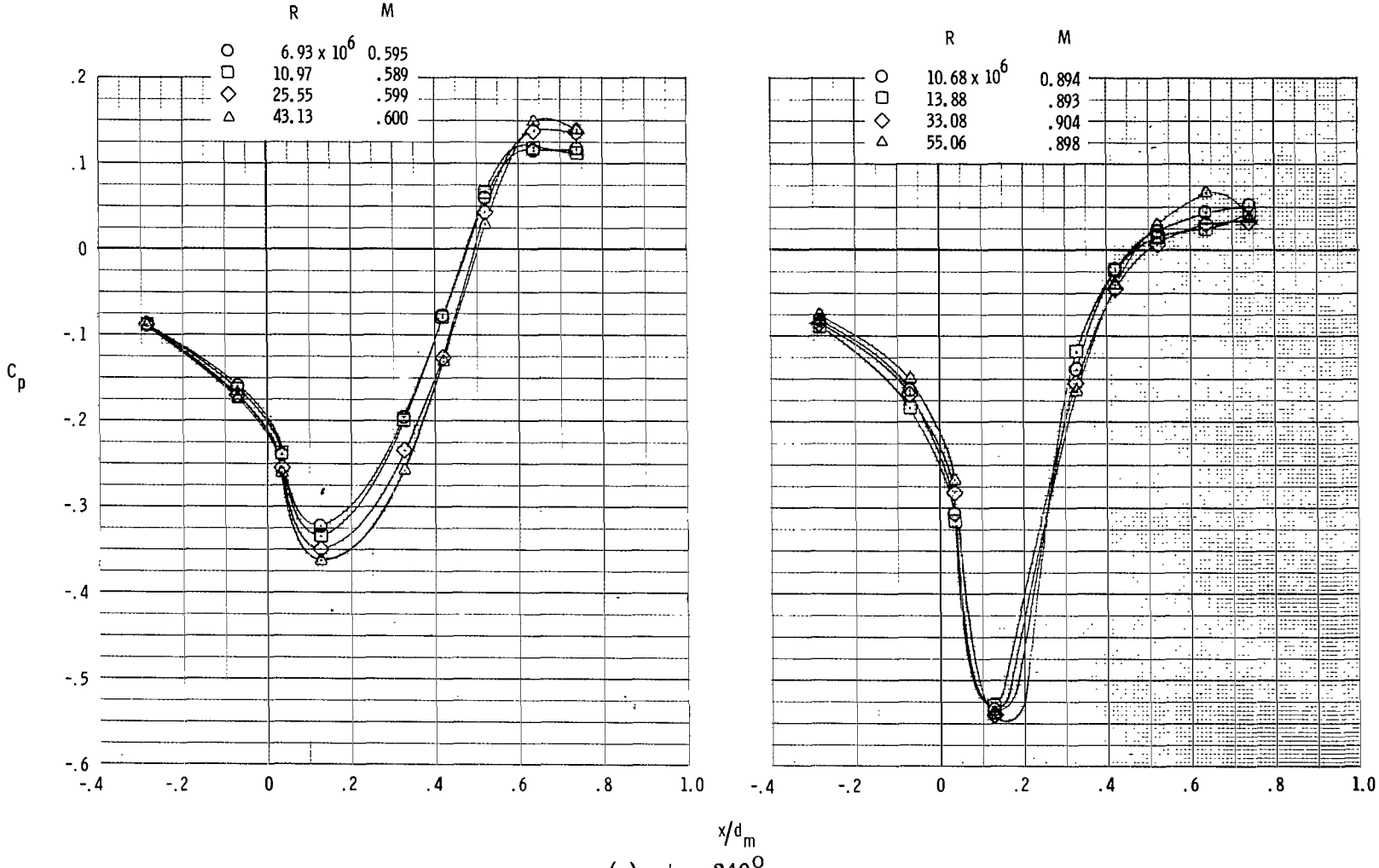

(c) $\phi = 240^{\circ}$.

Figure 14.- Concluded.

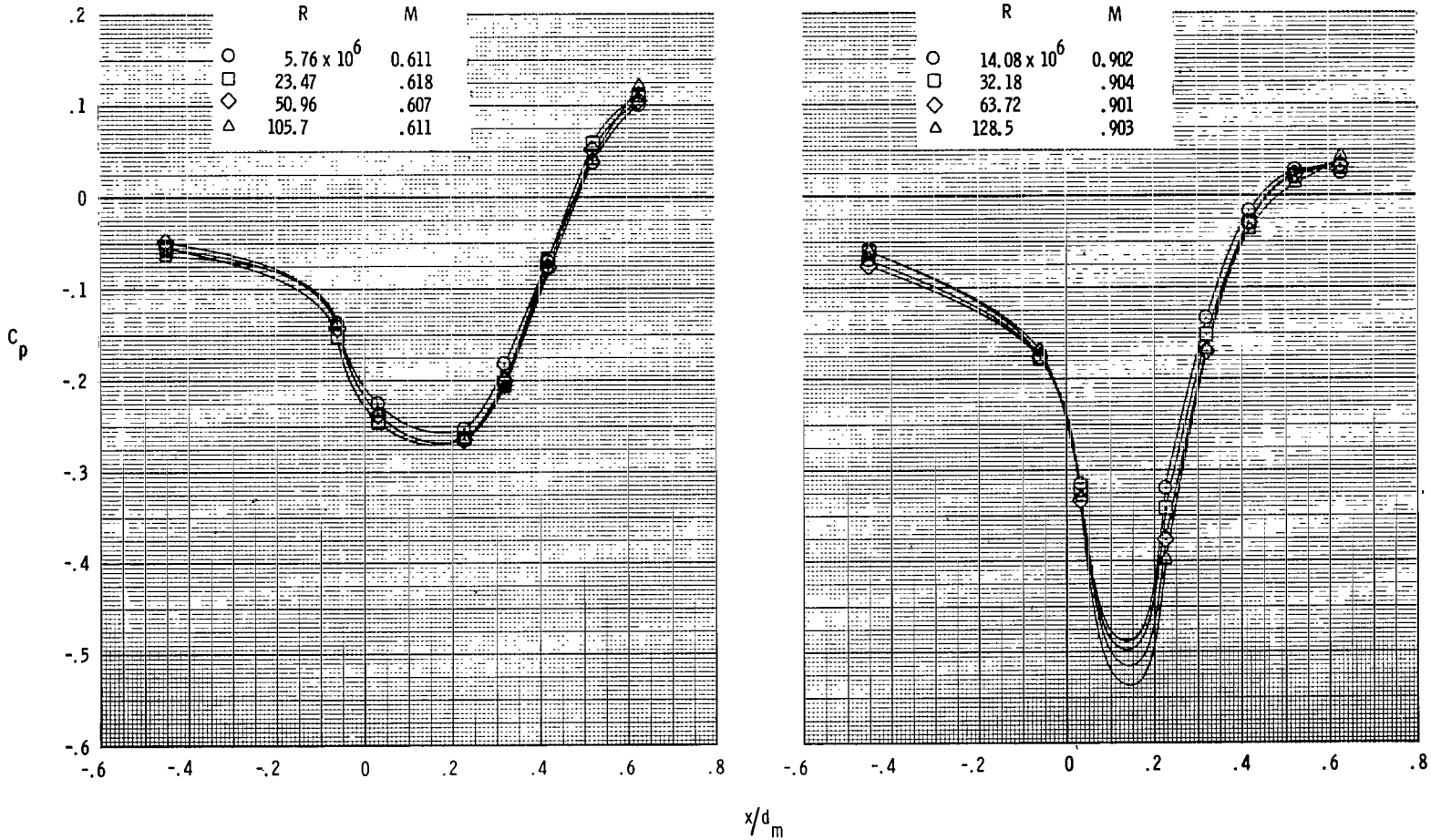

(a) $\phi = 0^{o}$.

Figure 15.- Comparison of boattail static pressure coefficients at four Reynolds numbers for $\frac{l}{d_m} = 0.80$ circular-arc boattail $\left(\frac{L}{d_m} = 16.0\right)$ for $M = 0.6$ and 0.9.

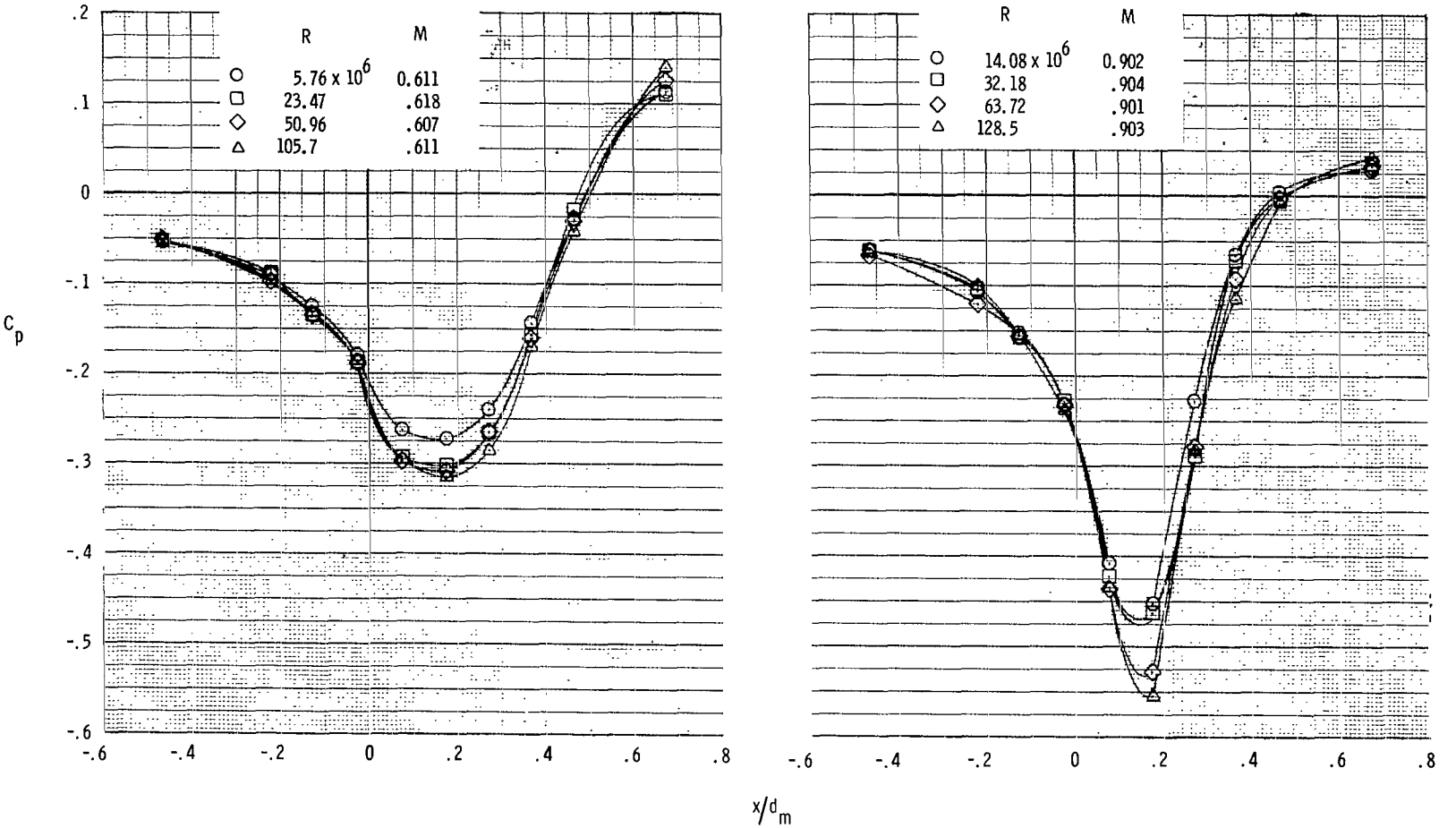

(b) $\phi = 120^{o}$.

Figure 15.- Continued.

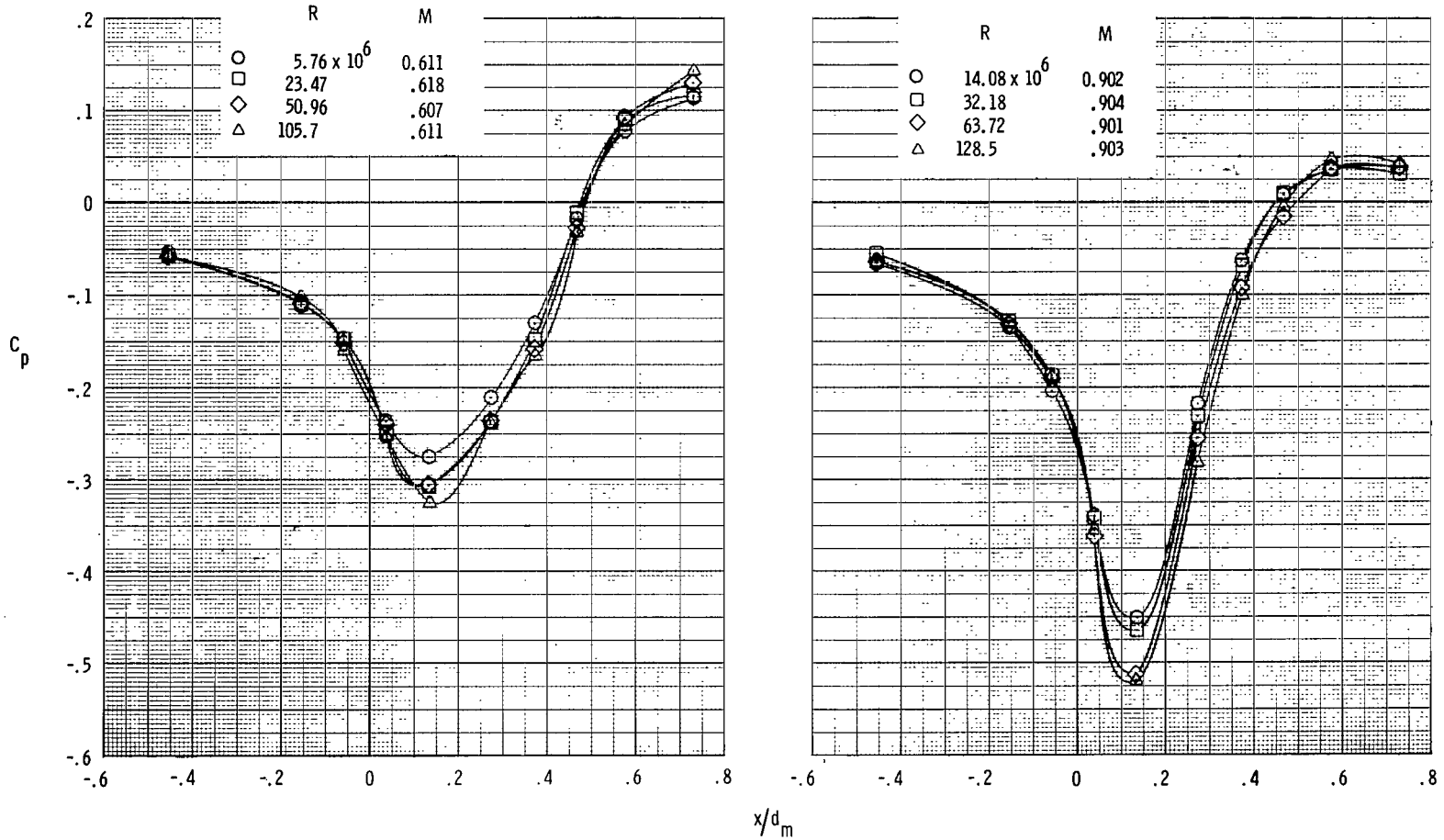

(c) $\phi = 240^{\circ}$.

Figure 15.- Concluded.

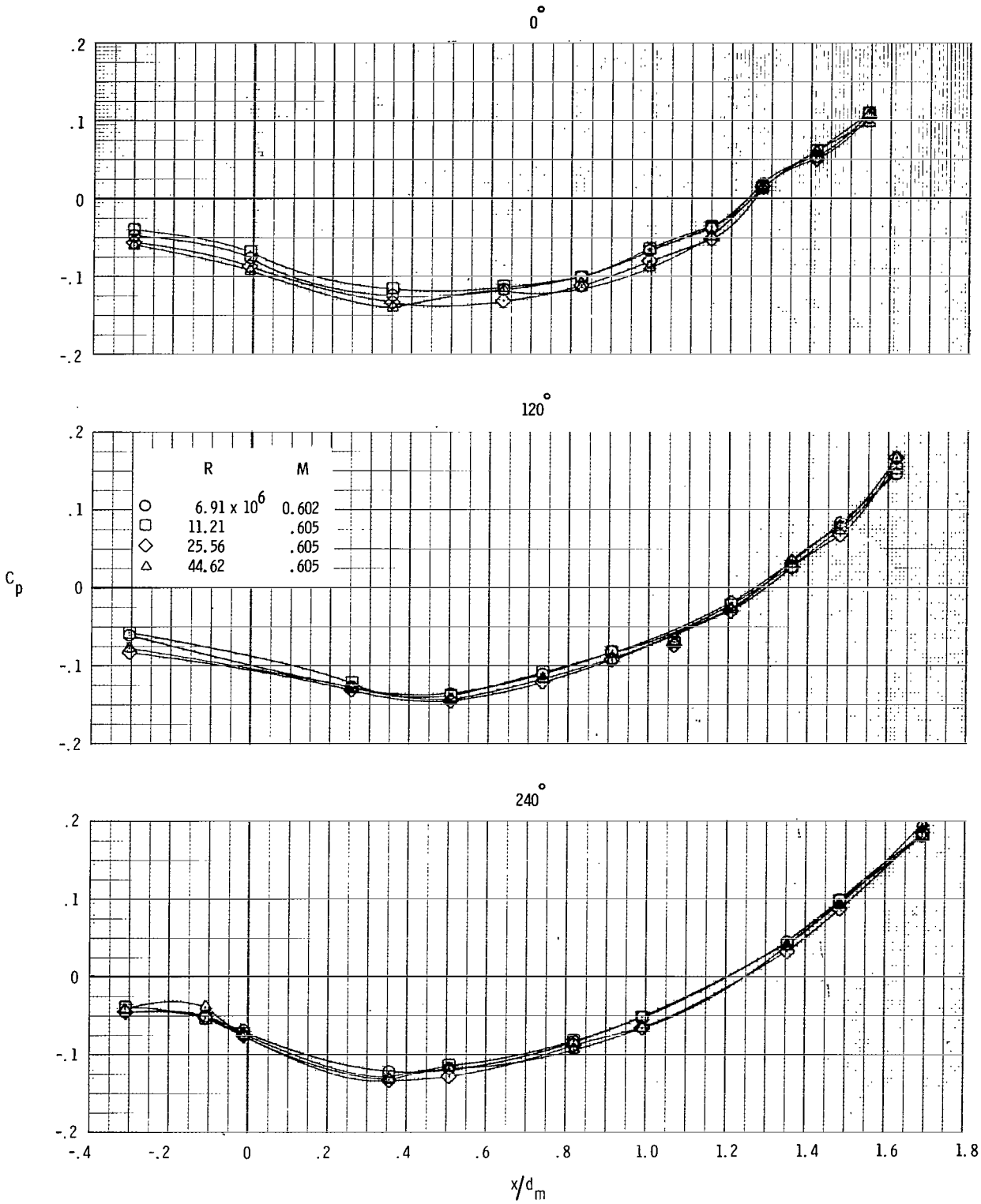

(a) M = 0.6.

Figure 16.- Comparison of boattail static pressure coefficients at four Reynolds numbers for $\frac{l}{d_m} = 1.77$ circular-arc boattail $\left(\frac{L}{d_m} = 8.0\right)$ for M = 0.6 and 0.9.

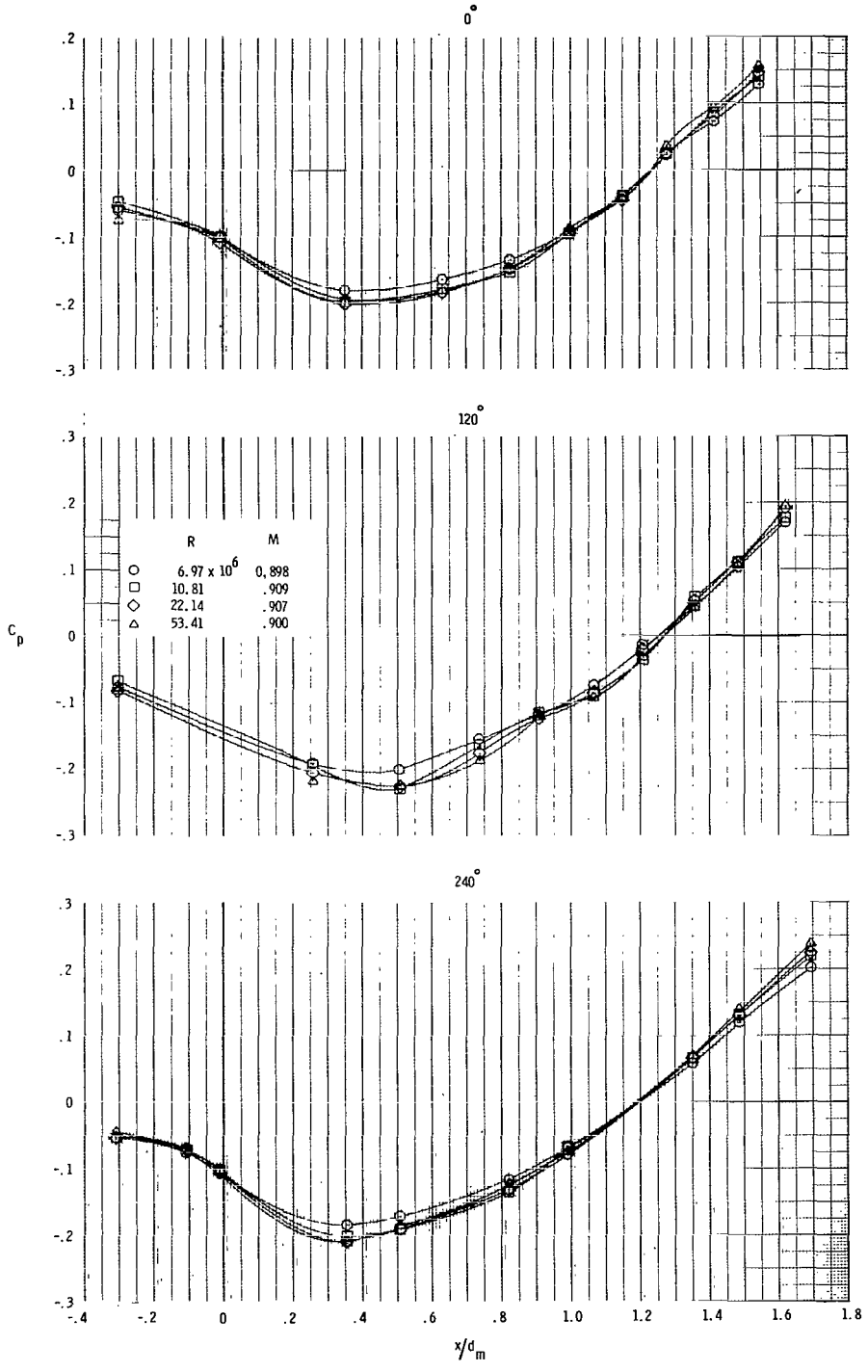

(b) M = 0.9.

Figure 16.- Concluded.

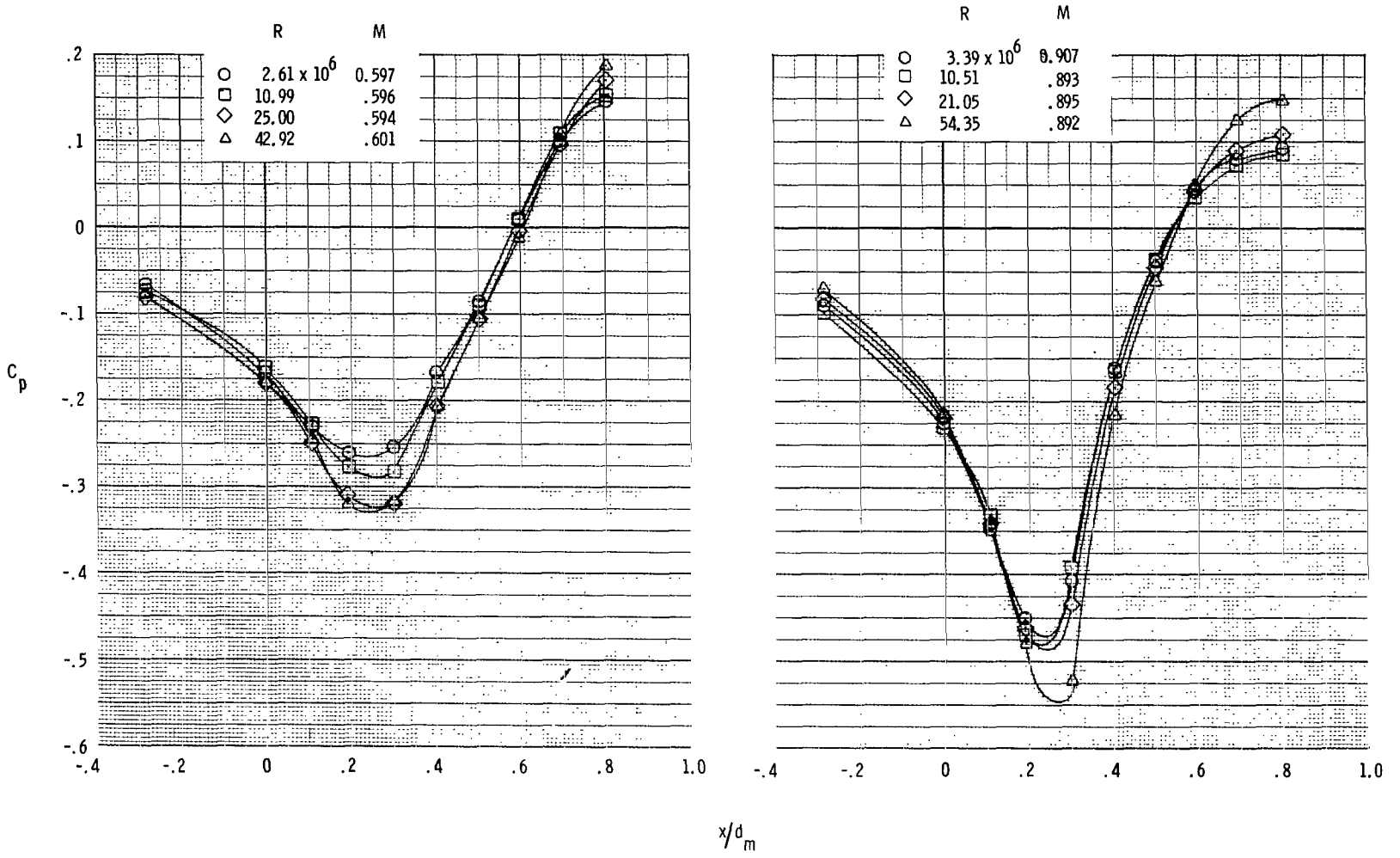

(a) $\phi = 0^{\circ}$.

Figure 17.- Comparison of boattail static pressure coefficients at four Reynolds numbers for circular-arc–conic boattail $\left(\frac{L}{d_m} = 8.0\right)$ for M = 0.6 and 0.9.

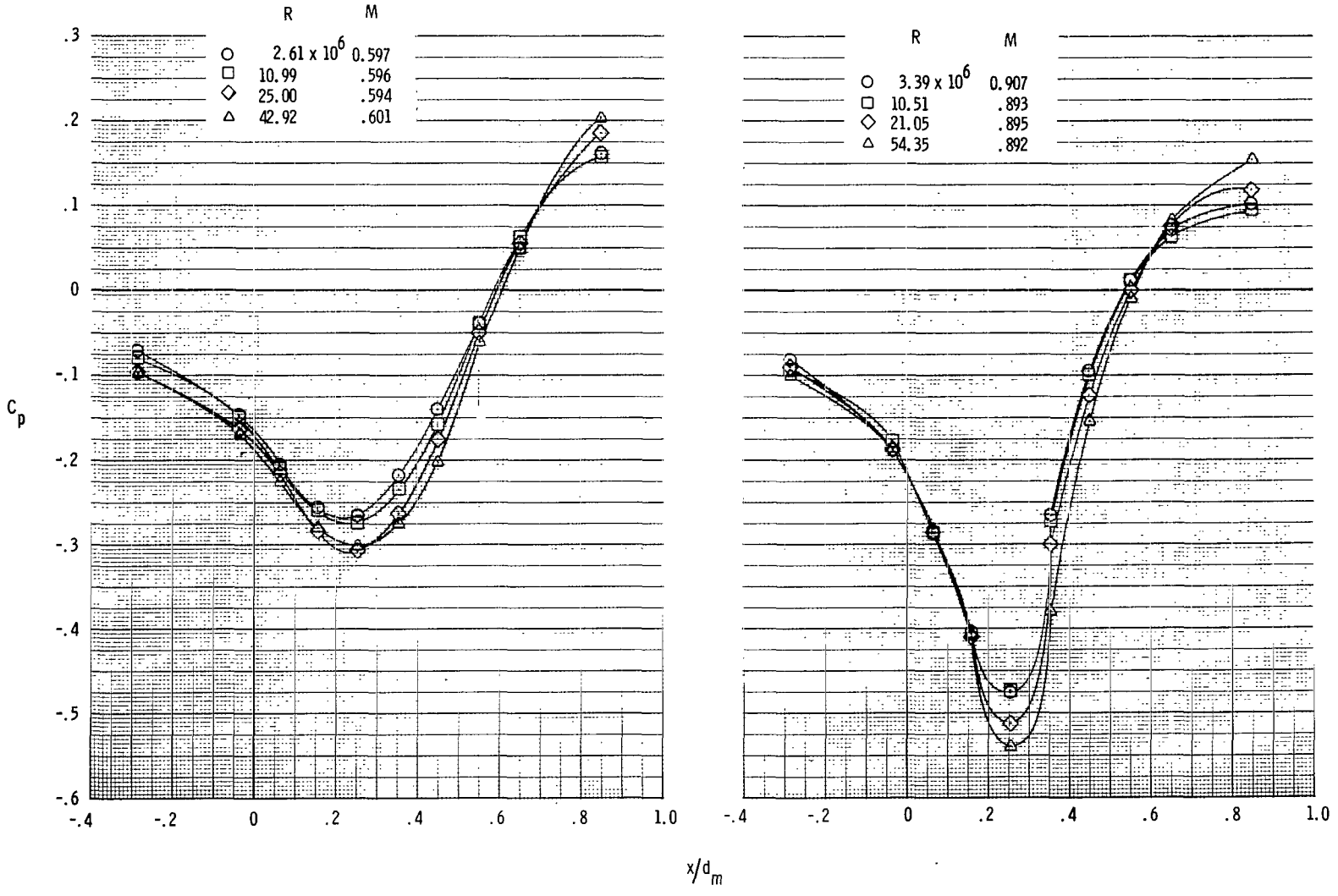

(b) $\phi = 120^{\circ}$.

Figure 17.- Continued.

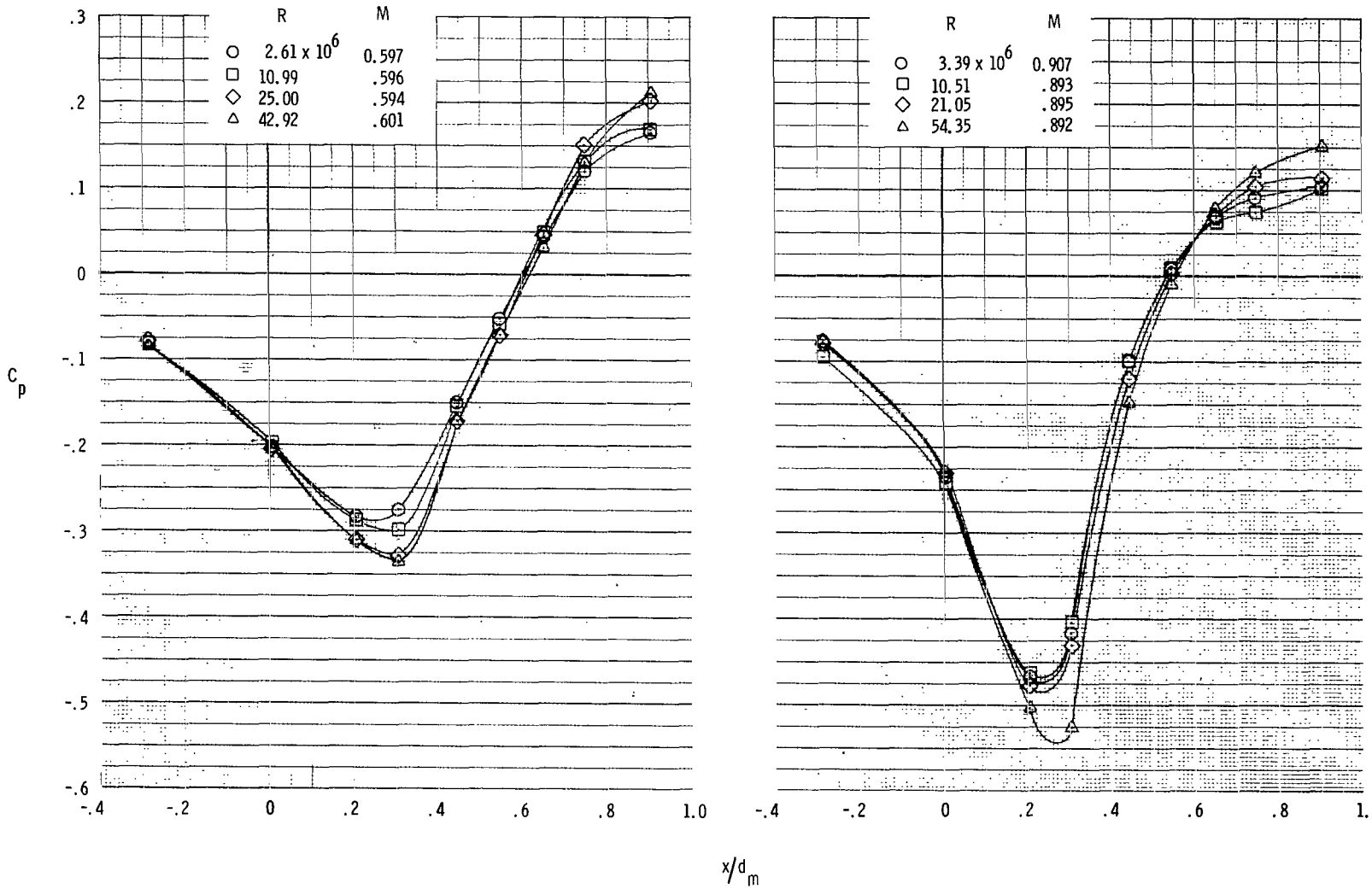

(c) $\phi = 240^{o}$.

Figure 17.- Concluded.

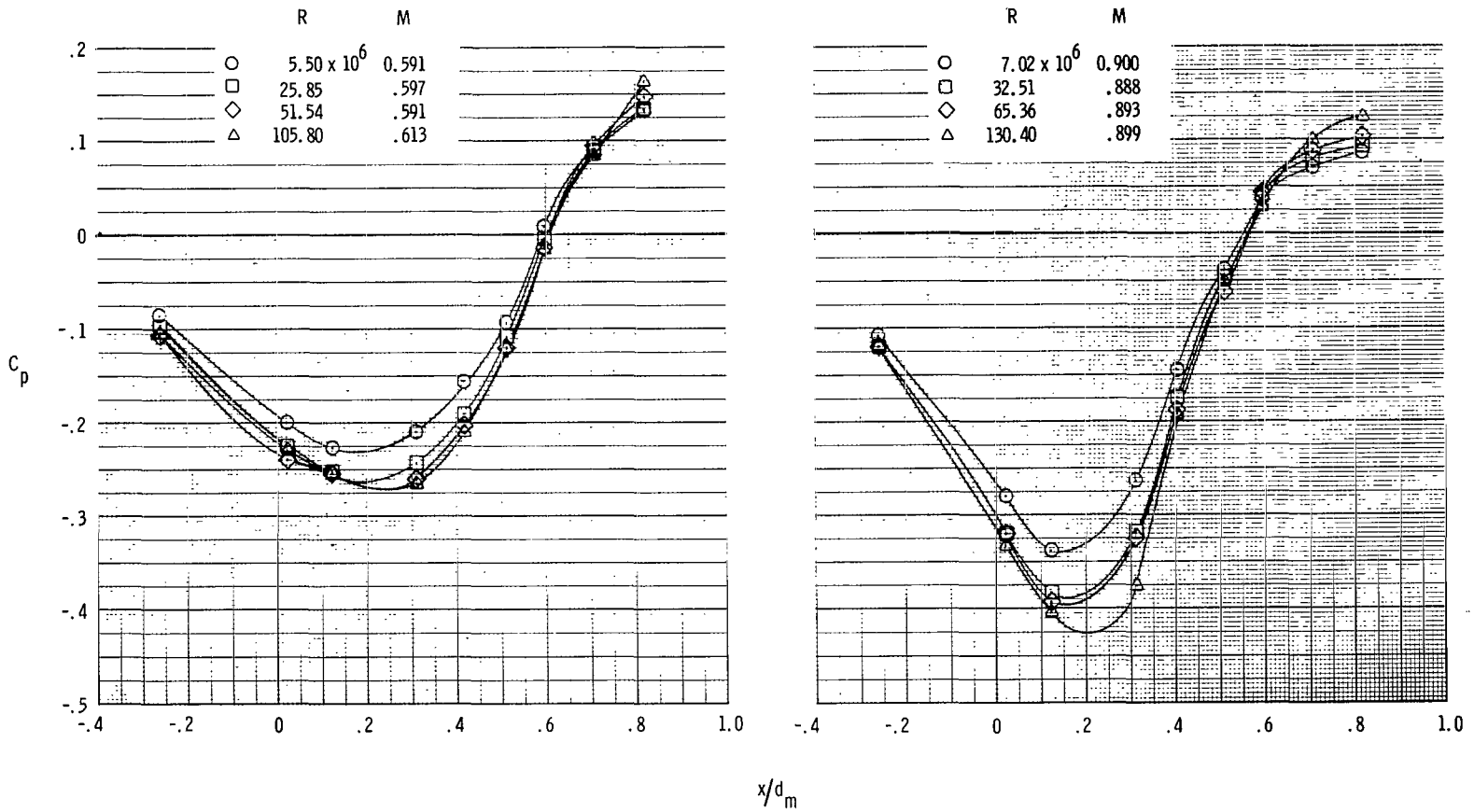

(a) $\phi = 0^{o}$.

Figure 18.- Comparison of boattail static pressure coefficients at four Reynolds numbers for circular-arc–conic boattail $\left(\frac{L}{d_m} = 16.0\right)$ for M = 0.6 and 0.9.

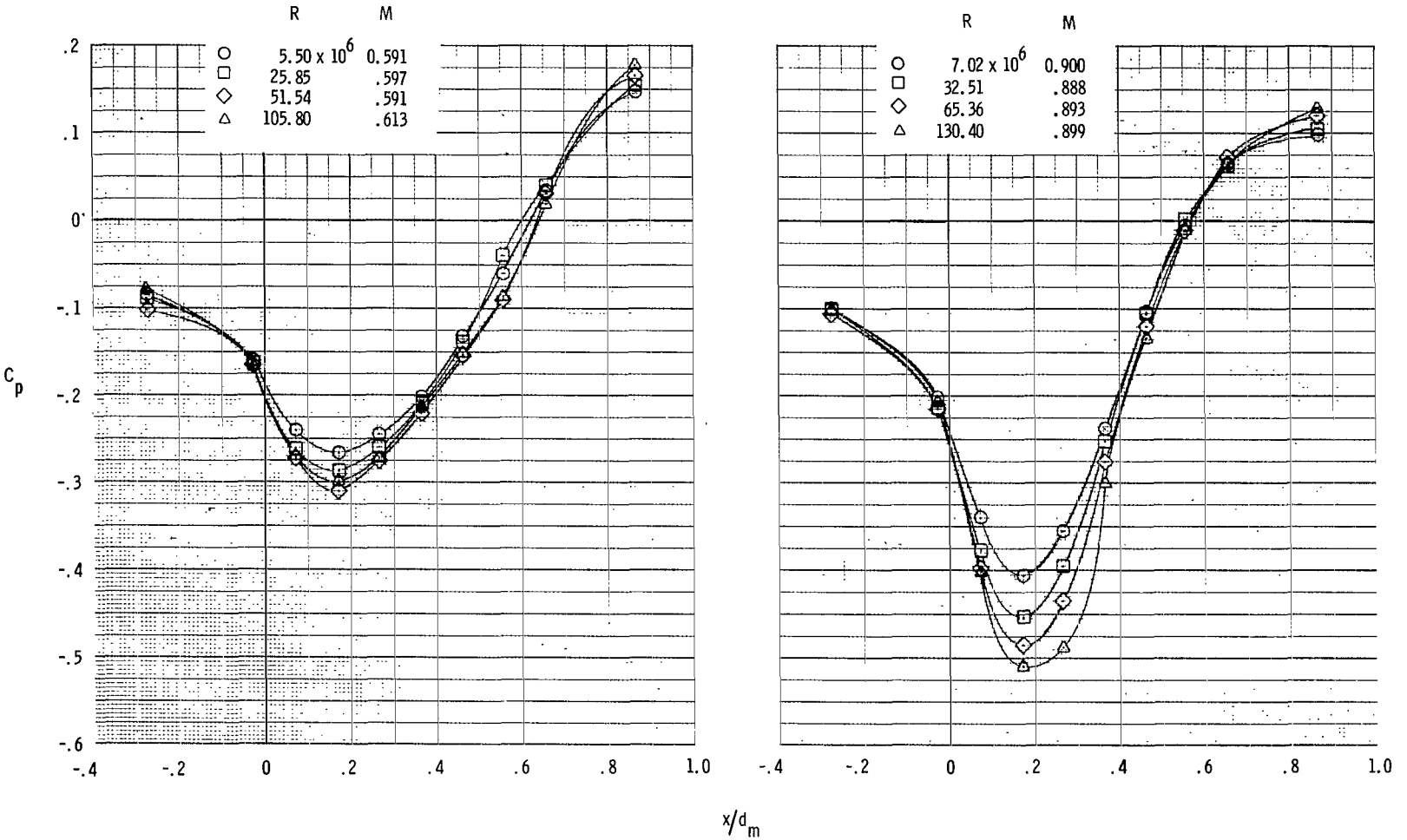

(b) $\phi = 120^{\circ}$.

Figure 18.- Continued.

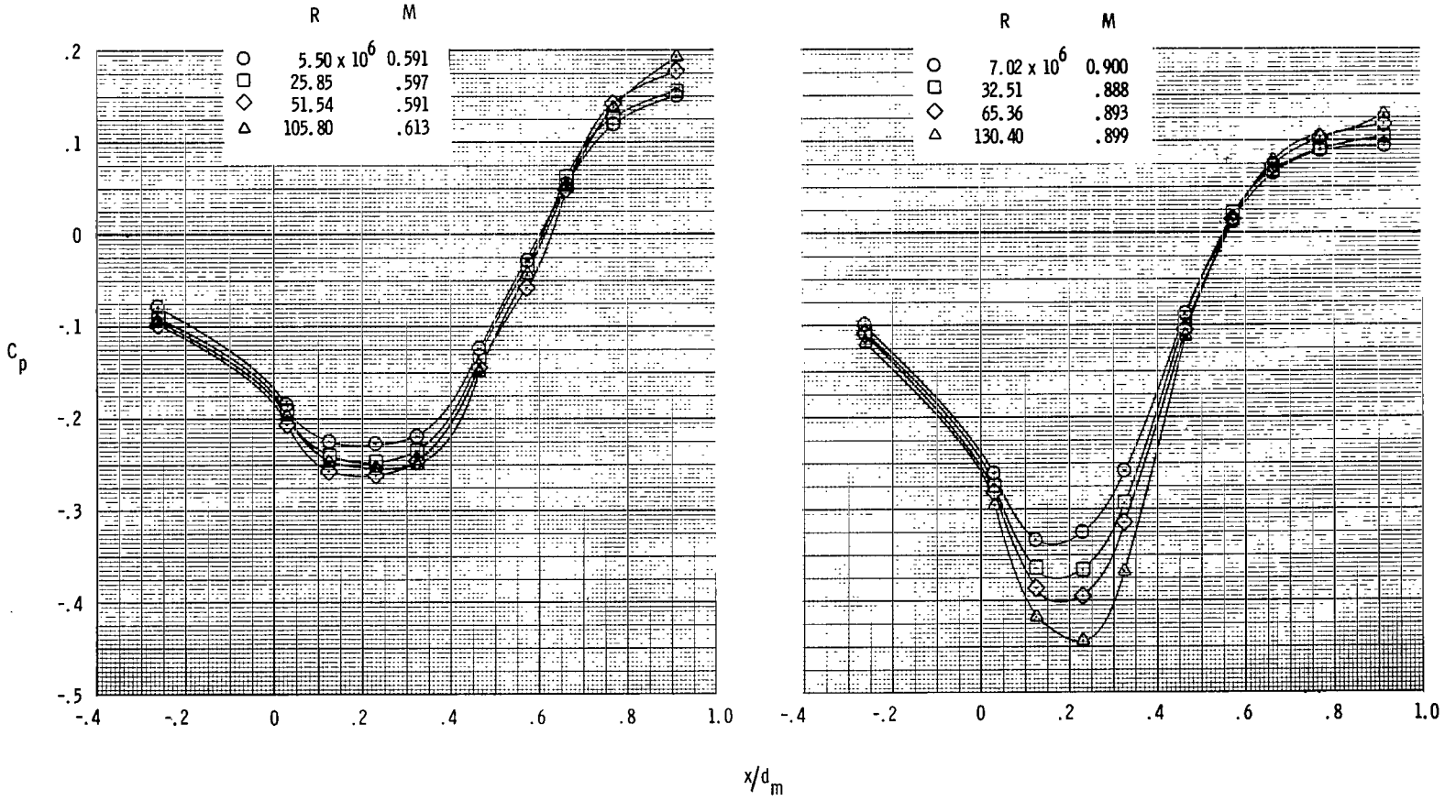

(c) $\phi = 240^{\circ}$.

Figure 18.- Concluded.

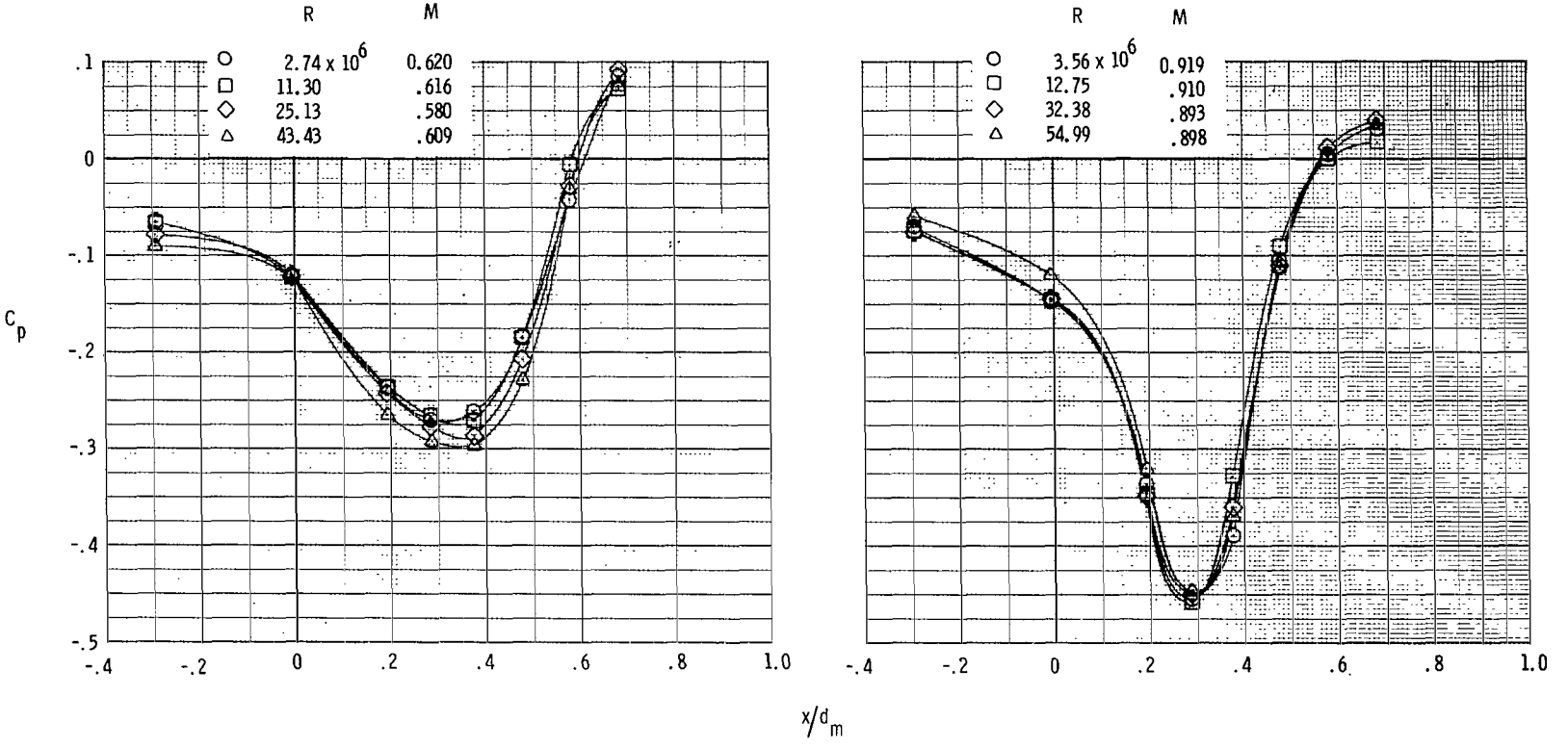

(a) $\phi = 0^{o}$.

Figure 19.- Comparison of boattail static pressure coefficients at four Reynolds numbers for contoured boattail $\left(\frac{L}{d_m} = 8.0\right)$ for M = 0.6 and 0.9.

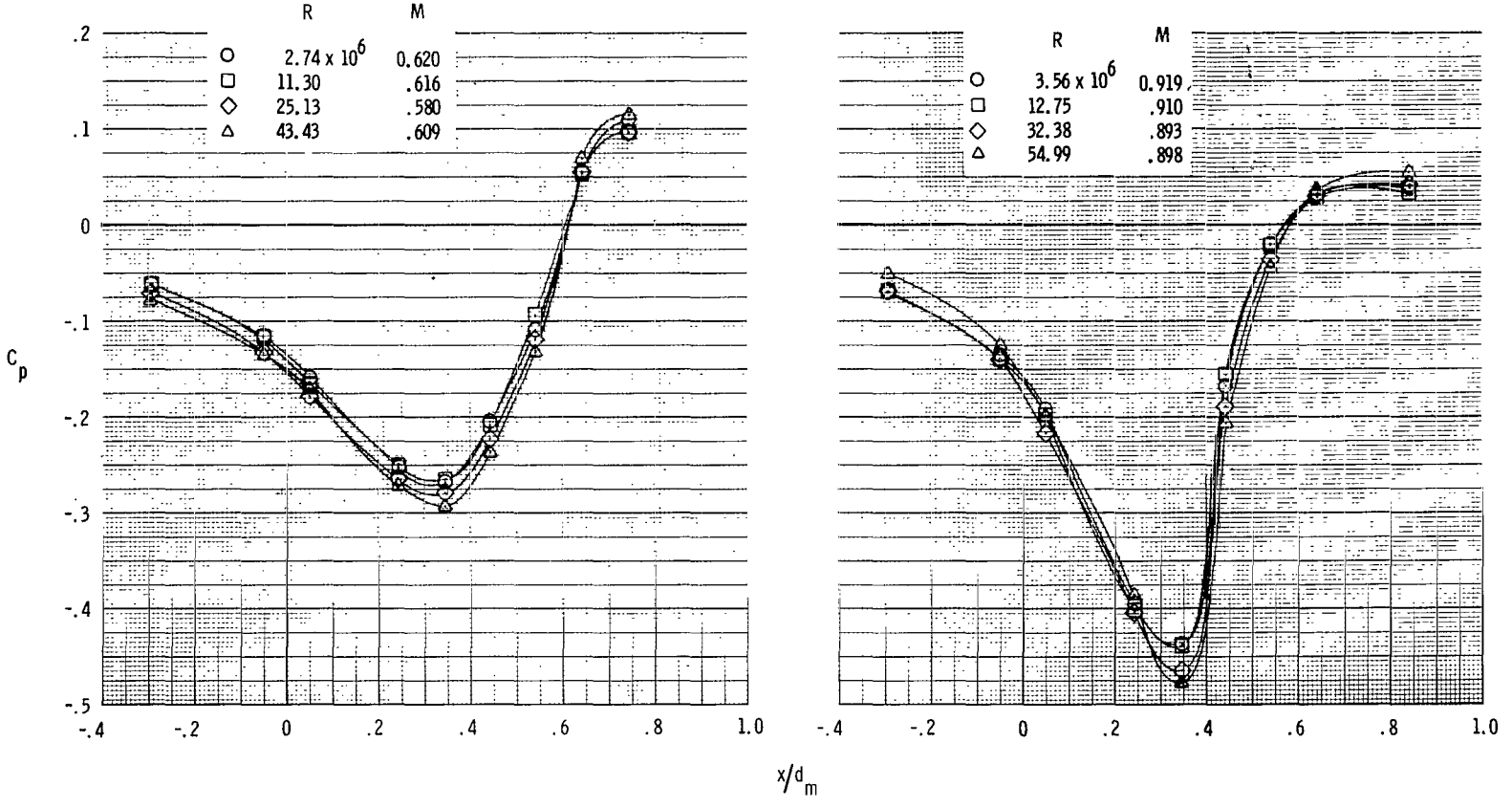

(b) $\phi = 120^{\circ}$.

Figure 19.- Continued.

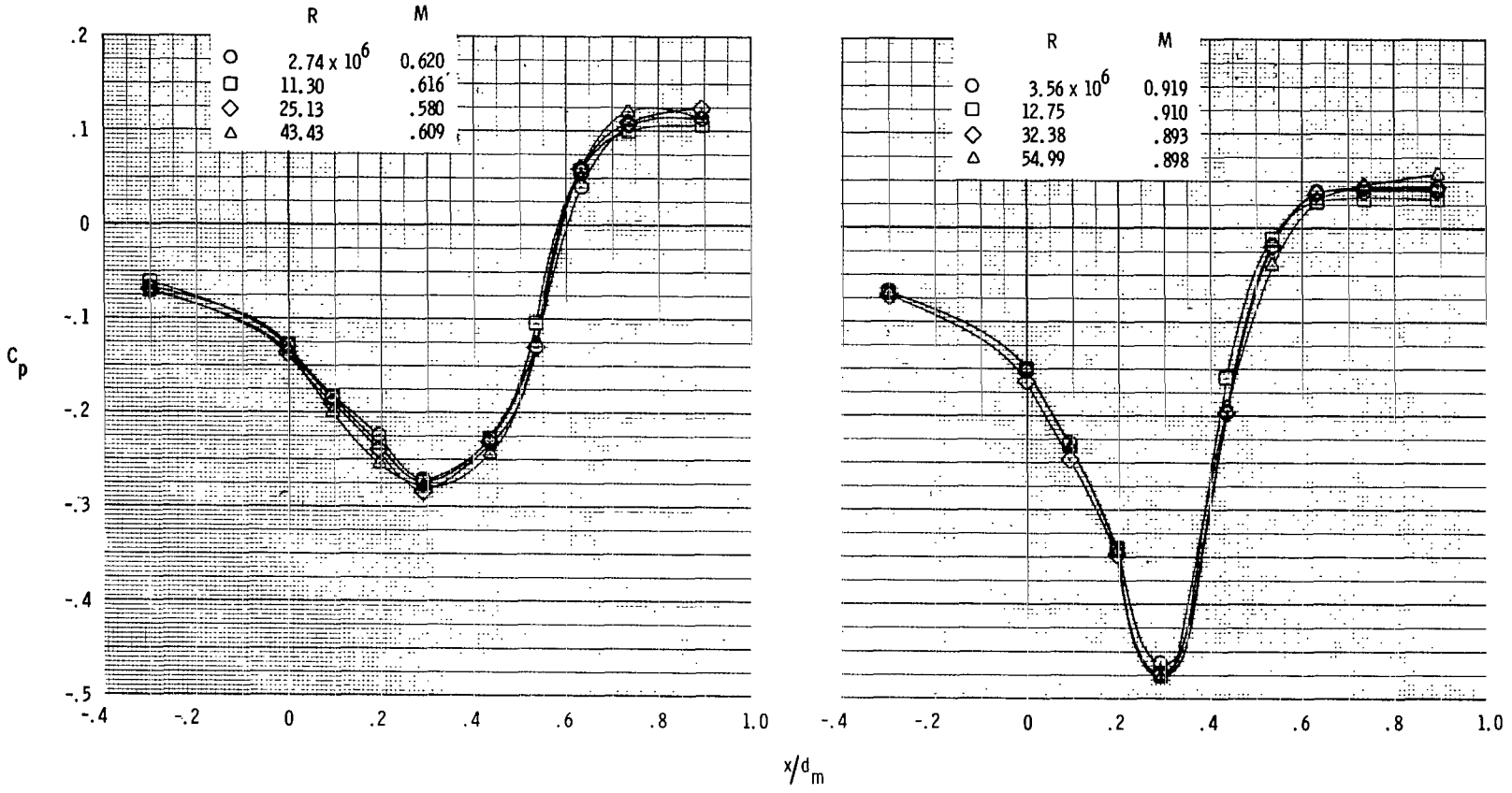

(c) $\phi = 240^{\circ}$.

Figure 19.- Concluded.

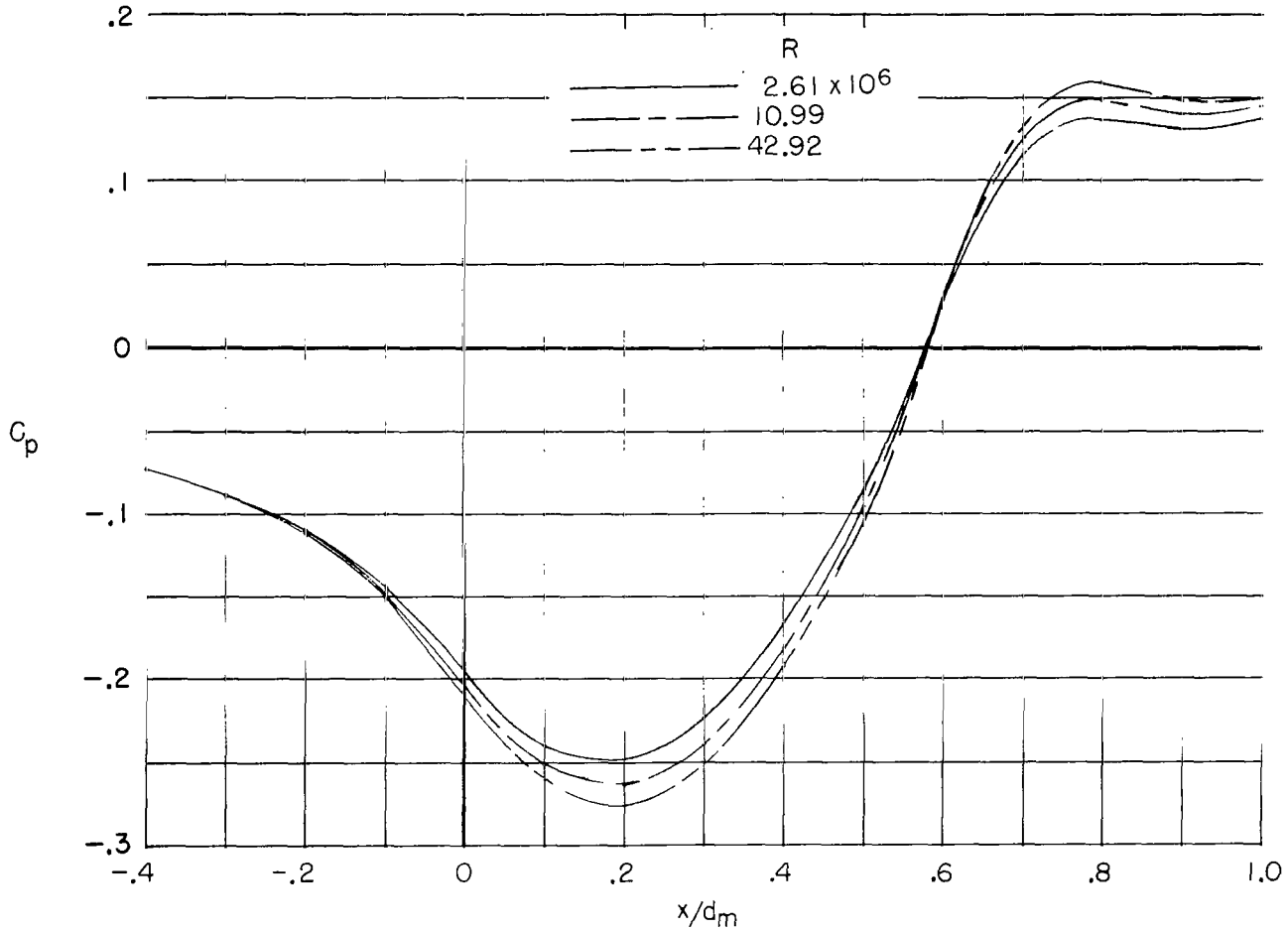

Figure 20.- Theoretical predictions of boattail static pressure coefficient distributions for circular-arc–conic boattail $\left(\frac{L}{d_m} = 8.0\right)$ at three values of Reynolds number at $M = 0.6$.

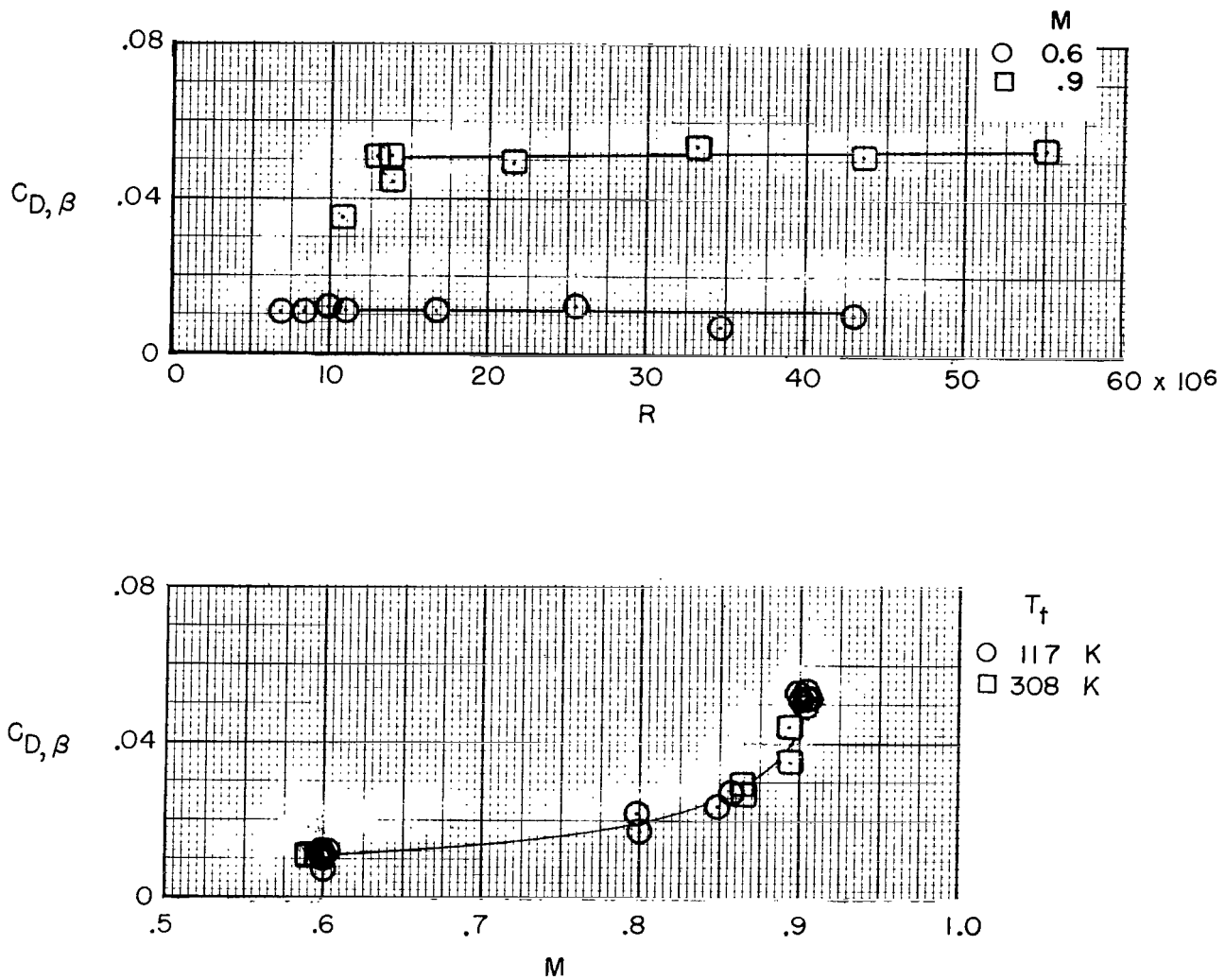

Figure 21.- Effect of Reynolds number and Mach number on boattail pressure drag for $\frac{l}{d_m} = 0.80$ circular-arc boattail $\left(\frac{L}{d_m} = 8.0\right)$.

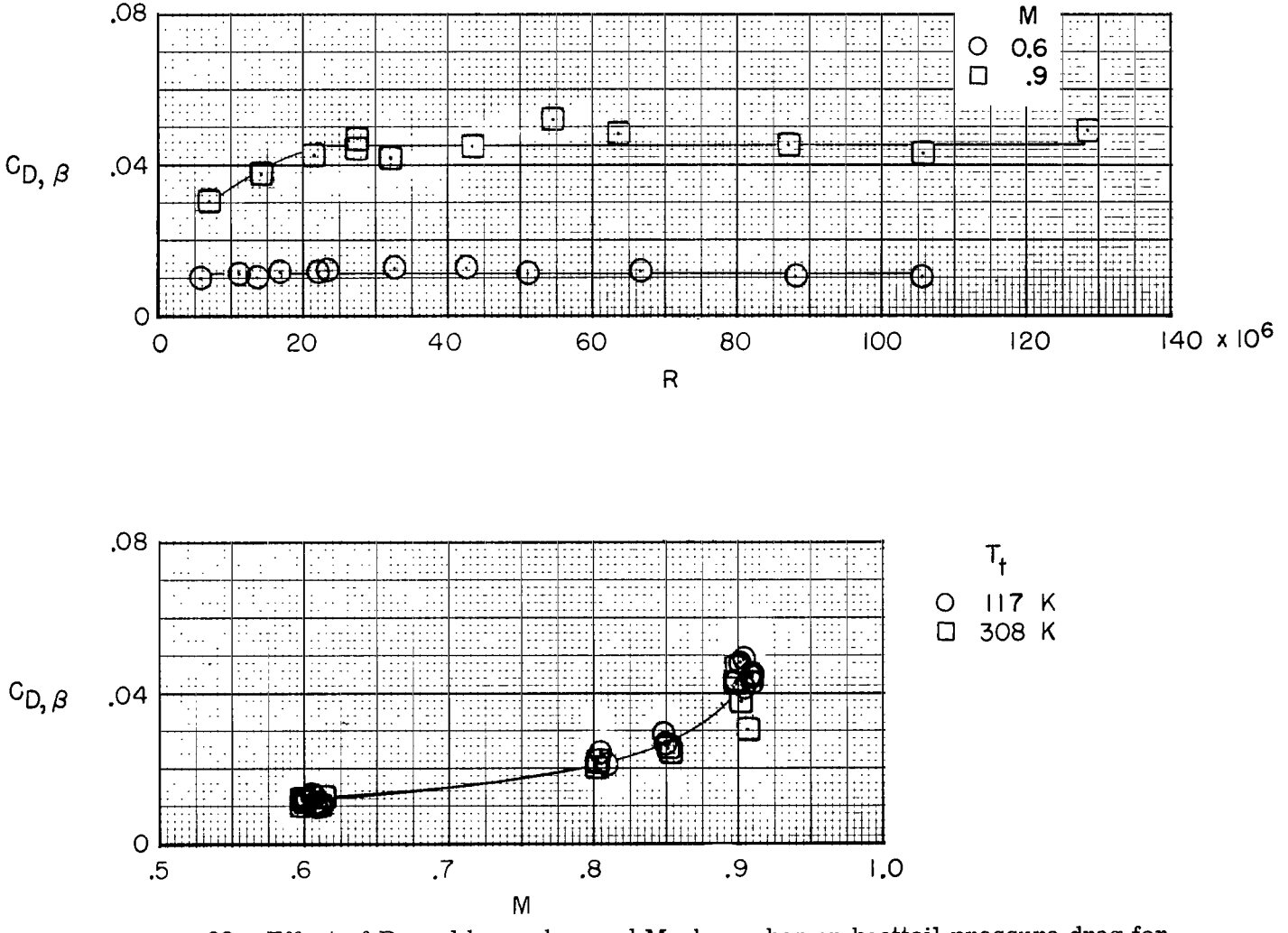

Figure 22.- Effect of Reynolds number and Mach number on boattail pressure drag for $\frac{l}{d_m} = 0.80$ circular-arc boattail $\left(\frac{L}{d_m} = 16.0\right)$.

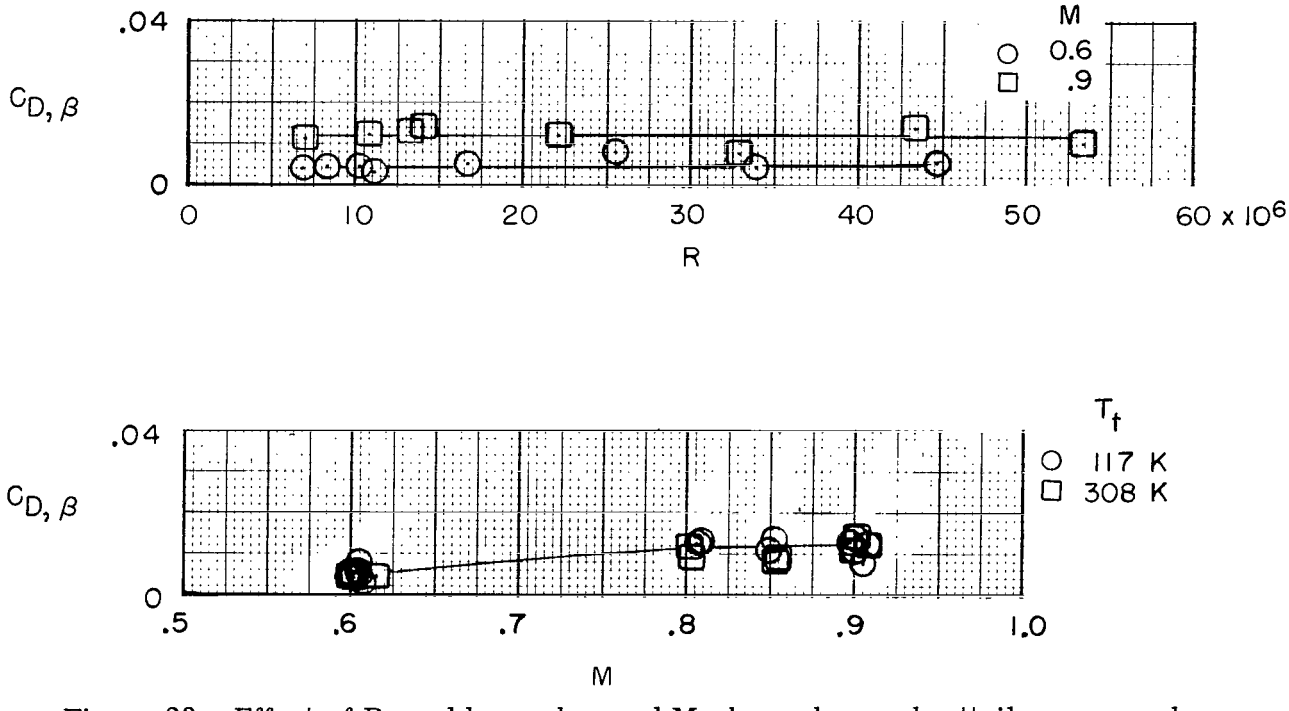

Figure 23.- Effect of Reynolds number and Mach number on boattail pressure drag for $\frac{l}{d_m} = 1.77$ circular-arc boattail $\left(\frac{L}{d_m} = 8.0\right)$.

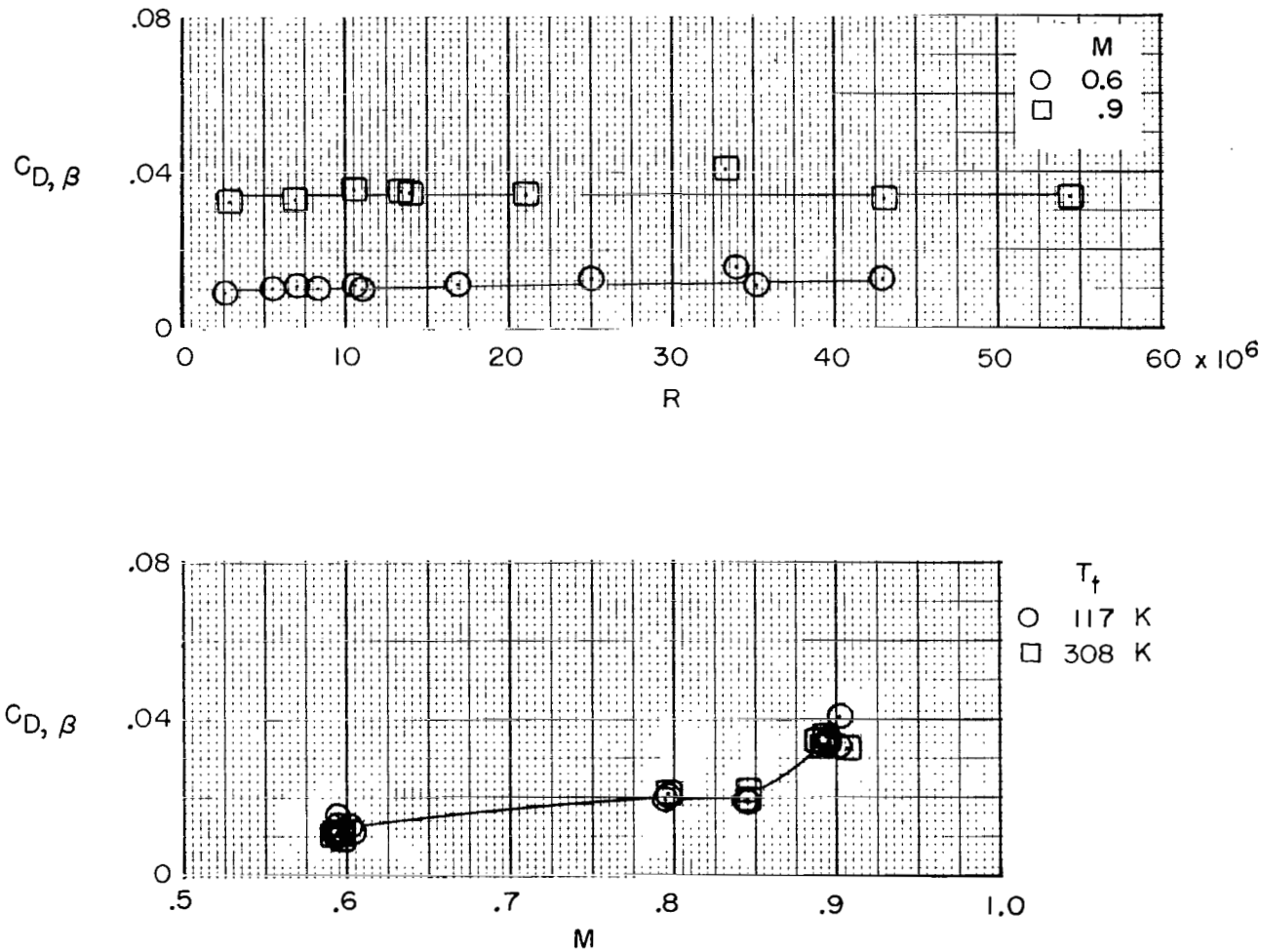

Figure 24.- Effect of Reynolds number and Mach number on boattail pressure drag for circular-arc–conic boattail $\left(\frac{L}{d_m} = 8.0\right)$.

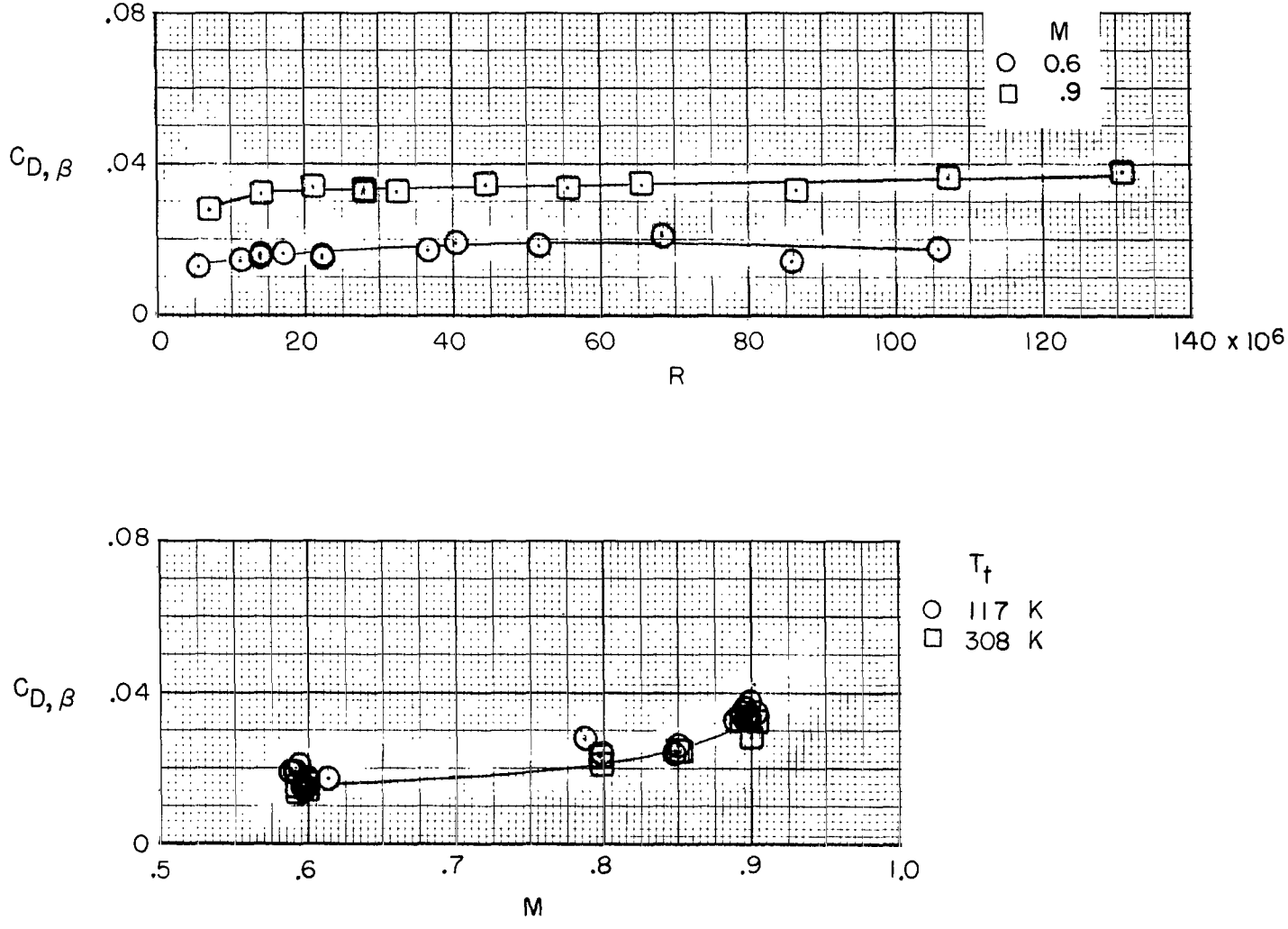

Figure 25.- Effect of Reynolds number and Mach number on boattail pressure drag for circular-arc–conic boattail $\left(\frac{L}{d_m} = 16.0\right)$.

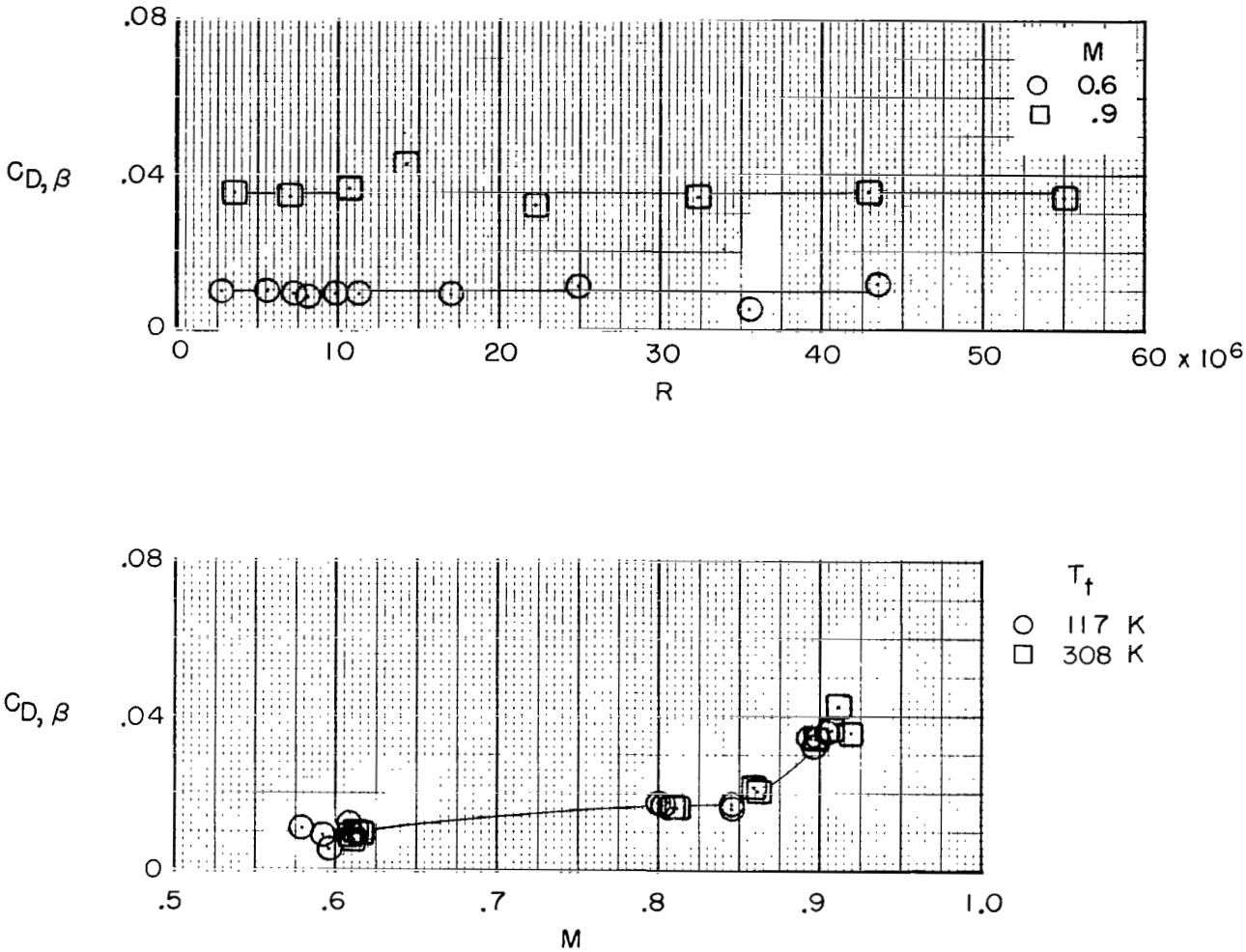

Figure 26.- Effect of Reynolds number and Mach number on boattail pressure drag for contoured boattail $\left(\frac{L}{d_m} = 8.0\right)$.

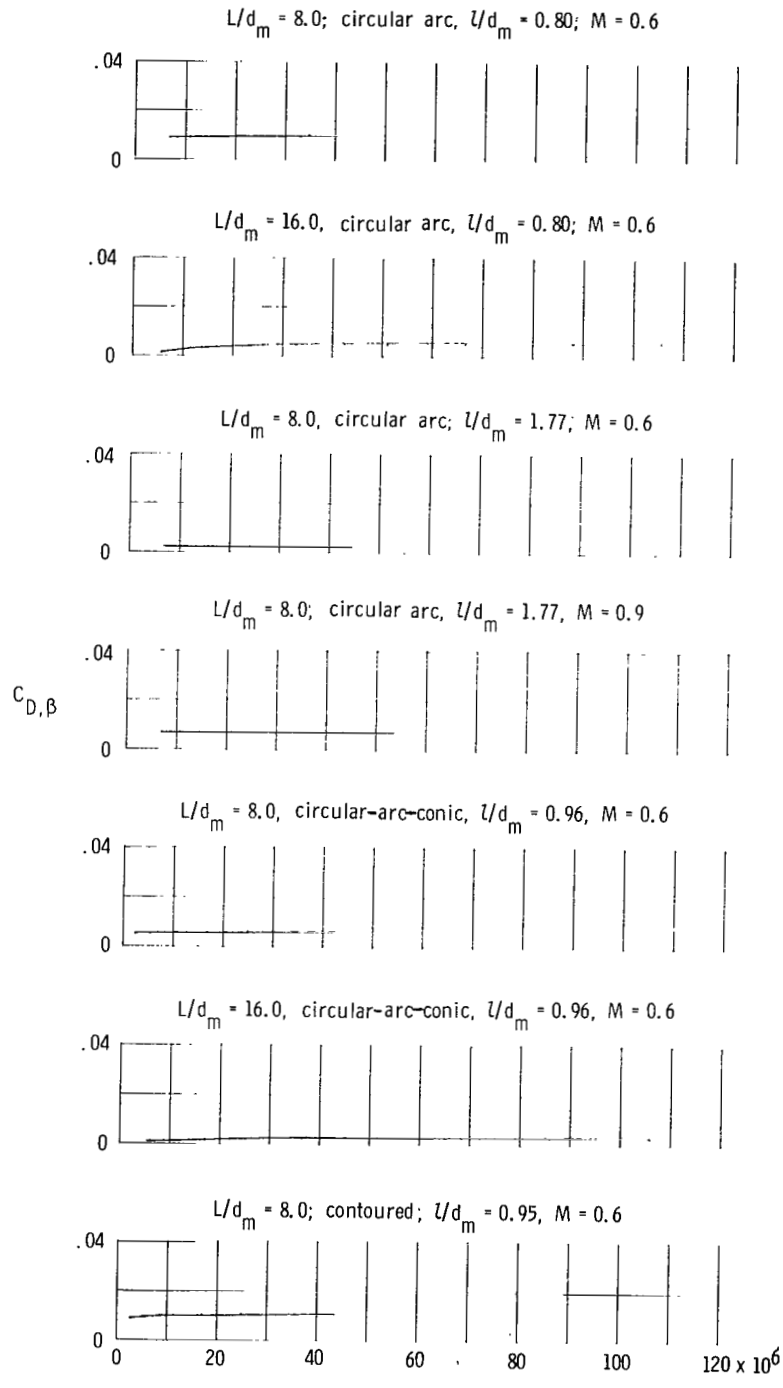

Figure 27.- Theoretical predictions of effect of Reynolds number on boattail pressure drag coefficients for various boattails.

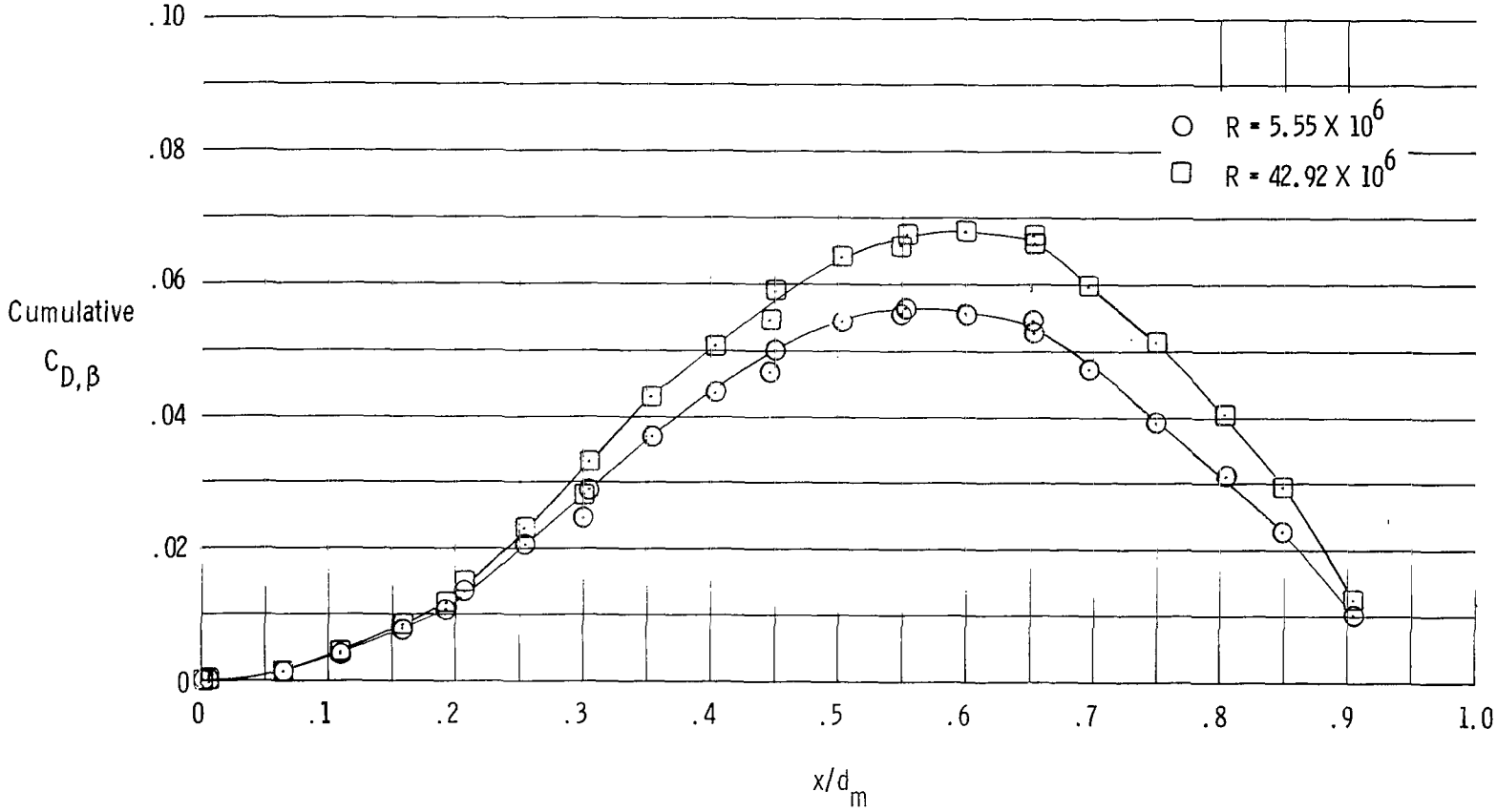

Figure 28.- Experimental boattail pressure drag coefficient as function of distance from start of boattail for circular-arc–conic boattail $\left(\frac{L}{d_m} = 8.0\right)$ at two Reynolds numbers at M = 0.6.

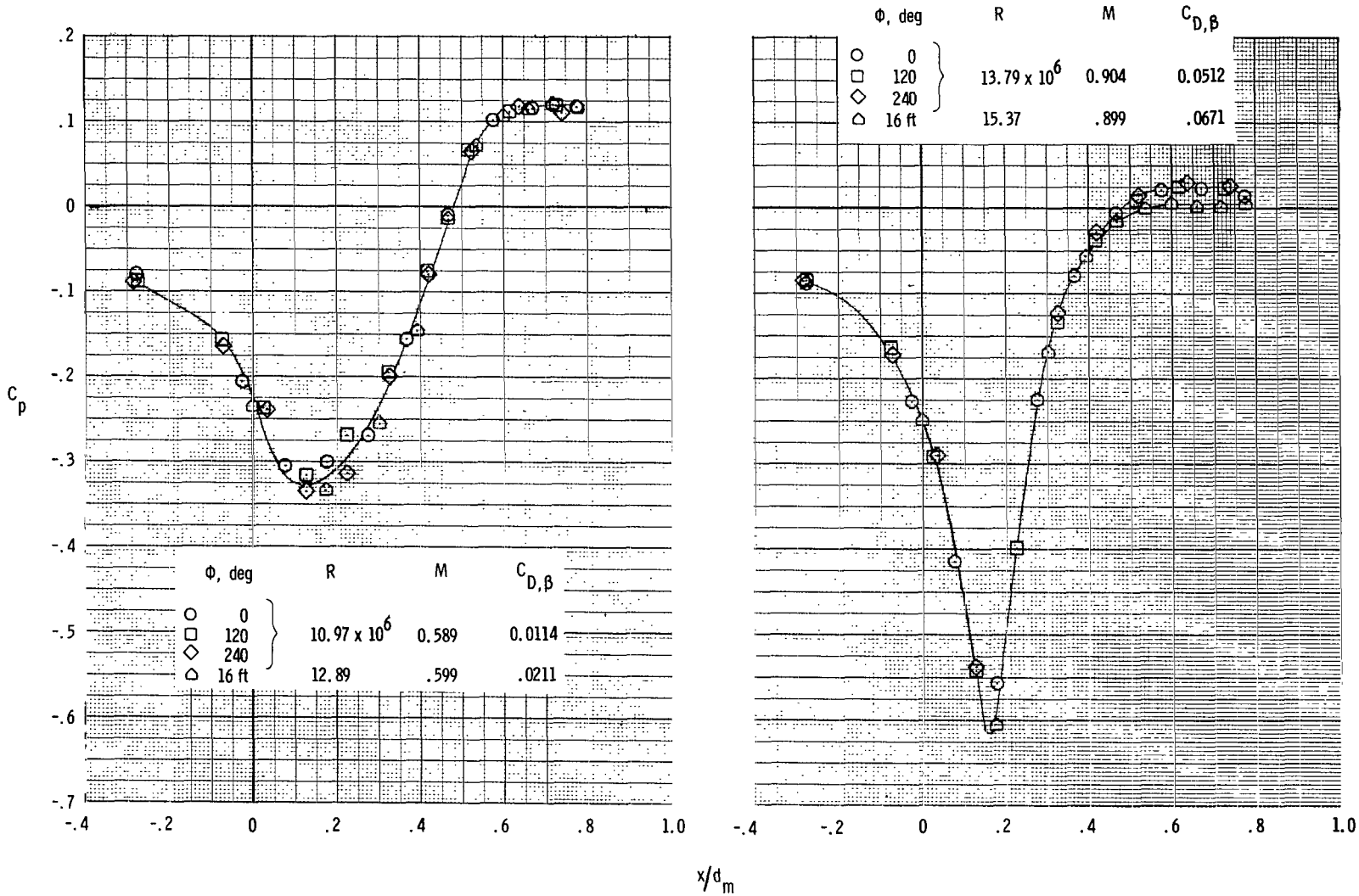

Figure 29.- Comparison of boattail static pressure coefficients for $\frac{l}{d_m} = 0.80$ circular-arc boattail $\left(\frac{L}{d_m} = 8.0\right)$ obtained in Langley 1/3-meter transonic cryogenic tunnel with those from larger scale model obtained in Langley 16-foot transonic tunnel.

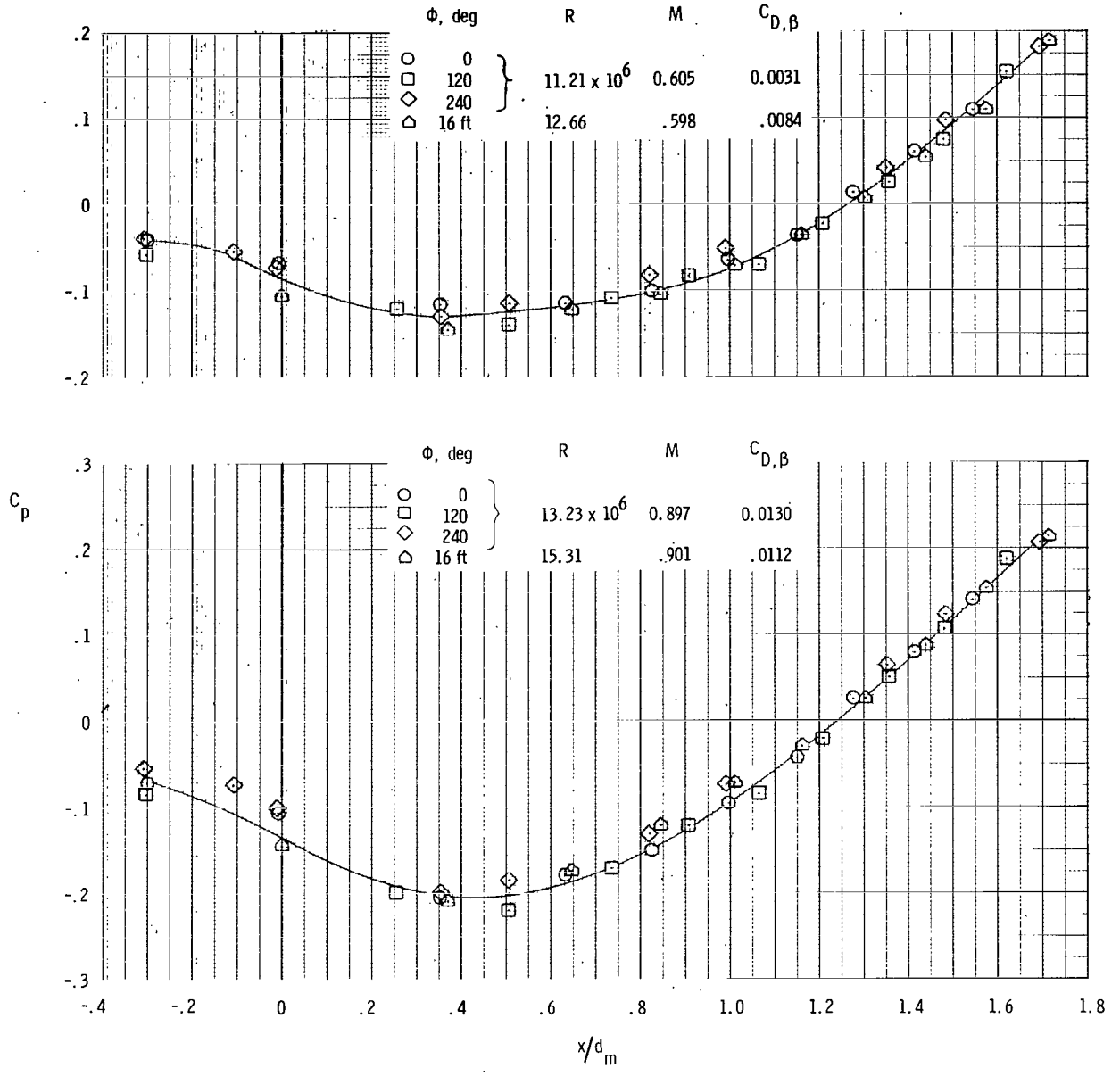

Figure 30.- Comparison of boattail static pressure coefficients for $\frac{l}{d_m} = 1.77$ circular-arc boattail $\left(\frac{L}{d_m} = 8.0\right)$ obtained in Langley 1/3-meter transonic cryogenic tunnel with those from larger scale model obtained in Langley 16-foot transonic tunnel.

NATIONAL AERONAUTICS AND SPACE ADMINISTRATION
WASHINGTON, D.C. 20546

OFFICIAL BUSINESS
PENALTY FOR PRIVATE USE $300

SPECIAL FOURTH-CLASS RATE
BOOK

POSTAGE AND FEES PAID
NATIONAL AERONAUTICS AND
SPACE ADMINISTRATION
451

U.S.MAIL

"The aeronautical and space activities of the United States shall be conducted so as to contribute . . . to the expansion of human knowledge of phenomena in the atmosphere and space. The Administration shall provide for the widest practicable and appropriate dissemination of information concerning its activities and the results thereof."

—NATIONAL AERONAUTICS AND SPACE ACT OF 1958

NASA SCIENTIFIC AND TECHNICAL PUBLICATIONS

TECHNICAL REPORTS: Scientific and technical information considered important, complete, and a lasting contribution to existing knowledge.

TECHNICAL NOTES: Information less broad in scope but nevertheless of importance as a contribution to existing knowledge.

TECHNICAL MEMORANDUMS: Information receiving limited distribution because of preliminary data, security classification, or other reasons. Also includes conference proceedings with either limited or unlimited distribution.

CONTRACTOR REPORTS: Scientific and technical information generated under a NASA contract or grant and considered an important contribution to existing knowledge.

TECHNICAL TRANSLATIONS: Information published in a foreign language considered to merit NASA distribution in English.

SPECIAL PUBLICATIONS: Information derived from or of value to NASA activities. Publications include final reports of major projects, monographs, data compilations, handbooks, sourcebooks, and special bibliographies.

TECHNOLOGY UTILIZATION PUBLICATIONS: Information on technology used by NASA that may be of particular interest in commercial and other non-aerospace applications. Publications include Tech Briefs, Technology Utilization Reports and Technology Surveys.

Details on the availability of these publications may be obtained from:

SCIENTIFIC AND TECHNICAL INFORMATION OFFICE

NATIONAL AERONAUTICS AND SPACE ADMINISTRATION

Washington, D.C. 20546